

**FUNCTIONALIZATION OF PARTICLES AND SELECTIVE
FUNCTIONALIZATION OF SURFACES FOR THE
ELECTROLESS METAL PLATING PROCESS**

Dissertation

zur Erlangung des akademischen Grades

Doctor rerum naturalium

(Dr. rer. nat)

vorgelegt

der Fakultät Mathematik und Naturwissenschaften

der Technischen Universität Dresden

von

M.Sc. Giovanni Mondin

geboren am 11. Mai 1986 in Zürich

eingereicht am 28.05.2014

Die Dissertation wurde in der Zeit von 08/2011 bis 05/2014 an der Professur für
Anorganische Chemie I der Fachrichtung Chemie und Lebensmittelchemie angefertigt

Gutachter: Prof. Dr. Stefan Kaskel
Prof. Dr. Alexander Eychmüller

Tag der Verteidigung: 28.11.2014

Acknowledgements

I would like to express my appreciation to my supervisor Prof. Dr. Stefan Kaskel. Thank you for encouraging my research, supporting my work and for allowing me to grow as a research scientist.

I would especially like to thank group leaders Dr. Julia Grothe and Dr. Susanne Dörfler for fruitful discussion and guidance throughout my PhD.

Many special thanks to my laboratory colleagues for all the help, patience and very nice working environment: Nasser Mohamed-Noriega, Benjamin Schumm, Julia Fritsch, Andreas Meier, Florian Wisser, Matthias Benusch and Annika Leifert. Also a big thank you to my assistants Holm Ackermann and Elke Schade for all the help in carrying out experimental work.

I would like to thank the staff at Leibniz Institute for Solid State and Materials Research (IFW Dresden) who assisted me during my TEM investigations: Nicole Geißler, Dr. Sandeep Gorantla, Dr. Mark Rümmeli, Gesine Kreutzer and Dr. Felix Börrnert. Many thanks also to the people working at the project ECEMP-C1, in particular to Christoph Großmann, Dr.-Ing. Jörg Zschetzsche and Prof. Dr. Uwe Füssel (Institute of joining technology and assembly), Marcel Haft, Dr. Silke Hampel and Prof. Dr. Büchner (IFW Dresden).

My sincere thanks to my great office colleagues Claudia Hoffmann, Martin Oschatz, Nasser Mohamed-Noriega and Jan Martin for constant help and first-class working environment.

I wish also to express my gratitude to all the staff of the Kaskel Group for help and support in scientific as well as general issues. Thank you!

Many hearty thanks to all my friends who supported me during my PhD and were always there for help.

My deepest thanks to my girlfriend Yulia and my family: my niece, my brother-in-law, my sister, my mother and my father. Words cannot express how grateful I am to you.

Table of contents

I	MOTIVATION	1
II	THEORETICAL PART	5
1.	ELECTROLESS PLATING	5
1.1	<i>Pretreatment</i>	8
1.2	<i>Silver electroless plating</i>	8
1.3	<i>Copper electroless plating</i>	9
1.4	<i>Nickel electroless plating</i>	10
1.5	<i>Cobalt electroless plating</i>	10
2.	METAL COATING OF PARTICLES	11
2.1	<i>Functionalization of particles</i>	12
2.1.1	<i>Functionalization with polydopamine</i>	12
2.2	<i>Metal coating of particles by electroless plating</i>	15
3.	METAL MATRIX COMPOSITES.....	17
3.1	<i>Metal matrix composites incorporating metal plated particles</i>	18
4.	SOFT LITHOGRAPHY	20
4.1	<i>Microcontact printing</i>	22
4.2	<i>Capillary Force Lithography</i>	23
4.3	<i>Fabrication of metal structures by soft lithography</i>	24
4.3.1	<i>Selective metallization by electroless plating</i>	25
5.	CHARACTERIZATION METHODS.....	28
5.1	<i>Transmission electron microscopy (TEM)</i>	28
5.1	<i>Atomic force microscopy (AFM)</i>	29
III	EXPERIMENTAL	32
1.	FABRICATION OF METAL-COATED PARTICLES	32
1.1	<i>Functionalization with 3-mercaptopropyltriethoxysilane</i>	32
1.2	<i>Functionalization with 3-aminopropylphosphonic acid</i>	33
1.3	<i>Functionalization with polydopamine</i>	33
1.4	<i>Metal deposition by electroless plating on functionalized particles</i>	34
1.4.1	<i>Silver electroless deposition</i>	34

1.4.2	Copper electroless deposition	35
1.4.3	Nickel electroless deposition	36
1.4.4	Cobalt electroless deposition	36
2.	FABRICATION OF METAL MATRIX COMPOSITES BY POWDER METALLURGY	37
2.1	<i>Cu composites reinforced with Cu@Al₂O₃ nanoparticles and Cu@WC microparticles</i>	37
3.	FABRICATION OF SILVER STRUCTURES BY SOFT LITHOGRAPHY.....	37
3.1	<i>Micro-contact printer “GeSiM μ-CP 3.0”</i>	37
3.1.1	Preparation of PDMS stamps.....	38
3.1.2	Preparation of PFPE stamps.....	39
3.2	<i>Fabrication of silver structures by micro-contact printing of 3-mercaptopropyltriethoxysilane and electroless plating</i>	42
3.3	<i>Fabrication of silver structures by capillary force lithography of PMMA and electroless plating</i>	43
4.	CHARACTERIZATION METHODS.....	45
4.1	<i>Transmission electron microscopy (TEM)</i>	45
4.2	<i>Scanning electron microscopy (SEM) and Energy-dispersive X-ray spectroscopy (EDX)</i>	45
4.3	<i>Atomic force microscopy (AFM)</i>	46
4.4	<i>Fourier transform infrared spectroscopy (FTIR)</i>	46
4.5	<i>Thermal gravimetric analysis (TGA)</i>	46
4.6	<i>X-Ray Diffraction (XRD)</i>	46
5.	LIST OF USED CHEMICALS.....	47
IV	RESULTS AND DISCUSSION.....	49
1.	FUNCTIONALIZED PARTICLES	49
1.1	<i>Particle characterization (as received)</i>	49
1.1.1	Al ₂ O ₃ nanoparticles	49
1.1.2	Al ₂ O ₃ microparticles.....	51
1.1.3	SiO ₂ nanoparticles	52
1.1.4	WC nanoparticles	53
1.1.5	WC microparticles.....	54
1.2	<i>Particle functionalization with 3-mercaptopropyltriethoxysilane</i>	55
1.2.1	MPTES@Al ₂ O ₃ nanoparticles	55

1.2.2	MPTES@SiO ₂ nanoparticles	57
1.3	<i>Particle functionalization with 3-aminopropylphosphonic acid</i>	58
1.3.1	3-APP@WC microparticles	58
1.4	<i>Functionalization with polydopamine</i>	60
1.4.1	Polydopamine@Al ₂ O ₃ nanoparticles	60
1.4.2	Polydopamine@Al ₂ O ₃ microparticles	62
1.4.3	Polydopamine@WC nanoparticles	64
1.4.4	Polydopamine@WC microparticles	66
2.	METAL PLATED PARTICLES	70
2.1	<i>Silver coated particles</i>	70
2.1.1	Ag@Pdop@WC microparticles	70
2.2	<i>Copper coated particles</i>	71
2.2.1	Cu@MPTES@Al ₂ O ₃ and Cu@MPTES@SiO ₂ nanoparticles	71
2.2.2	Cu@3-APP@WC microparticles	75
2.2.3	Cu@Pdop@Al ₂ O ₃ nanoparticles	76
2.2.4	Cu@Pdop@WC microparticles	78
2.3	<i>Nickel coated particles</i>	80
2.3.1	Ni@3-APP@WC microparticles	80
2.4	<i>Cobalt-coated particles</i>	81
2.4.1	Co@3-APP@WC microparticles	81
2.4.2	Co@Pdop@WC microparticles	81
3.	METAL MATRIX COMPOSITES FABRICATED BY POWDER METALLURGY	83
3.1	<i>Cu composites reinforced with Cu@Al₂O₃ nanoparticles</i>	83
3.2	<i>Cu composites reinforced with Cu@WC microparticles</i>	84
4.	SILVER STRUCTURES BY SOFT LITHOGRAPHY	85
4.1	<i>Microcontact printed 3-mercaptopropyltriethoxysilane</i>	85
4.2	<i>Ag structures on printed 3-mercaptopropyltriethoxysilane patterns</i>	86
4.3	<i>PMMA resist structures by Capillary Force Lithography</i>	89
4.4	<i>Silver structures from patterned PMMA resist</i>	93
V	CONCLUSIONS AND OUTLOOK	97
VI	REFERENCES	102

List of abbreviations

γ	Surface tension
η	Viscosity of a fluid
μCP	Microcontact printing
ρ	Density of a liquid
3-APP	3-aminopropylphosphonic acid
AFM	Atomic force microscopy
APTES	Aminopropyltriethoxysilane
CFL	Capillary force lithography
DiT	3,5-diiodotyrosine
DMAB	Dimethylamine borane
EDTA	Ethylenediaminetetraacetic acid
EDX	Energy-dispersive X-ray spectroscopy
EP	Electroless plating
FTIR	Fourier transform infrared spectroscopy
h	Height of the capillary rise of a fluid through a narrow channel
ITO	Indium tin oxide
MMC	Metal matrix composite
MPTES	3-mercaptopropyltriethoxysilane
NPs	Nanoparticles
PAMAM	Polyamide-amine
PDMS	Poly(dimethylsiloxane)
Pdop	Polydopamine
PFPE	Perfluoropolyether
PTFE	Polytetrafluoroethylene
PTMS	n-propyltrimethoxysilane
R_a	Roughness (arithmetic average)
R_q	Roughness (root mean square)

SAM	Self-assembled monolayer
SEM	Scanning electron microscopy
TEM	Transmission electron microscopy
TGA	Thermogravimetric analysis
Tris-HCl	Tris(hydroxymethyl)aminomethane-HCl
XRD	X-ray diffraction

I Motivation

Electroless plating is a metal deposition technique widely used in the coating industry [1–3]. It is the method of choice to plate substrates with complex geometries and nonconductive surfaces, such as polymers and ceramics, since it is based on a chemical reduction in solution rather than on an external electrical energy source like the electroplating method [4]. Among others, examples of well-established applications are the electroless deposition of decorative metal coatings such as gold and silver, wear and corrosion resistant nickel coatings, particularly to coat drive shafts, rotors, and bathroom fixtures, as well as the electroless deposition of copper in electronic devices as diffusion barriers and conductive circuit elements [1–3]. Compared to physical vapor deposition techniques, electroless plating offers much simpler and less expensive equipment, in particular the absence of high temperatures, vacuum and cooling systems. On the other hand, it is a wet chemical method and hence not suitable for all applications [5].

In the academic research, electroless plating is extensively used thanks to its low cost, simple equipment and versatility that allow rapid prototyping. Two common applications are the coating of small particles and the selective plating of flat surfaces [6–12]. Electroless plating is the only practical way to uniformly coat small particles. Physical methods such as vapor deposition might also be used, but it is inadequate for particles in the submicron and nanometer range mainly because they lead to inhomogeneous coatings [13,14]. Metal coated ceramic particles are of enormous interest in many scientific fields, e.g. fluorescent diagnostics in biochemistry, catalysis, and fabrication of photonic crystals [15]. Metal coated ceramic nanoparticles and microparticles are also gaining attention as potential candidates in the fabrication of higher quality metal matrix composites [16–18], which is one of the applications addressed by this work. Metal coated ceramic particles are easier to integrate in metal matrix composites, avoiding aggregation caused by the low wettability of the particles by the matrix metal, and are potentially shielded from oxidation and undesired chemical reactions that take place at the interface between the particles and the metal matrix [18]. The use of electroless plating to selectively fabricate metallic patterns on flat surfaces is also extensively used in scientific research, especially in microelectronics, opto-electronics, and plasmonics, as well as in the electronics and microelectronics industries, especially for the fabrication of circuit lines in printed circuits and electronic packaging [1].

Electroless plating is an autocatalytic process, meaning that the deposited metal atoms catalyze the deposition of further metal. In order to achieve the first stable metal seeds on a surface, the latter has to be functionalized. Without this functionalization the metal ions in the electroless plating bath are not reduced or are simply reduced to metal nanoparticles in solution [19–22]. The traditional activation step for nonconductive surfaces is performed by immersion of the substrate in palladium based solutions, which is very time-consuming and extremely expensive. In particular for nanoparticles, previous work showed that at least 10^{15} Pd atoms/cm² are required for a uniform activation of a surface, meaning that in the case of nanoparticles with a surface area of about 100 m²/g are necessary 6.4 g of palladium for each gram of substrate. Assuming a price of about 150 €/g (laboratory scale) for palladium nanoparticles and palladium precursors used for surface activation, it results that the activation of 1 g of nanoparticles costs around 1000 € [23,24]. Such costs are suboptimal considering the typical production scale, and therefore alternative functionalization methods are desired. In this work, new organic-based functionalization methods based on (3-mercaptopropyl)triethoxysilane to functionalize oxide particles, 3-aminopropylphosphonic acid to activate carbide particles and a substrate-independent method based on the bioinspired polydopamine are developed and investigated in detail, together with the respective electroless plating baths, which often have to be specifically tailored regarding the different reactivity of the different molecules and substrates. Furthermore, in the fabrication of metallic patterns on substrates by electroless plating, new, simple, and cost-effective activation and metal deposition processes are desired. In this work, two new methods are presented, one based on the printing of (3-mercaptopropyl)triethoxysilane by microcontact printing, the other based on the capillary force lithography of polymethylmethacrylate.

This thesis describes the fabrication by electroless plating of metal coated ceramic micro- and nanoparticles as well as the manufacture of silver patterns on glass substrates, as shown schematically in figure 1, focusing on the use of new, simple and cost-effective functionalization methods as alternative to the expensive state of the art functionalization method based on Pd catalysts. Overall, five new processes are investigated and presented, showing that the combination of organic-based functionalization methods and of the electroless plating technique lead to simple, reliable and cost-effective approaches for the metal deposition, especially on nano- and microparticles.

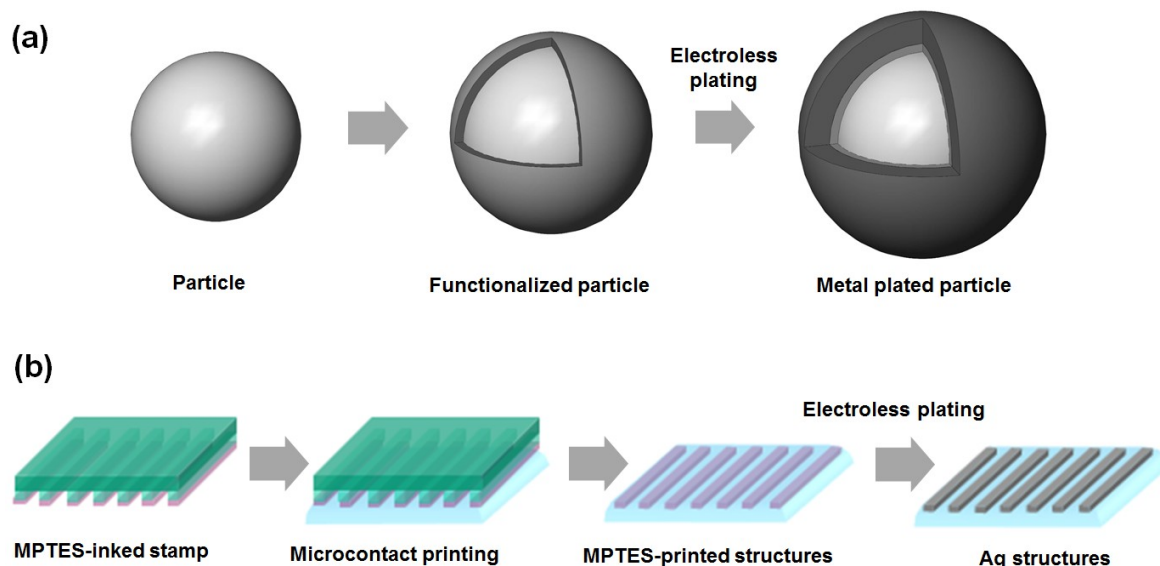


Fig. 1: Schematic illustration of the two processes used in this work. (a) Chemical functionalization of ceramic micro- and nanoparticles followed by electroless deposition for the fabrication of metal plated particles. (b) Selective functionalization of glass substrates by soft lithography followed by electroless plating for the development of silver structures.

In particular, the objectives of this work can be summarized in the following points:

- Develop and investigate scalable functionalization process for oxide nanoparticles (Al_2O_3 and SiO_2) based on (3-mercaptopropyl)triethoxysilane. The thiol group has a high affinity towards metal ions and can therefore promote the electroless deposition process, while the ethoxy groups can react with the hydroxyl groups of a glass substrate, promoting the adhesion of the molecule.
- Establish a functionalization process for the more chemically inert WC particles based on 3-aminopropylphosphonic acid. The phosphonic acid group binds strongly with metals (tungsten in this case), while the amino group has a high affinity towards metal ions and can therefore promote the subsequent electroless plating process
- Develop a substrate-independent functionalization method based on polydopamine and systematically investigate the different coating thickness against polymerization time for particles of different size and material. The alkylamine and catechol functionalities of polydopamine are used to promote particle electroless plating.
- Fabricate Cu, Ni and Co plated particles by electroless deposition, developing specifically tailored plating baths according to the different particle functionalization.

- Investigate the use of the copper plated particles in the fabrication of copper matrix composites fabricated by powder metallurgy.
- Fabricate silver patterns on glass substrates by microcontact printing of (3-mercaptopropyl)triethoxysilane and electroless plating.
- Develop a substrate independent method to fabricate silver patterns on surfaces based on the use of soft lithography and PMMA, followed by electroless deposition.

II Theoretical Part

1. Electroless plating

Electroless plating (EP) is a chemical non-galvanic method used to deposit a metal layer on a substrate. The metal deposition takes place by the controlled reduction of metal ions in solution without the use of external electrical energy and the need for an electrical contact between substrate and energy source, as shown in figure 2. EP is a very versatile technique since electrically conductive as well as nonconductive substrates, such as polymers and ceramics, can be plated with a metal layer [4,25,26]. Moreover, EP is the method of choice for the metal deposition on substrates with complex geometries and on nanoscaled particles [4,25,26]. EP is extensively used in the microelectronics industry, especially for the fabrication of circuit lines in printed circuits and electronic packaging, and in the plating industry for the deposition of decorative coatings as well as wear and corrosion resistant coatings [27,28]. Besides its ability to plate nonconductive and complex-shaped objects, EP is inexpensive since only basic equipment is needed, has a fast deposition rate, is carried out at low temperatures and is suitable for mass production and scaling-up [29,30]. It is also possible to plate alloys and to finely control their composition, hence allowing the tuning of the metal coatings properties, for example electrical conductivity, wear resistance and color [31,32].

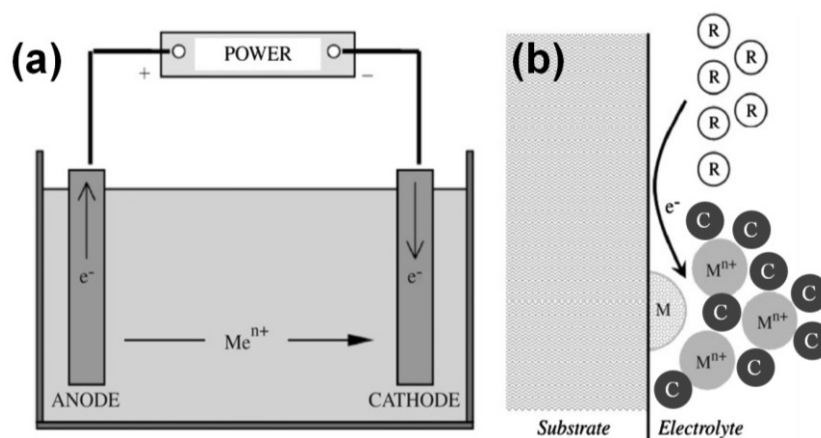


Fig. 2: schematic illustrations of the (a) electroplating process and (b) electroless plating process, where a reducing agent (R) is used instead of an external power source to reduce the complexed (C) metal ions (M^{n+}). Modified after Sudagar *et al.* [2].

A broad range of metals and alloys, among them copper, silver, gold, nickel, cobalt, iron, tin, nickel alloy, and cobalt alloy has been plated on different substrates [4,33]. Electroless plated coatings show a grainy morphology and homogeneous thicknesses regardless of the substrate shape, as shown in figure 3 [2]. This is a great advantage over electroplating, in which the thickness of the plated metal layer depends on the electron density of the substrate, with the consequence that sharp corners and hedges are plated with a thicker metal coating than flat areas. The first deposited metal seeds act as catalysts for the subsequent metal deposition, leading to a continuous autocatalytic reaction until the reactant is consumed [4]. A typical electroless plating solution contains the following features: a source of metal ions, a reducing agent, one or more complexing agents, and one or more stabilizers or inhibitors [34,35].

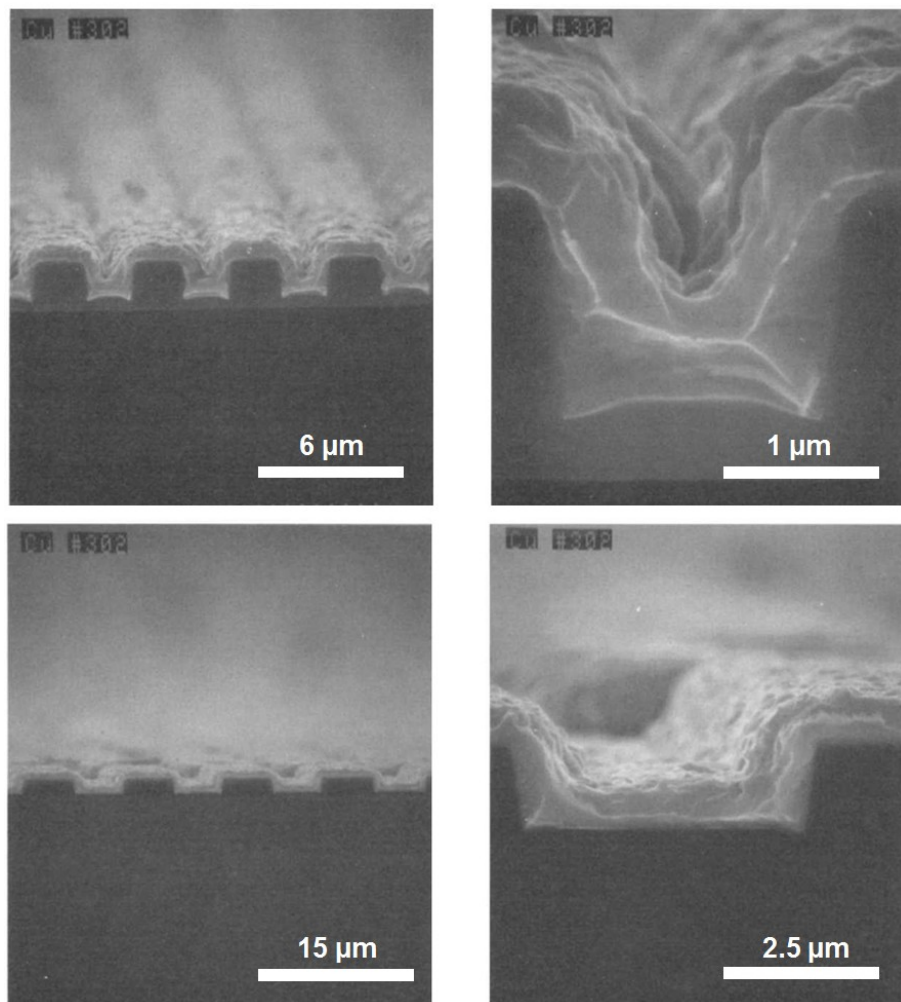


Fig. 3: SEM cross sections of microstructures plated with a layer of copper approximately $0.75 \mu\text{m}$ thick (in white) by electroless plating, showing the typical grainy morphology and constant thickness. Modified after Dubin *et al.* [28].

In general, the source of metal ions can be any salts such as chlorides, sulfates and cyanides. The choice of one over the other depends on the desired final properties of the deposited metal layer, the stability of the solution as well as safety and environmental aspects [4]. The nature of the reducing agent depends on the plating conditions, the redox potential of the metal to be plated and on the desired properties of the metal or alloy coating, e.g. reducing agents containing boron or phosphorus lead to the inclusion of these elements in the plated metal layer, greatly affecting its properties such as corrosion resistance, crystallinity and hardness [4]. Electroless plating of pure metals is possible using reducing agents which do not contain boron or phosphorus, such as hydrazine, formaldehyde and glucose [35]. The choice of a suitable complexing agent is more difficult. The essential functions of complexing agents are the reduction of the concentration of free aqueous metal ions and the prevention of hydroxides and salts precipitation [34]. Additionally, complexing agents affect the properties of the plated metal and, most importantly, they influence the metal ions reduction rate and hence the metal deposition rate. The majority of complexing agents used in electroless metal plating are organic acids or their salts, e.g. ethylenediaminetetraacetic acid (EDTA) and tartrate, with some exceptions including ligands such as NH_4^+ and CN^- [4]. Stabilizers are used to ensure the stability of the plating bath over a longer period of time by preventing the decomposition of the solution. The use of stabilizers hinders the spontaneous reduction of the metal ions until an activated substrate is immersed into the electroless plating solution. The concentration of stabilizers is very important because it also determines the rate of deposition, to the point that if the concentration is too high it may completely inhibit the plating process [4]. The most common features of the electroless plating baths for the metals used in this work (copper, silver, nickel and cobalt) are described in the next sections.

Prior to the plating process, the substrates are generally pretreated to promote a good adhesion of the metal layer and to avoid pore formation [36]. The pretreatment process usually includes cleaning and activation. The cleaning step is used to remove dirt, oils and other undesired chemicals that may be on the substrate surface, while activation refers to the process that is required to make a surface catalytic, i.e. able to initiate the autocatalytic electroless metal deposition process. Therefore, activation is a crucial step when plating nonconductive substrates such as plastics and ceramics, but also some metal substrates are not catalytic when immersed in the electroless plating solution, such as steel and aluminum, and therefore need to be activated [37]. Given its central importance in the electroless plating, the pretreatment process is described in details in chapter I.1.1.

1.1 Pretreatment

The pretreatment process is used to clean and activate the substrate to be plated by electroless deposition. The cleaning step is carried out to remove contaminants from the substrate surface. Even though a common approach does not exist, the most general way includes degreasing with solvents such as acetone and ethanol, followed by alkaline soak cleaning. Soak cleaners contain a combination of surfactants and alkaline sodium compounds like hydroxide, carbonate and phosphates. The choice of a soak cleaner is based on the substrate material and on the nature of the contaminants [38]. After the cleaning step, the activation of the substrate is carried out in order to make the surface able to generate stable metal seeds and thus, able to start the reduction of the metal ions when immersed in the electroless plating solution. This is necessary for the autocatalytic plating process to start on the substrate surface, otherwise the metal ions in the electroless plating solution are not reduced or are simply reduced to metal nanoparticles in solution without conformal metal coating [19–22]. The activation step must be carried out for nonconductive surfaces like plastics and ceramics as well as for metals that are not already catalytic when immersed in the electroless plating solution. The traditional activation step for nonconductive surfaces is performed by immersion of the substrate in tin-based and palladium-based solutions [39,40]. Palladium catalyzes the subsequent metal deposition, ensuring a better initiation of the EP process. This method has the main advantage of being substrate-independent, but is also very time consuming and extremely expensive, especially for the activation of high surface area materials like nanoparticles [41,42]. A central aspect in this thesis is the development of alternative activation treatments for electroless plating to overcome the drawbacks of the palladium based activation, especially the high cost. Three organic-based, cost-effective and simple activation methods are presented.

1.2 Silver electroless plating

The electroless deposition of silver is a well-known example of the EP process and was introduced in the 1830 by Drayton and later improved by Liebig [43–45]. Electroless deposition of silver was commonly used for the fabrication of mirrors and is still nowadays

widely employed for decorative coating of nonconductive objects and as undercoating to promote adhesion of a subsequent coated metal layer, in particular copper and gold [43]. Silver electroless deposition is attractive because silver is relatively easy to plate, shows unique physical properties in the nanometer regime, is a noble metal and having the highest electrical conductivity can be used in the fabrication of electrodes [28,43].

Generally silver nitrate is used as the silver source while ammonia is used as complexing agent [43]. Since the standard reduction potential of silver is very high (+ 0.8 V) compared to other metals, many compounds can be used as reducing agent since the electromotive force will always be positive and great, i.e. the difference in voltage between the silver reduction potential and the reducing agent oxidation potential will always be high [43]. Some frequently used and commercially available reducing agents are potassium sodium tartrate (also known as Rochelle salt), glucose, formaldehyde, dimethylamine borane (DMAB) and tartaric acid [46,47]. The high standard reduction potential of silver is however a problem regarding the bath stability: the plating bath decomposes as soon as the electroless deposition reaction starts, becoming dirty and muddy [4]. To overcome this bath instability problem it is necessary to accurately control the pH and to use a specific amount of stabilizers. Typical stabilizers used to improve the stability of the silver electroless plating bath are 3,5-diiodotyrosine (DiT), cysteine and metal ions [43].

1.3 Copper electroless plating

Electroless copper plating is widely used in the electronics and microelectronics industries, e.g. for the fabrication of printed circuit boards [1]. Copper electroless deposition is preferred over silver plating in the electronics industry because of its higher stability, much lower costs and comparable conductivity of the plated metal patterns. Normally, copper sulfate is used as copper source and EDTA is used as complexing agent [1]. Copper plating baths are more stable than silver plating baths given that the standard reduction potential of copper is lower than for silver, + 0.34 V against + 0.8 V, but still high enough, so that even mild reducing agents can be employed. Typically used reducing agents are hydrazine, formaldehyde, DMAB and sodium hypophosphite [1]. Occasionally, stabilizers such as thiourea, 2-mercaptobenzothiazole, diethyldithiocarbamate and vanadium pentoxide may be used [1].

1.4 Nickel electroless plating

The EP of nickel from an aqueous solution was already noted by Wurtz in 1844 and Roux in 1911, but usually the work published in 1946 by Brenner and Riddell is considered the beginning of the nickel electroless plating development [2,19]. The authors observed that the use of the additive sodium hypophosphite in the nickel electroplating process led to cathode efficiencies of more than 100 %, meaning that also a chemical reduction was taking place in the plating bath. In the following year, Brenner and Riddell systematically investigated and further improved the process [20]. Nickel electroless plating is almost exclusively employed for the deposition of functional coatings, as opposed to silver plating which is also extensively used in decorative coatings. In particular, electroless plated nickel is used for its wear and corrosion resistance, lubricity, hardness and magnetic properties [2].

Typical bath constituents are nickel sulfate or nickel chloride as metal source, EDTA and sodium citrate as complexing agents and thiourea or heavy metal salts as stabilizers. Nickel plating baths are relatively stable since the standard reduction potential of nickel is -0.25 V, and mild to strong reducing agents are commonly used, in particular sodium hypophosphite, hydrazine and sodium borohydride [2]. Because of the constituents of the nickel plating bath, electroless deposited nickel is not a pure metal but includes other elements derived from the reducing agent, usually boron or phosphorus. Depending on the content of these two elements, the nickel coating shows different features, which can also be finely tuned. In example, electroless plated nickel with a high phosphorus content (> 10 %) has a very high corrosion resistance and is non-magnetic, while plated nickel with low phosphorus content (1 – 4 %) shows a high wear resistance [2].

1.5 Cobalt electroless plating

The EP of cobalt was introduced by Brenner and Riddell in 1947, shortly after the development of nickel EP by the same authors in 1946 [19,20]. Cobalt EP has several applications, such as the fabrication of corrosion, wear and oxidation resistance coatings, as well as ferromagnetic functional coatings [3]. Typical bath constituents are similar to those used with nickel: cobalt sulfate or cobalt chloride as metal source, EDTA and sodium citrate as complexing agents, imidazole or heavy metal salts as stabilizers. The standard reduction

potential of cobalt is -0.28 V, similar to nickel and hence the same reducing agents are typically used, i.e. sodium hypophosphite, hydrazine and sodium borohydride [3].

2. Metal coating of particles

Metal coated ceramic particles have been traditionally investigated for their optical properties and find a plethora of applications in the fields of photonics, biochemistry, catalysis and electronics [15]. Metal coated microparticles and nanoparticles are also gaining attention in recent years as potential candidates in the fabrication of improved metal matrix composites (MMCs) [16–18]. The main problem in the fabrication of MMC is the ceramic particle aggregation caused by the low wettability of the particles by the metal due to the significant difference in surface energy and density between the two materials. This in turn causes inhomogeneous particle distributions and porosity, resulting in MMCs with inadequate mechanical properties [48,49]. Another issue during the production of MMCs are chemical reactions that take place at the interface between the particles and the metal matrix, resulting in the formation of undesired products, such as the formation of aluminum carbide at the interface between an aluminum matrix and silicon carbide particles. Furthermore, oxidation of the ceramic particles if the composite material is manufactured at high temperature may be a problem, e.g. the oxidation of tungsten carbide to tungsten oxide [50]. An elegant and simple solution for all these drawbacks is to coat the ceramic particles with a thin metal film prior to the MMC fabrication process, hence minimizing the surface energy difference between the metal matrix and the particles, and furthermore, acting as a barrier layer [18]. This promotes a homogeneous particle distribution in the metal matrix composite and prevents undesired reactions at the interface with the metal and particle oxidation.

Metal coated ceramic particles can be produced with many techniques, including ball milling [51], sputtering [52], metal vapor deposition [53], seed growth [54], electroless plating and other solution-based processes [7,8,55–59]. While physical methods like vapor deposition and sputtering show cost-intensive scaling up and inhomogeneous coatings, electroless plating is gaining interest as metal coating method because of its simplicity, versatility, conformal coating, high potential for mass production and high deposition rate. However, prior to the electroless plating process, the ceramic particles must be functionalized in order to selectively promote the metal deposition of their surface. This is discussed in the next section.

2.1 Functionalization of particles

In order to be electroless plated, nonconductive particles have to be activated as in the case of macroscopic objects. The traditional activation step for nonconductive surfaces is performed by immersion of the substrate in tin-based and palladium-based solutions [39,40]. This method is substrate-independent, but on the other hand is very time-consuming and extremely expensive, in particular for the activation of materials with a very high surface like nanoparticles [41,42]. Previous work showed that at least 10^{15} Pd atoms/cm² are required for a uniform activation of a surface [23,24]. In the case of nanoparticles with a surface area of about 100 m²/g, 6.4 g of palladium for each gram of substrate are necessary as previously discussed, assuming a price of about 150 €/g for palladium nanoparticles and palladium precursors, resulting in costs of about 1000 € for the activation of 1 g of nanoparticles. Such costs are very high in the field of research and development and surely a disadvantage in the industrial scale production. Hence, new, cost-effective and environmentally friendly functionalization processes for the electroless plating are highly desired.

Over the last few years, the use of polydopamine has been investigated as a new, substrate-independent functionalization process. This method, described in the next section along with the relevant literature, is very promising and is extensively investigated and applied to nanoparticle functionalization in this work. Alongside with polydopamine functionalization, in this work other two organic-based functionalization methods are investigated, one using 3-mercaptopropyltriethoxysilane (MPTES) to functionalize oxides and one using 3-aminopropylphosphonic acid (3-APP) to functionalize carbides. These methods were specifically designed as simple and cost-effective functionalization processes for particles, as alternatives to the standard palladium based activation, but can be used also for the functionalization of macroscopic objects.

2.1.1 Functionalization with polydopamine

Polydopamine is a bioinspired polymer developed for multifunctional coatings by Lee *et al.* in 2007 by drawing inspiration from the adhesive proteins found in mussels (fig. 4.a) [60]. They developed a facile approach to generate surface-adherent polydopamine coatings on different

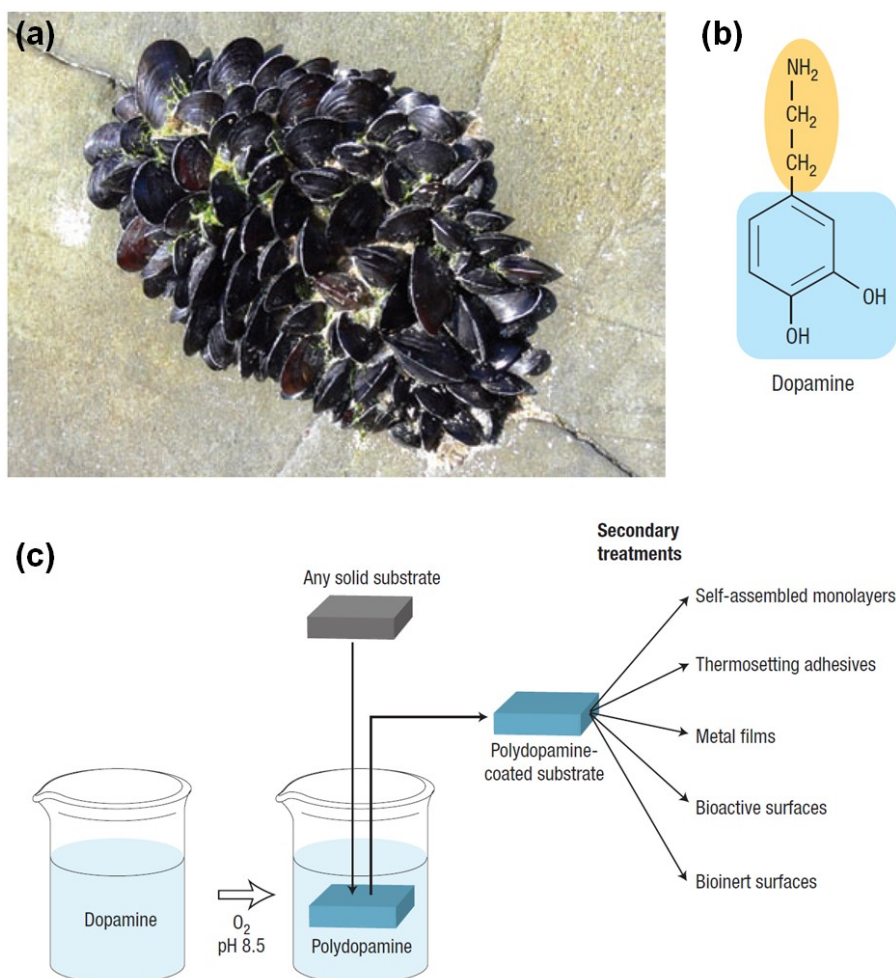


Fig. 4: Polydopamine is a bioinspired polymer with properties similar to the adhesive proteins found in mussels. (a) Mussels in their natural environment. (b) The structure of dopamine, consisting of a catechol (in blue) and an alkylamine (in yellow) functional groups. (c) Schematic illustration of the dopamine polymerization process and of the several possible secondary reactions. Modified after Waite *et al.* [61].

objects by simply immersing a substrate in an aqueous solution of dopamine buffered at pH 8.5. Many oxides, noble metals, polymers, and ceramics were successfully coated with a 50 nm thick polydopamine layer by Lee *et al.* showing the substrate-independence of this method. Thanks to the alkylamine and catechol functionalities of dopamine (fig. 4.b), polydopamine can be used to carry out a wide range of secondary reactions, such as grafting of organic molecules for the fabrication of bioactive or bioinert surfaces (fig. 4.c) [61].

The polydopamine structure and the dopamine polymerization process are still not well understood. Lee *et al.* propose a mechanism that involves the oxidation of the catechols and a subsequent melanin-like polymerization as shown in figure 5.a [60]. Analogous mechanisms were also proposed by others [62–64]. Conversely, Dreyer *et al.* showed that polydopamine may not be made of covalently bonded units, but of monomers which interact with each other

through non-covalent interactions like hydrogen bonding, π -stacking and charge transfer, as shown in figure 5.b [65].

Thanks to its versatility, the use of polydopamine has attracted considerable attention in a variety of research fields and applications, such as the fabrication of separators and anodes for Li-Ion batteries [66–69], the fabrication of capsules for drug delivery [70–72], antibacterial materials [73–75], surface wetting control [76,77], tissue engineering [78,79] and functionalization of carbon nanotubes [80,81]. Despite the growing interest in polydopamine and catecholic chemistry in general, only very few works deal with the polydopamine coating of particles. Zhou *et al.* and Si *et al.* successfully synthesized polydopamine coated Fe_3O_4 nanoparticles [82,83], while Li *et al.* fabricated polydopamine coated Fe_3O_4 particles decorated with silver [84].

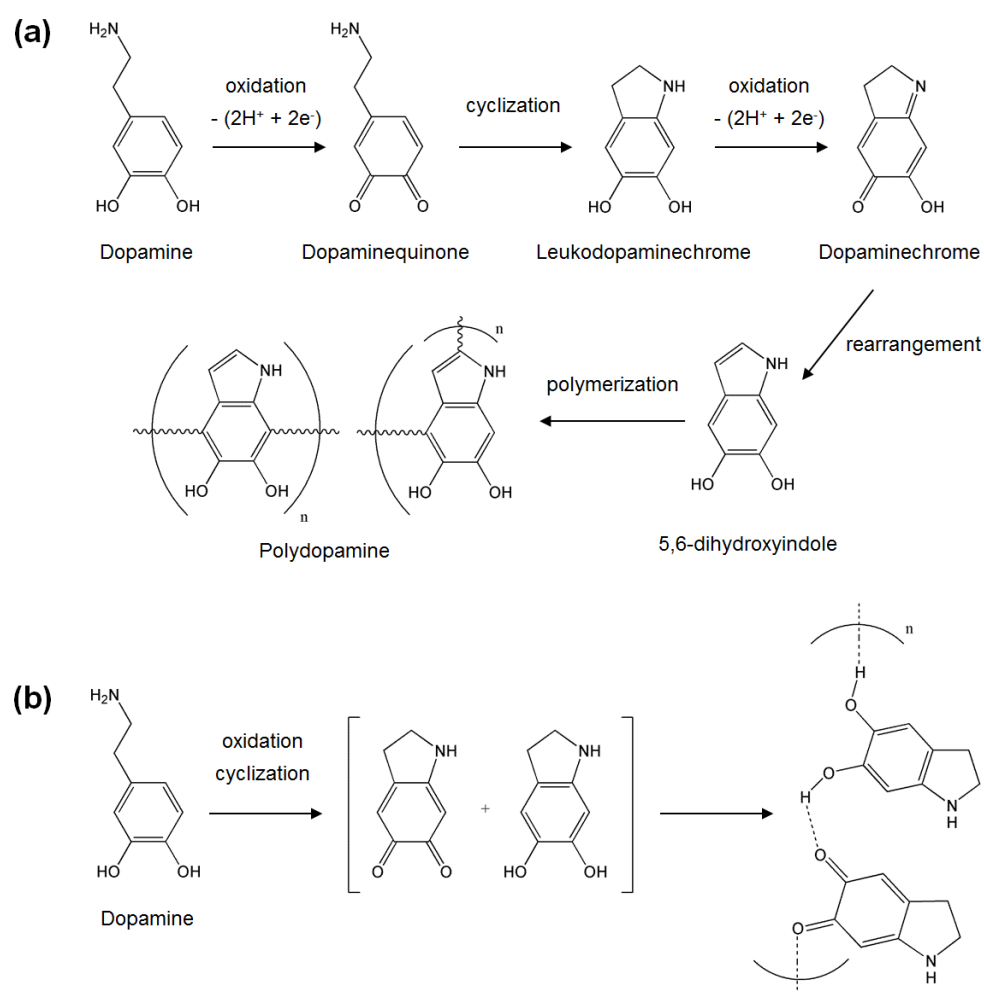


Fig. 5: (a) Possible self-polymerization mechanism of dopamine and hypothetical polydopamine structure (modified after [60,62,63]). (b) Proposed polymerization mechanism of dopamine and hypothetical polydopamine structure by Dreyer *et al.* [65].

Also Wang *et al.* explored the use of polydopamine for the fabrication of metal coated particles, but only the plating with silver of 25 μm silica spheres is investigated [85]. In this thesis, the use of polydopamine for particle functionalization is further investigated by systematically analyzing the polydopamine layers regarding its thickness and morphology on different substrates, such as oxides and carbides.

2.2 Metal coating of particles by electroless plating

There are several examples in the literature of metal coating of particles by electroless plating (listed in table 1). In the majority of works the standard tin-based and palladium-based activation process is used [6–9]. Only a small number of works explore the use of organic molecules, not as a promoter for the plating process, but rather only to help the adhesion of palladium ions or palladium nanoparticles, which are the actual catalyst [86–88]. The work by Zou *et al.* is interesting, reporting on SiC nanoparticles with a size of about 20 nm that are uniformly plated with nickel (fig. 6) [7]. Particularly interesting is also the work by Leon *et al.*, in which both the nickel coating by EP of SiC particles and the production of a MMC are investigated (fig. 6) [6]. In general, the most plated metal is nickel, given its many applications and useful properties, while the most used ceramic particles are carbides and oxides, and only the tin- and palladium-based activation process is used, sometimes with the help of organic molecules to promote adhesion.

Table 1: List of selected publications investigating the metal coating of particles by electroless plating.

Reinforcing particles	Coated metal	Ref.
SiC (78 μm , 49 μm and 18 μm)	Ni	[6]
Al ₂ O ₃ (74 μm , 46 μm and 17 μm)	Ni	[6]
SiC (20 nm)	Ni	[7]
Al ₂ O ₃ /SiO ₂ mixture (100 μm)	Cu	[8]
Al ₂ O ₃ (5 μm)	Cu	[9]
SiO ₂ (240 nm)	Ni	[86]
SiO ₂ (227 nm)	Au	[87]
Mica powder (30-120 μm)	Ni	[88]

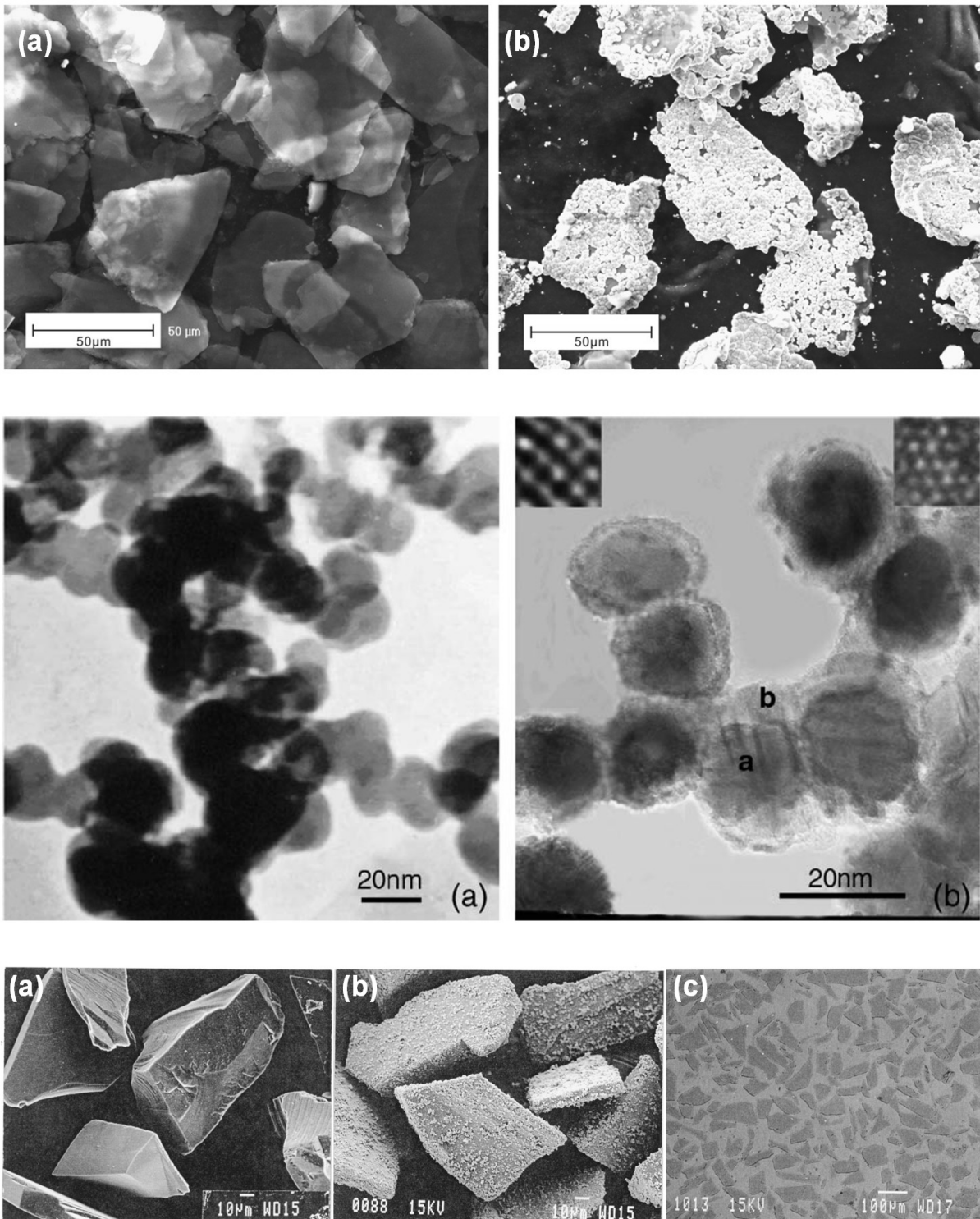


Fig. 6: Examples of ceramic particles coated with a metal layer by electroless plating. Top: SEM images of (a) uncoated mica powder and (b) nickel coated mica powder, modified after Dai *et al.* [88]. Middle: TEM images of (a) SiC nanoparticles and (b) nickel coated SiC nanoparticles, modified after Zou *et al.* [7]. Bottom: SEM images of (a) uncoated SiC powder, (b) nickel coated SiC powder and (c) SiC/Al composite fabricated using the coated powder from (b), modified after Leon *et al.* [6].

3. Metal matrix composites

Metal matrix composites are materials based on a metal or metal alloy matrix incorporating ceramic particles, commonly nitrides, carbides and oxides. As a result of the combination of the toughness and ductility of the metal matrix with the stiffness and specific strength of the ceramic particles, the MMCs show many significant improvements over monolithic metals like higher strength and wear resistance, better high temperature properties and higher chemical resistance [89,90]. In particular, nanoparticle reinforced MMCs have superior mechanical properties as compared with microparticles reinforced MMCs having a similar volume content of particles [18]. This is due to the grain boundary strengthening (or Hall-Petch effect): grain boundaries impede the movement of dislocations and therefore, metals with smaller grains show better mechanical properties. Incorporating nanoparticles in a metal is a way of effectively reducing the size of the grains, however the particle volume content must not exceed a limit value of around 4 %, otherwise the strengthening effect level off because of the particle agglomeration [18].

Metal matrix composites can be classified in ex-situ and in-situ: in the former case the reinforcing particles are prepared separately prior to the MMC fabrication, while in the latter case the reinforcing particles are formed in situ by exothermal reactions between elements and compounds [18]. Ex-situ metal matrix composites are the most common MMCs and are the ones addressed by this work. Ex-situ metal matrix composites are fabricated with a variety of techniques which can be grouped in two classes according to the physical state of the metal during processing: solid state and liquid state methods [91]. Solid state methods involve the blending of a metal powder with a ceramic powder, followed by the pressing and consolidation phases. The material can then be worked, e.g. by extrusion, to produce the final composite component, as shown in figure 7. Liquid state methods are based on the incorporation of ceramic particles in a molten metal matrix, followed by mixing and casting [92]. Many variations exist, such as the widely used melt infiltration technique, in which the molten metal is infiltrated in a preformed ceramic body [48]. In both the liquid and solid state fabrication processes, the main drawbacks in the fabrication of MMC is the ceramic particle aggregation caused by the low wettability of the particles by the metal, the oxidation of the ceramic particles if the composite material is manufactured at high temperature and undesired chemical reactions that take place at the interface between the particles and the metal, as discussed in chapter II.2. Moreover, the MMC fabrication processes are rather complex and

time-consuming and therefore a faster integration of the reinforcing particles, i.e. a shorter processing time, is desired. An elegant and simple solution for these problems is to coat the ceramic particles with a thin metal film prior to the MMC fabrication process [18]. This assures a faster and homogeneous particle distribution in the metal matrix composite and the prevention of particle oxidation and undesired reactions at the interface with the metal. Thanks to their superior mechanical and physical properties, MMCs are used in many applications in the automotive, aerospace, electronics and coating industries [16–18,89,90].

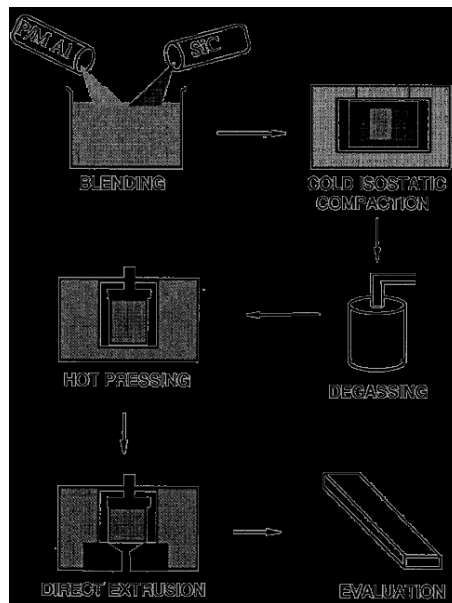


Fig. 7: The Alcoa process, a solid state method for the fabrication of ex-situ metal matrix composites (MMCs), based on the mixing of a metal powder with a ceramic powder, followed by compaction, degassing, pressing and extrusion [89].

3.1 Metal matrix composites incorporating metal plated particles

The idea of coating ceramic particles prior to the incorporation in the metal matrix during the fabrication of composite materials was developed in the 90s of the last century, mainly using carbides as ceramic particles, nickel as particle coating and aluminum as metal matrix [89,93]. The most interesting and influencing literature is reported here, while for a comprehensive overview the reader is referred to Drew *et al.* [94]. One of the first articles was published by Chung *et al.* in 1996, in which a vacuum infiltration method was used to fabricate aluminum composites containing 50 vol% of nickel coated SiC particles. The authors reported nickel

macrosegregation as a major problem, explained with the dissolution of the nickel coating during the melt infiltration [95].

In 1997 Yih *et al.* successfully fabricated copper matrix composites using a powder metallurgy method [96]. The use of uncoated and copper coated reinforcing particles made of silicon carbide, molybdenum and titanium diboride was investigated. All the composite materials fabricated using copper coated reinforcing particles show superior properties as compared with the composites fabricated with uncoated particles, in particular higher hardness, higher thermal conductivity, higher electrical conductivity and lower porosity. Moreover, composites with coated reinforcing particles show a stronger bond and a cleaner interface between the particles and the copper matrix. The optimal reinforcing particles content was 33 vol% for silicon carbide, 60 vol% for molybdenum and 42 vol% for titanium diboride. In 2000 Drew *et al.* fabricated and systematically investigated aluminum matrix composites using nickel plated SiC and alumina particles [6]. From the same authors is also the influential work from 2002 about the influence of the nickel coatings on the wettability of aluminum on ceramic reinforcing particles [97]. More recently, Ramesh *et al.* fabricated aluminum matrix composites incorporating nickel plated Si_3N_4 particles using the stir cast method, leading to a material with superior hardness [98,99]. Among other applications, copper composites reinforced with copper coated particles can be potentially used as reinforced electrodes for resistance spot welding (fig. 8.a,b) and reinforced overhead wire and sliding contact for trains and other vehicles (fig. 8.c).

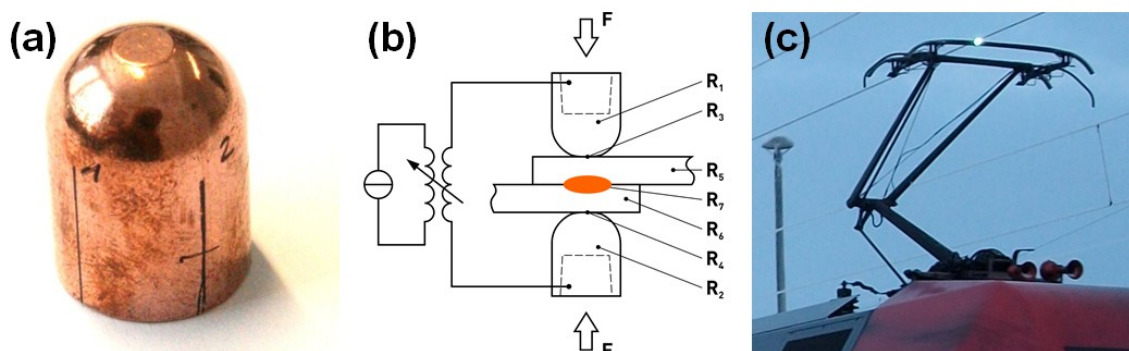


Fig. 8: (a) Picture of a $\text{Cu}/\text{Cu}@\text{Al}_2\text{O}_3$ composite electrode for resistance spot welding, fabricated by powder metallurgy using Cu powder and 1 wt% of Cu plated Al_2O_3 nanoparticles. (b) The resistance spot welding principle. (c) Picture of an overhead wire and of the sliding contact of a train, both potential applications of composite reinforced electrodes. Courtesy of C. Großmann, J. Zschetsche, U. Füssel.

4. Soft lithography

Soft lithography is a term used to describe a broad set of unconventional micro- and nanofabrication methods based on printing and molding using patterned elastomeric stamps, as opposed to rigid photomasks used in conventional photolithography [100]. The most common techniques include replica moulding, microcontact printing (μ CP), micromoulding in capillaries, and microtransfer moulding, all shown in figure 9.

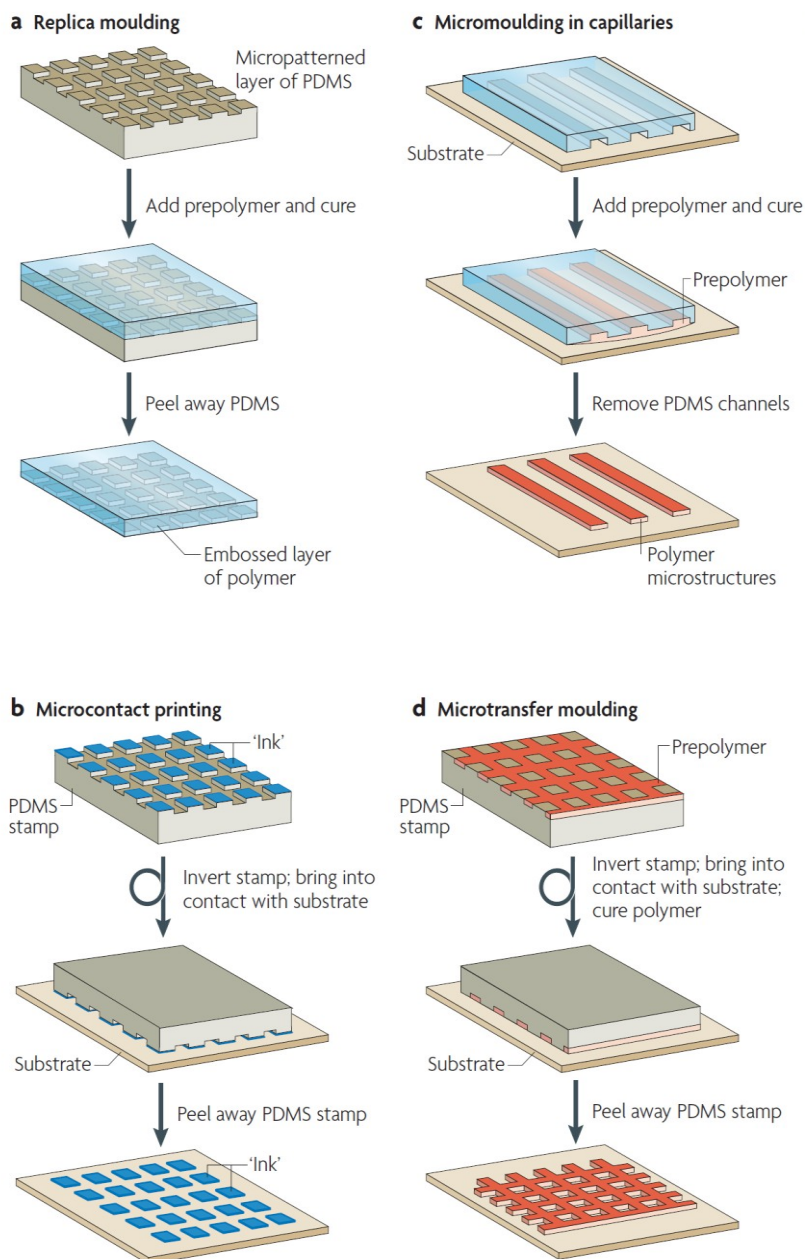


Fig. 9: The main fabrication methods of the soft lithography technique. (a) Replica moulding, (b) microcontact printing, (c) micromoulding in capillaries and (d) microtransfer moulding [101].

Soft lithography is a very simple, fast and cost-effective alternative to photolithography, which is attracting considerable attention in applications in which uniformity and alignment of the patterns are not a major concern, such as in the fabrication of sensors and microelectrodes [100]. Moreover, soft lithography allows the patterning of nonplanar surfaces and of functional groups, can be used with liquid materials, allows the fabrication of three-dimensional structures and can be transferred to a roll-to-roll process [100].

The key element in soft lithography is the patterned elastomeric stamp, which is usually made of poly(dimethylsiloxane) (PDMS) by cast molding, but also other materials such as polyimides, polyurethanes and polytetrafluoroethylene (PTFE) are used for specific applications [102]. The main advantages of PDMS are its chemical and thermal stability, flexibility, durability and nontoxicity. Moreover, it is commercially available and inexpensive [103,104]. At room temperature, PDMS is available as a liquid prepolymer with a glass transition temperature of approximately $-120\text{ }^{\circ}\text{C}$ and a melting point of $-50\text{ }^{\circ}\text{C}$ [105]. To fabricate a patterned PDMS stamp the prepolymer is blended with a curing agent, poured on a non-adhesive micropatterned master (usually made of silicon), and cured in order to crosslink the polymer, as shown below in figure 10.

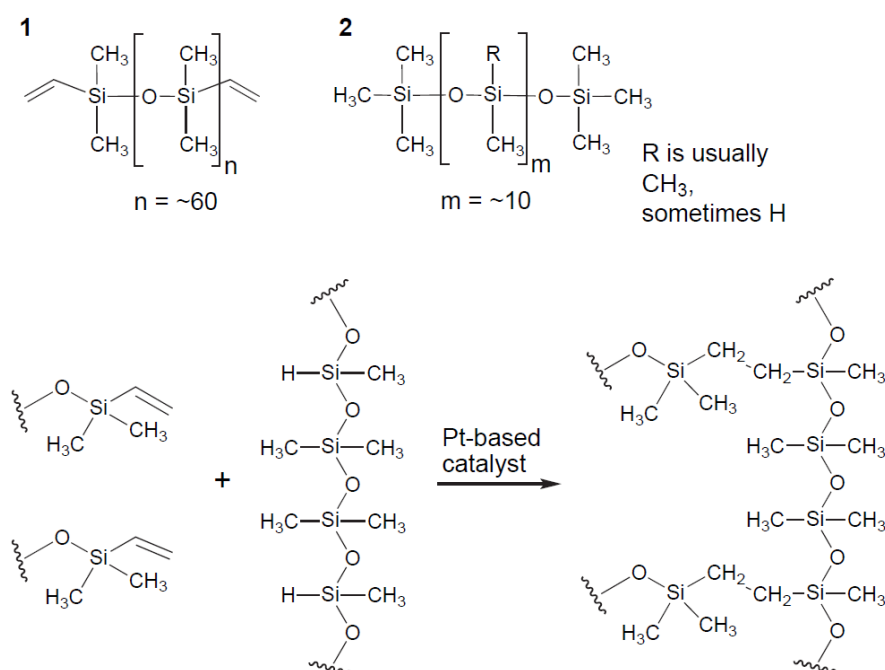


Fig. 10: Mechanism of PDMS cross-linking: siloxane oligomers terminated with vinyl groups (1) are mixed with cross-linking siloxanes oligomers (2) and a platinum-based catalyst which cures the elastomer by an hydrosilation of the double bonds forming Si-CH₂-CH₂-Si linkages, allowing the three-dimensional cross-linking of PDMS. Modified after Campbell *et al.* [106].

However, there are some drawbacks related to the PDMS stamps which limit their range of use. A major disadvantage is the resolution: in theory, PDMS stamps can be fabricated with features down to the nanometer range, but the mechanical characteristics of the elastomeric PDMS molds provide adequate stability for printing only with features down to 500 nm [107], since stamp deformation during contact with the substrate and also during stamp removal from the master reduces the patterning resolution [108]. Because the patterned PDMS molds are flexible, another problem is related to the aspect ratio of the features: if the aspect ratio is too high, the stamp features collapse against the substrate during the printing process [105]. On the other hand, if the aspect ratio is too low, e.g. in broad noncontact areas, roof collapse may occur, leading to contact between the mold and the substrate where it is actually undesired [108].

Another limit of PDMS lies in its hydrophobicity meaning that water-based inks do not wet PDMS molds and hence cannot be homogeneously printed on the substrate. This severely reduces the usage of inorganic complexes and biomolecules such as DNA and proteins as inks for PDMS stamps [107]. To overcome the aforementioned drawbacks of PDMS in soft lithography, either chemical or mechanical modifications of the PDMS mold or the use of a different polymer with higher Young's modulus and polarity is required. A common treatment process is the oxidation of the PDMS mold surface, e.g. by oxygen plasma, generating a chemically modified stamp with a polar and thin silica-like surface, allowing the printing of polar inks. In the next sections, the two soft lithography methods used in this work, microcontact printing and capillary force lithography, are described in detail.

4.1 Microcontact printing

Microcontact printing is a soft-lithographic technique for surface patterning in which a patterned elastomeric stamp is inked and then pressed on a substrate to transfer the molecules of the ink from the stamp to the substrate, as shown in figure 9.b. Developed as an alternative patterning processes to photolithography by Whitesides *et al.* in 1993, μ CP is extremely versatile, simple, and with a resolution down to the nanometer range [107,109,110]. Microcontact printing was first used to pattern self-assembled monolayers (SAMs) on gold substrates [102,111,112], but a plethora of applications and fabrication strategies were investigated since then [107]. For example, a patterned SAM on a substrate can control the

deposition of a material onto that substrate by metallization [113], crystal growth [114] and chemical amplification [115], and it can regulate the wetting and adhesion features of the substrates on which they are printed [116]. Also the printing of metal nanofilms and nanoparticles on different substrates were investigated [110], as well as the printing of biomolecules such as proteins, lipids and DNA [105].

The crucial steps in microcontact printing are the inking and printing processes. Inking is generally done either by placing an ink droplet on the patterned area of the stamp or by dipping the whole stamp into the ink solution [105,107]. The ink molecules do not only stay on the PDMS stamp surface but they also diffuse into the bulk of the stamp, creating an ink reserve [117]. The most commonly used solvent in the inking process is ethanol because of its low boiling point and the little swelling effect on the elastomer stamp [105,107]. After the inking process, the stamp is pressed against the substrate to be printed. Only the regions with protrusions are in conformal contact with the substrate, allowing a selective transfer of the ink molecules from the stamp. During the printing step the surface chemistries of stamp and substrate play a very important role in the transfer process efficiency, because the ink molecules will transfer to the substrate surface only if it is more energetically favorable than staying on the PDMS mold [107]. For example, the strong interactions of thiols with gold or the interactions of silanes with silica surfaces drive the transfer of these molecules from the mold to the surface [118].

4.2 Capillary Force Lithography

Capillary force lithography (CFL) is a polymer patterning method which combines the basic aspect of nanoimprint lithography, molding a polymer, with the key feature of soft lithography, the use of an elastomeric stamp [119]. The CFL process is carried out as follow: a patterned elastomeric mold is placed on a polymer layer and the temperature is raised above the polymer glass-transition point. Capillary force causes the melted polymer to rise in the narrow channels between the stamp and the substrate. After cooling, a hardened negative replica of the mold is left on the substrate. An ingenious variation of the CFL technique is the softening of the polymer by dissolving it in a solvent instead of heating it. In this case the process is also known as soft molding or solvent-assisted molding [119,120]. Soft molding is a very simple and efficient method for the patterning of polymers at room temperature, over

large areas, down to sub-100 nm resolution and without the need of complex and expensive instrumentation. Capillary force lithography was introduced by Suh *et al.* in 2001 using a commercial novolac resin and commercial polystyrene [119,121]. In the following years the method was further improved, smaller and more complex polymer structures were fabricated [122,123], and the use of other polymers such as polyvinylpyrrolidone and poly(ethylene glycol) was also studied [124,125]. In this thesis a new soft molding approach is investigated by using a solution with a polymer content of only 5 % in weight, much lower as usual in literature. This ensures a very fast rising of the polymer solution through the channels and hence a faster patterning time.

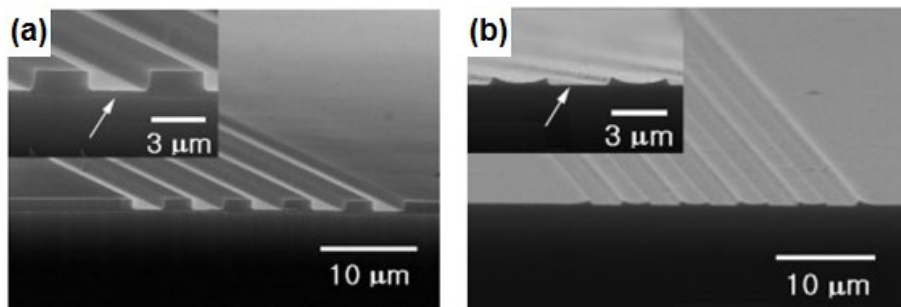


Fig. 11: SEM images showing polymer patterns fabricated using two approaches of the capillary force lithography process: (a) the use of a thick polymer layer (1.5 μm) and (b) the use of a thin polymer layer (180 nm). In the latter case the patterns show the meniscus caused by the capillary action. Modified after [119, 122].

4.3 Fabrication of metal structures by soft lithography

The fabrication of metal nano- and microstructures by unconventional fabrication processes like soft lithography is attracting increasing interest in different materials science areas, especially in opto-electronics, microelectronics and plasmonics [126–129]. The standard processes to fabricate metal nano- and microstructures are based on beam lithography or photolithography in combination with electroplating, ion sputtering or metal evaporation. Unfortunately, these conventional methods have low throughput, require sophisticated equipment, are time-consuming, use environmentally unfriendly chemicals for etching, waste a large amount of material and generally allow the patterning of only very small regions on the planar surface of a small number of inorganic substrates [13,14]. This explains why

several alternative methods, usually called “soft lithographic” processes, are receiving more and more attention from the scientific community [107].

Unconventional fabrication techniques such as soft lithography can circumvent many disadvantages of the conventional processes, above all cost, complexity and speed, but on the other hand they are difficult to use in the production of highly integrated and complex devices, where uniformity, reproducibility and alignment of the final metal patterns are critical concerns [100,127]. Nevertheless, soft lithographic techniques are very well suited for an extensive range of applications such as manufacturing of metal etching masks, the realization of sensors and biosensors [130,131], wiring of printed circuits [11], plasmonics [129], and the fabrication of transparent electrodes in solar cells and displays [132,133]. Extensive research has been done in the last decade in the development of new methods for the manufacturing of metallic nano- and microstructures [105,127,129]. For this reason, only the existing literature involving both electroless plating and microcontact printing is exhaustively reviewed in the next section.

4.3.1 Selective metallization by electroless plating

A patterned metal layer can be fabricated by electroless deposition either by directing the plating process or by plating a metal layer on the whole substrate and afterwards etching it selectively. In general, the first approach is preferred because it does not involve an extra etching process and thus it is simpler and more cost-effective. On the other hand, selectivity problems have been reported [12,134]. The use of microcontact printing in combination with electroless plating for the fabrication of metal microstructures was at first reported by Hidber *et al.* in 1996, three years after the introduction of the microcontact printing process by Whitesides *et al.* Previously, only non-soft lithographic patterning methods like photolithography and beam lithography were used. Hidber *et al.* printed palladium colloids stabilized by tetraoctadecyl-ammonium bromide on a substrate which was initially coated with siloxanes to promote adherence, followed by the electroless plating of copper catalyzed by the palladium colloids. They fabricated copper lines and other complex structures with a lateral dimension down to 0.5 μm (figure 12). The process was also used to manufacture free-standing copper structures by dissolution of the glass substrate in a dilute HF solution. In addition, both glass and polymers substrates were successfully patterned, showing the

versatility of the method [10]. Also other research groups applied an analogous approach based on electroless deposition on a substrate selectively activated with palladium-based catalysts. In 2000, Kind *et al.* successfully produced copper lines with lateral dimensions of 170 nm and 500 nm on substrates covered with titanium employing a precursor based on a Pd(II)-complex with organic ligands [135]. This work is of particular importance because it is the first that systematically investigate many parameters involved in the selective electroless deposition by microcontact printing, such as ink stability and ink adhesion to the stamp and substrate. However, this technique has a few major disadvantages: the ink solution is highly unstable and the PDMS mold must be hydrophilized with a plasma treatment before the inking and printing processes.

Other authors used a passivation process to fabricate metal patterns by stamping a passivation layer or a resist on a substrate. Exposing the passivated substrate to an electroless deposition solution allows the metal to deposit exclusively on the exposed non-passivated regions [136,137]. In 2002, Bittner *et al.* developed an interesting process based on the electroless metallization of dendrimer-coated micropatterns [138]. First a passivation layer was printed by microcontact printing, then polyamide-amine (PAMAM) dendrimers were transferred on the not passivated regions. Afterwards, palladium ions were bound to the PAMAM dendrimers by immersing the substrate into a Pd²⁺ solution. The Pd²⁺ ions are then reduced to palladium particles using an aqueous NaBH₄ solution, which act as seeds for the subsequent electroless plating step. Metallic lines and dots with a size of 10 μm were successfully fabricated. Although this method is a very interesting approach for the manufacturing of metal microstructures, it includes too many fabrication steps and is very complicated. In 2003, Moran *et al.* fabricated silver and gold lines with a lateral dimension in the submicrometer range using a passivation microcontact printing process which involves the stamping of n-propyltrimethoxysilane (PTMS) molecules as a patterned passivation layer [139]. Exposing the substrate printed with PTMS to a solution of SnCl₂ activates exclusively the non-printed regions, i.e. the PTMS-free regions, which can be afterwards selectively metallized by electroless plating. The resulting metal patterns were also used to investigate the propagation of surface plasmons within periodic and confined structures.

In 2004, Carmichael *et al.* introduced a new organic ink containing phosphonic acid groups to bind the ink to a glass substrate and phosphine groups to bind the colloidal palladium catalyst that starts the metal deposition during the electroless plating process [11]. Using this ink, the authors selectively deposited patterned layers of nickel and copper on glass substrates, with

areas as large as 15 cm^2 and with a lateral dimension of the metal structures down to $2 \text{ }\mu\text{m}$ (figure 12). This work is noteworthy since it is the first effort to overcome many of the drawbacks related to the direct microcontact printing of palladium-based catalysts by developing a new organic-based ink. However, the metal layers show major irregularities and lack of adhesion. In 2006, Mewe *et al.* fabricated metal microstructures on a silicon dioxide substrate using a seeded-growth method based on gold nanoparticles [12]. The authors used microcontact printing to print aminopropyltriethoxysilane (APTES), generating functionalized patterns with a high affinity towards gold. By immersing the substrate into a colloidal suspension of gold nanoparticles, the authors observed that gold nanoparticles selectively adhere on the printed APTES patterns.

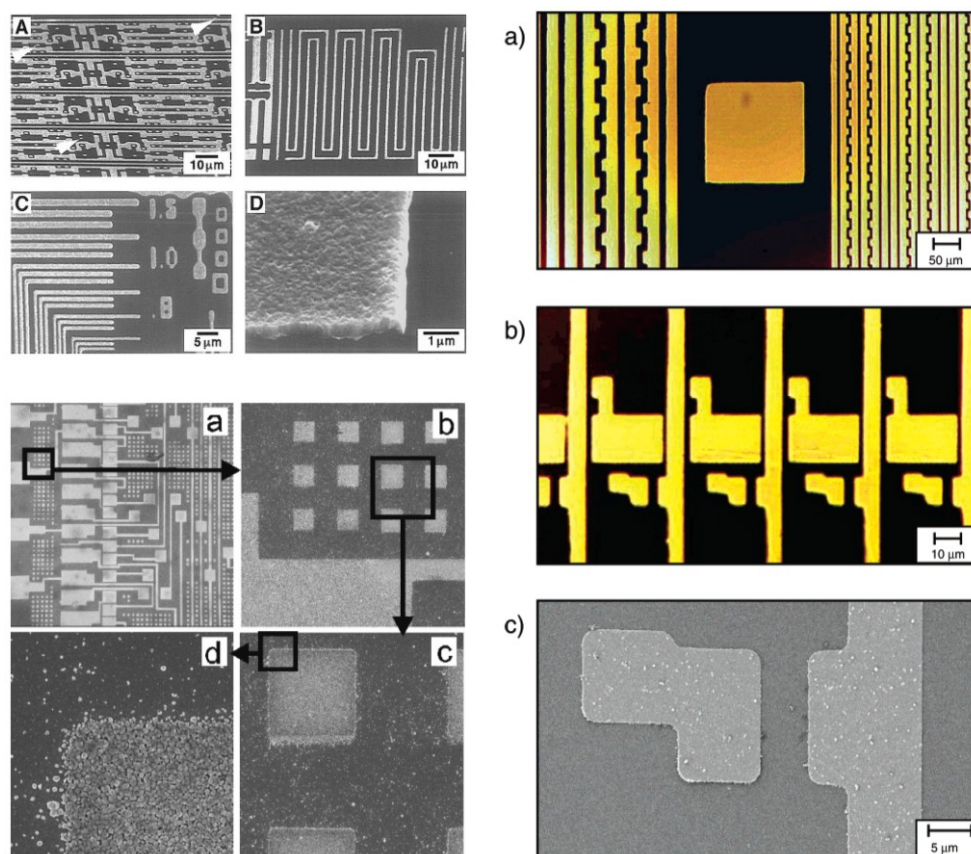


Fig. 12: Examples of metal structures fabricated by μCP and selective EP. Top-left: Cu structures fabricated by Hidber *et al.* by μCP of Pd colloids stabilized by tetraoctadecyl-ammonium bromide, followed by EP of copper [10]. Right: Ni patterns manufactured by Carmichael *et al.* by μCP of an organic ink containing phosphonic acid groups to bind the ink to the glass substrate and phosphine groups to bind the colloidal Pd catalyst, followed by EP [11]. Bottom-left: Au structures fabricated by Mewe *et al.* by μCP of aminopropyltriethoxysilane, followed by immersion of the substrate into a colloidal suspension of gold nanoparticles and subsequent EP. The image sizes are: (a) $1 \times 1 \text{ mm}^2$, (b) $100 \times 100 \text{ }\mu\text{m}^2$, (c) $25 \times 25 \text{ }\mu\text{m}^2$ and (d) $4 \times 4 \text{ }\mu\text{m}^2$ [12].

Afterwards, the isolated gold nanoparticles were grown above the percolation threshold by electroless plating, generating metal structures with high conductivity, although a selectivity problem is reported since there are some undesired gold depositions in the APTES-free areas (figure 12). Hsu *et al.* in 2007 were the first who reported the direct printing of an inorganic catalyst on a substrate, eliminating one process step in comparison with the previous methods [134]. They fabricated patterns made of silver lines with linewidths in the 0.6 – 10 μm range and a thickness of 50 nm by directly printing a SnCl_2 solution on a glass substrate, followed by the metallization process of the Sn-stamped areas via electroless plating. In 2008, Yoon *et al.* manufactured gold microstructures with a lateral dimension down to approximately 20 μm on a polyimide substrate [140]. The method is based on the selective activation of the polyimide substrate by microcontact printing of an aqueous solution of potassium hydroxide, which makes the printed areas hydrophilic, followed by activation of such areas with Pd^{2+} ions by immersing the film in a PdCl_2 solution. In this thesis a new method based on the direct printing of an organic promoter followed by selective electroless plating is investigated.

5. Characterization methods

The samples were characterized with standard and commonly used methods for chemical analysis: scanning electron microscopy (SEM), Fourier transform infrared spectroscopy (FTIR), thermogravimetric analysis (TGA) and X-ray diffraction (XRD). Other less common characterization techniques were used, namely transmission electron microscopy (TEM) and atomic force microscopy (AFM) which are described in the next sections.

5.1 Transmission electron microscopy (TEM)

A transmission electron microscope (TEM) operates basically in a similar way to the optical microscope, but instead of light a beam of electrons is used. The electron beam collides with the sample and the directly transmitted electrons are focused on an imaging device such as a fluorescent screen. The contrast of the image is caused by the absorption of electrons by the

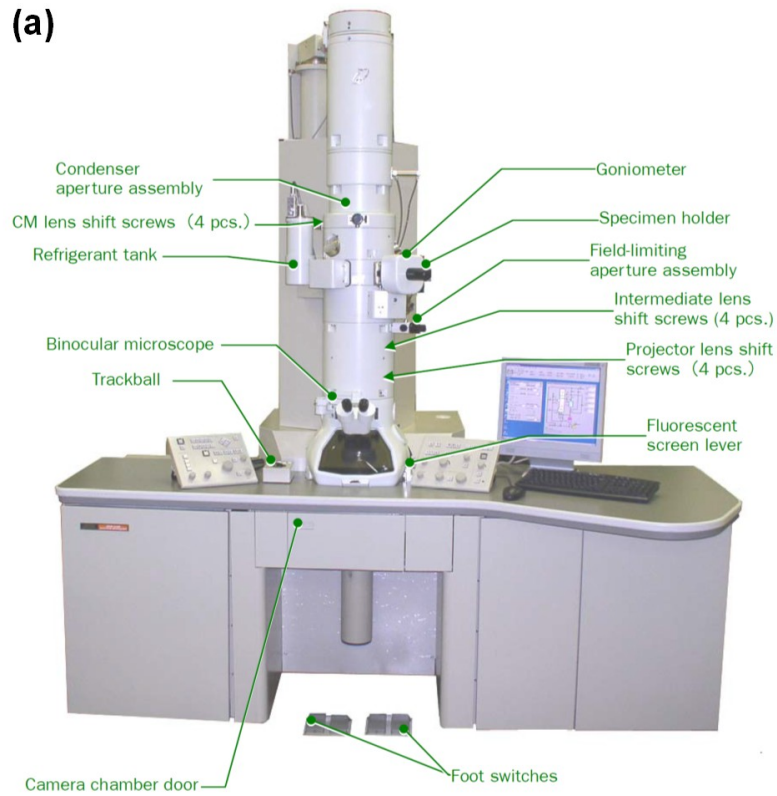
sample. Given the small de Broglie wavelength of electrons, TEM can reach very high resolutions. In fact, single rows of atoms can be seen in crystalline materials as a result of the diffraction of the electrons by the specimen. The resolution of TEM microscopes is constantly improved, e.g. Meyer *et al.* were able to see single carbon and hydrogen atoms on a graphene substrate [141]. In figure 13, the principal parts of a TEM are shown. The TEM is basically a column containing an electron gun and several electromagnetic lenses operating in vacuum. The electrons are generated by the electron gun and accelerated and focused by a set of condenser lenses. The beam then reaches the sample, which must be thin enough for the electron beam to pass through it. The samples are usually placed on specifically designed TEM grids, with a diameter of approximately 3 mm and a thickness of a few micrometers. The grid is fixed on a specimen holder and inserted in the TEM column. Afterwards, the electrons which are not absorbed by the sample are focused by a set of objective lenses and projector lenses before reaching the imaging device, usually a fluorescent screen or a CCD camera.

TEM is a very powerful analysis method and is necessary in the investigation of nanomaterials. It has however a few limitations: the preparation of the microscope and of the samples is very time consuming, the high energy of the electron beam can damage the sample, usually by amorphization or melting, and the small amount of sample volume investigated may lead to false interpretations [142].

5.1 Atomic force microscopy (AFM)

In an atomic force microscope, the specimen surface is sampled by a probing tip attached to a cantilever, usually made of silicon or Si_3N_4 by chemical etching (figure 14). Generally, when the tip is brought close to the specimen surface it experiences an interaction force, leading to the deflection of the cantilever. This deflection is usually determined by measuring with photodiodes the movement of a laser spot reflected from the cantilever. The measurement of the cantilever deflection along the z-direction as a function of the tip lateral position (x,y) leads to a 3D image of the sample surface. The interaction forces that the tip experiences when in proximity of the sample surface depends on the nature of both sample and tip and include, among others, electrostatic forces, mechanical contact forces, van der Waals forces, magnetic forces and capillary forces.

(a)



(b)

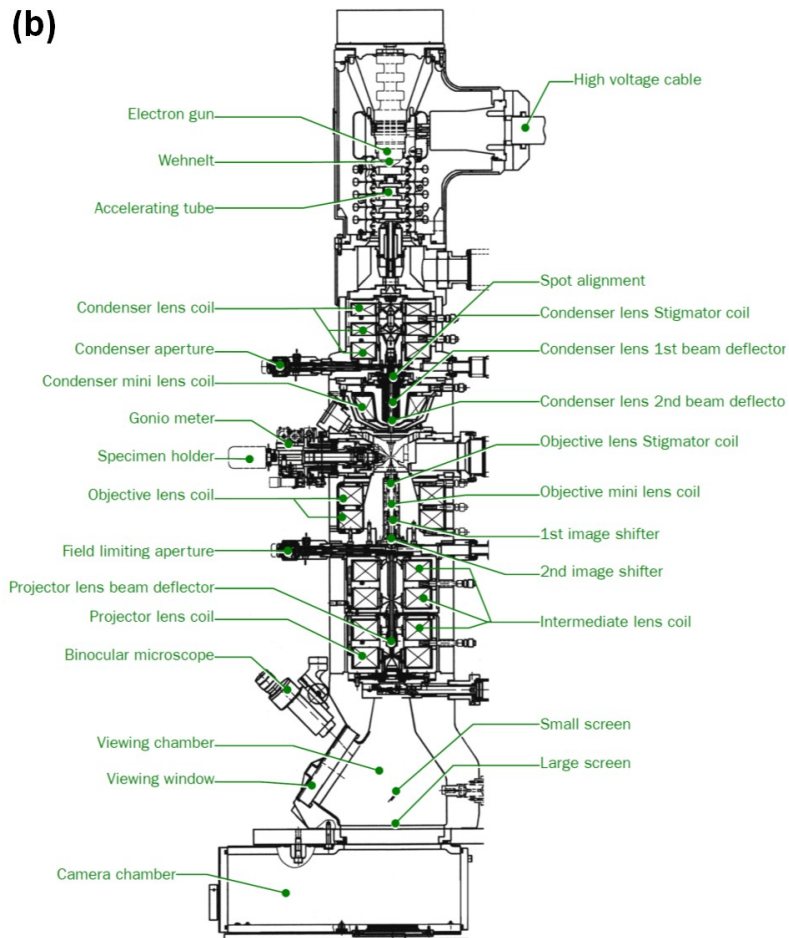


Fig. 13: (a) picture and (b) schematic illustration of a “JEOL JEM 2010” TEM. Modified after [142].

Depending on the application, the AFM can be operated in several ways. Generally, the operating modes are grouped into contact modes, where the tip is dragged across the surface of the sample in a repulsive force regime, and tapping modes, where the cantilever is vibrated. In this work an AFM operating in tapping mode was used. Tapping mode is a dynamic operating mode in which the cantilever is vibrated near its resonance frequency in proximity of the surface (usually 0 – 10 nm above the surface). If the distance between tip and surface becomes smaller, the intensity of the van der Waals and electrostatic forces experienced by the tip becomes stronger, leading to a decrease of the oscillation amplitude of the cantilever. In this way, the surface morphology can be measured and the above mentioned 3D image generated. From this image, also the roughness of the sample surface can be determined. The surface roughness is usually expressed with R_a and R_q , defined as:

$$R_a = \frac{1}{n} \sum_{i=1}^n |y_i| \quad (1)$$

$$R_q = \sqrt{\frac{1}{n} \sum_{i=1}^n y_i^2} \quad (2)$$

R_a is defined as the arithmetic average of the absolute values of the collected roughness data points (y_i), while R_q is the root mean square of the collected roughness data points (y_i) [143,144].

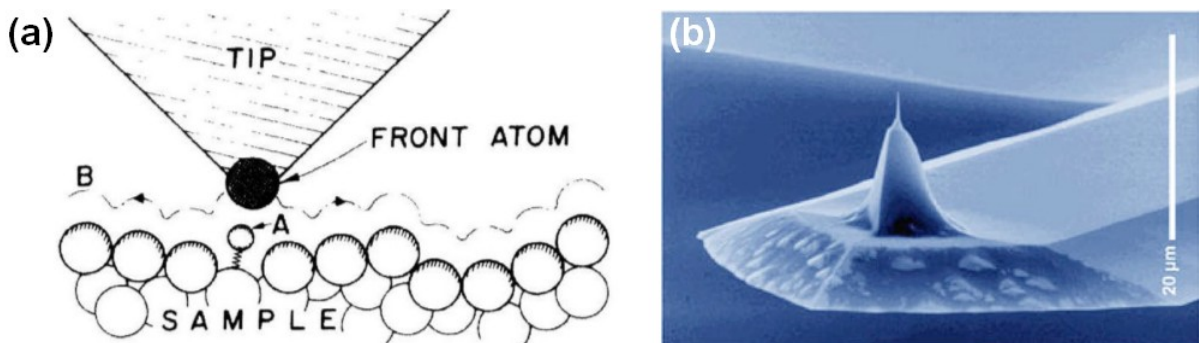


Fig. 14: (a) AFM operating principle: a probing tip attached to a cantilever is brought close to the specimen surface where it experiences an interaction force, leading to the deflection of the cantilever. By measuring the deflection of the cantilever along the z-direction as a function of the tip lateral position (x,y) a 3D image of the sample surface can be produced. (b) SEM image of a typical AFM tip.

III Experimental

1. Fabrication of metal-coated particles

1.1 Functionalization with 3-mercaptopropyltriethoxysilane

Silica nanoparticles (10 – 20 nm particle size) and alumina nanoparticles (13 nm average primary particle size) were functionalized with MPTES by hydrolysis and condensation reactions, as summarized in figure 15. Silica nanoparticles were used as received, whereas alumina nanoparticles were pretreated with hydrochloric acid to increase the number of hydroxyl groups on the particle surface. The pretreatment with HCl was carried out as follows: 1 g of alumina nanoparticles were suspended in 50 ml of a mixture of deionized water and 37 % HCl (1:1, v/v), sonicated for 15 min and then left in this solution overnight under intense stirring to avoid aggregation. Afterwards, the pretreated Al₂O₃ nanoparticles were carefully washed via centrifugation with distilled water. The MPTES functionalization reaction was performed in the same way for both alumina and silica: 1 g of nanoparticles were suspended in 50 ml deionized water and sonicated for 15 min. The coating reaction was carried out in reflux at 100°C for 2 h after the addition of 0.05 g MPTES.

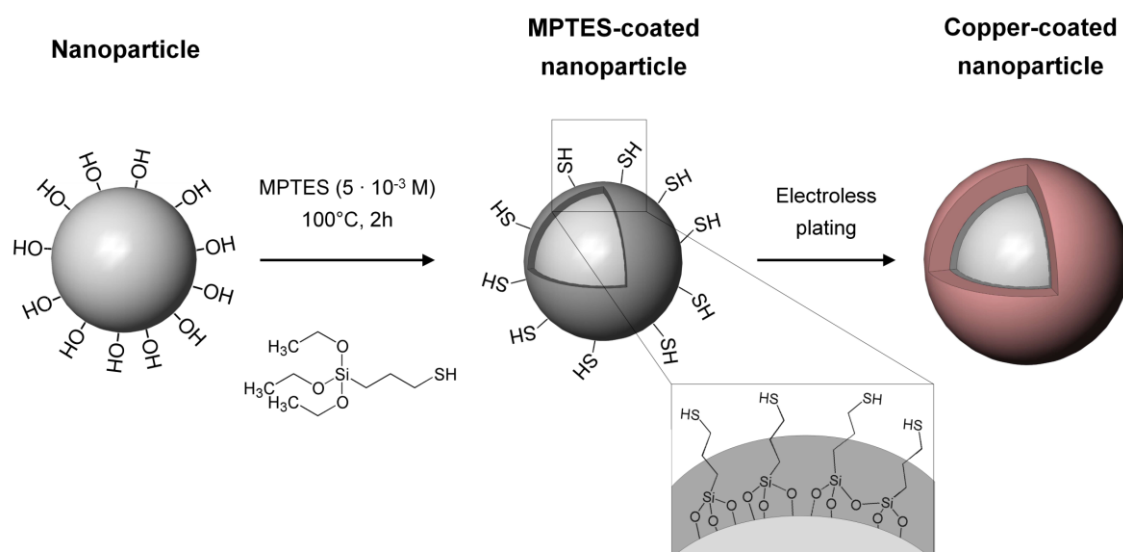


Fig. 15: Schematic illustration of the functionalization process of oxide particles with 3-mercaptopropyltriethoxysilane. The high affinity of the thiol groups towards metal ions promotes the subsequent metal deposition on the MPTES coated particles [145].

Synthesis of self-condensed MPTES as a reference for the FTIR analysis was done via a sol-gel process by mixing 1 ml deionized water, 1 ml acetone, 1 ml HCl (1 M), 10 ml ethanol and 1 g MPTES at room temperature. The resulting gel was dried in air for 12 h at 60°C [145].

1.2 Functionalization with 3-aminopropylphosphonic acid

Tungsten carbide microparticles (1 μm average size) were functionalized with 3-aminopropylphosphonic acid (3-APP) as follows: 20 g/l WC particles were suspended in a $5 \cdot 10^{-3}$ M aqueous solution of 3-APP, sonicated for 5 min and then left in this solution for 24 hours under stirring. Afterwards, the functionalized particles were washed via consecutive centrifugation cycles with deionized water and ethanol and then vacuum dried.

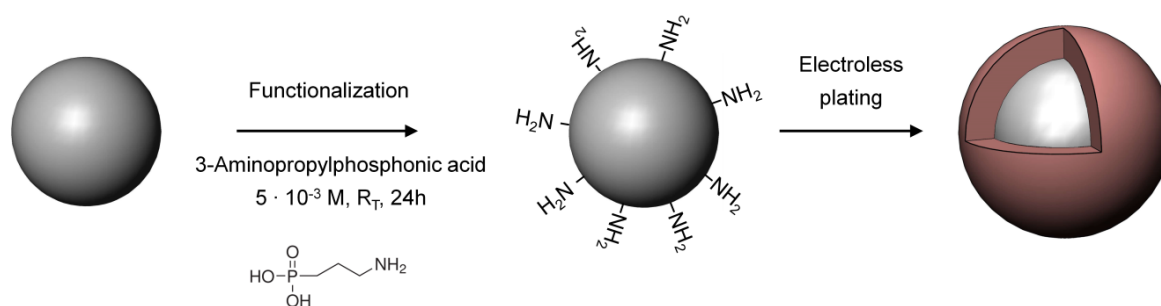


Fig. 16: Schematic illustration of the functionalization process of tungsten carbide particles with 3-aminopropylphosphonic acid. The high affinity of the amino groups towards metal ions promotes the subsequent metal deposition on the functionalized particles.

1.3 Functionalization with polydopamine

Tungsten carbide microparticles (1 μm average size) and alumina microparticles (4 – 10 μm average size) were coated with polydopamine using the same procedure for both materials: 1 g of particles was suspended in 33 ml of a Tris-HCl (tris(hydroxymethyl)aminomethane-HCl) buffer solution (10 mM, pH = 8.5) containing 2 g/l dopamine, sonicated for 5 min and then left in solution with stirring for a certain amount of time between 1 h and 24 h. A similar procedure was used with alumina nanoparticles (13 nm average primary particle size) and tungsten carbide nanoparticles (approx. 50 nm average primary particle size): 1 g of nanoparticles was suspended in 500 ml of a Tris-HCl buffer solution (10 mM, pH = 8.5)

containing 2 g/l dopamine, sonicated for 15 min and then left in solution under intense stirring for a certain amount of time. After the polymerization of dopamine, the polydopamine coated particles were washed via consecutive centrifugation cycles with deionized water and ethanol, until the solution became clear. The particles were then vacuum dried at 40°C. Pure polydopamine used in the FTIR analysis as a reference was synthesized in the same way as previously described, but without the addition of particles and sonication (2 g/L dopamine, 10 mM Tris-HCl buffer solution at pH = 8.5, 24 h polymerization time) [146].

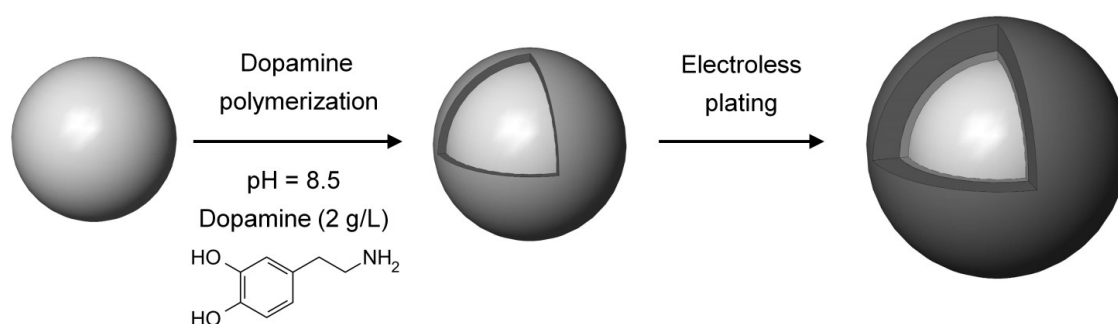


Fig. 17: Schematic illustration of the functionalization process with polydopamine by self-polymerization of dopamine on the particle surface. The affinity of the amino and catechols groups toward metal ions promotes the subsequent electroless metal deposition [146].

1.4 Metal deposition by electroless plating on functionalized particles

The nano- and microparticles functionalized with MPTES, 3-APP or polydopamine were coated with silver, copper, nickel or cobalt. The composition of the electroless plating bath used is summarized in table 2 and described in detail, along with operating conditions, in the next chapters.

1.4.1 Silver electroless deposition

Silver electroless deposition was carried out using an aqueous plating bath containing 4.5 g/l AgNO₃ as silver source, 13.5 ml/l ethylenediamine as complexing agent, 0.3 g/l 3,5-diiodo-L-tyrosine dihydrate as stabilizer, 12.0 g/l potassium sodium tartrate as reducing agent and

10 g/L of the particles to be plated. The pH was adjusted to 12.0 with the addition of NaOH, the suspension was sonicated for 5 min and then the deposition was carried out for 1 h at 35°C. The particles were afterwards washed via consecutive centrifugation cycles with deionized water and ethanol, then vacuum dried at 40°C [146].

Table 2: Composition of the electroless plating baths used in this work to fabricate metal coated particles. “ μ ” indicates the plating baths used to coat microparticles while “nano” indicates the plating bath used to coat nanoparticles.

	Ag-μ	Cu-μ	Cu-nano	Ni-μ	Co-μ
Metal source	AgNO ₃ (4.5 g/l)	CuSO ₄ ·5H ₂ O (7.5 g/l)	CuSO ₄ ·5H ₂ O (13.5 g/l)	NiCl ₂ ·6H ₂ O (10 g/l)	CoCl ₂ ·6H ₂ O (30.0 g/l)
Complexing agent(s)	Ethylenediamine (13.5 ml/l)	EDTA (5.5 g/l)	EDTA (10 g/l)	EDTA (16 g/l)	Sodium citrate (35.0 g/l) NH ₄ Cl (50 g/l)
Stabilizer	DiT (0.3 g/l)	-	-	-	-
Reducing agent(s)	Potassium sodium tartrate (12.0 g/l)	Hydrazine hydrate 80% (18.5 ml/l)	Hydrazine hydrate 80% (33 ml/l)	NaBH ₄ (3.2 g/l)	NaPO ₂ H ₂ (20 g/l) NaBH ₄ (7 g/l)
Particles	10 g/l	10 g/l	3 g/l	10 g/l	10 g/l
Temperature	35°C	R _T	R _T	R _T	60°C
pH	12.0	-	-	-	9.0

1.4.2 Copper electroless deposition

Copper electroless deposition on nanoparticles was carried out in an aqueous plating solution containing 13.5 g/l CuSO₄·5H₂O as copper source, 10 g/l EDTA as complexing agent and 3 g/l nanoparticles. The suspension was sonicated for 15 min before adding 33 ml/l hydrazine hydrate as reducing agent, which triggers the metal deposition reaction. After 2 h in the

plating solution at room temperature, the particles were removed and washed with distilled water and ethanol by consecutive centrifugation cycles, then vacuum dried at 40°C and stored under argon to avoid oxidation. Copper electroless deposition on microparticles was carried out in an aqueous plating solution containing 7.5 g/l $\text{CuSO}_4 \cdot 5\text{H}_2\text{O}$ as copper source, 5.5 g/l EDTA as complexing agent and 10 g/l nanoparticles. The suspension was sonicated for 5 min before adding 18.5 ml/l hydrazine hydrate as reducing agent. After 2 h in the plating solution at room temperature, the particles were removed and washed with distilled water and ethanol by consecutive centrifugation cycles, then vacuum dried at 40°C and stored under argon to avoid oxidation [145,146].

1.4.3 Nickel electroless deposition

Nickel electroless deposition was carried out using an aqueous plating bath containing 10 g/l $\text{NiCl}_2 \cdot 6\text{H}_2\text{O}$ as nickel source, 16.0 g/l EDTA as complexing agent and 10 g/l of the particles to be plated. The suspension was sonicated for 5 min before adding 3.2 g/l NaBH_4 as reducing agent. After 1 h in the plating solution at room temperature, the particles were removed and washed via consecutive centrifugation cycles with deionized water and ethanol, then vacuum dried at 40°C.

1.4.4 Cobalt electroless deposition

Cobalt electroless deposition on microparticles was carried using a plating bath modified after Brenner and Riddell [20]. The plating bath is made of an aqueous solution containing 30.0 g/l $\text{CoCl}_2 \cdot 6\text{H}_2\text{O}$ as cobalt source, 35.0 g/l sodium citrate and 50.0 g/l ammonium chloride as complexing agents, 20.0 g/l sodium hypophosphite and 7.0 g/l NaBH_4 as reducing agents, and 10 g/l of the particles to be plated. The pH was adjusted to 9.0 with the addition of ammonia and the suspension was sonicated for 5 min. Afterwards, the plating process was carried out for 1 h at 60°C, then the particles were removed, washed with distilled water and ethanol by consecutive centrifugation cycles and vacuum dried at 40°C.

2. Fabrication of metal matrix composites by powder metallurgy

2.1 Cu composites reinforced with Cu@Al₂O₃ nanoparticles and Cu@WC microparticles

The copper matrix composites were fabricated by powder metallurgy by CEP- Compound Extrusion Products GmbH and the Institute of joining technology and assembly of the Technical University of Dresden. First, Cu coated Al₂O₃ nanoparticles were synthesized as described in chapter III.1.4.2 by using the MPTES functionalization method followed by electroless plating, dried for 24 h at $3 \cdot 10^{-5}$ bar and stored under nitrogen. Afterwards, 1 wt% of the plated particles and a 99 wt% of copper powder (4.5 – 7.0 μm in size) were mixed in a drum hoop mixer, placed in a copper vessel and extruded in small rods of 1.5 cm in diameter. In the same way, copper matrix composites reinforced with 1 wt% of copper coated tungsten carbide microparticles were manufactured using the Cu coated WC microparticles synthesized as described in chapter III.1.4.2 by using the 3-APP functionalization method.

3. Fabrication of silver structures by soft lithography

All the soft lithographic processes were carried out with the semiautomatic micro-contact printer “GeSiM μ-CP 3.0”. The printer, the printing process, the stamps fabrication and the metallization procedures are described in following chapters.

3.1 Micro-contact printer “GeSiM μ-CP 3.0”

The device is a benchtop station (fig. 18.a) with a width of 63 cm, a length of 53 cm, a height of 37 cm and a weight of 35 kg. It has an inking station on the left side and a printing station on the right side. Up to four stamps can be placed on the stamps holder, which can be moved from the inking station to the printing station. A substrate is placed on the substrate holder in the printing station and its position is adjusted in two spatial directions and by rotation using vernier drives. During the printing process, the stamps are picked up from the stamps holder

by the printing head and pressed against the substrate. A built-in video microscope allows the perfect alignment of substrate and stamp, making it possible to print on defined regions only, or to print multiple layers exactly side by side or on top of each other. Before the stamping process, many parameters such as printing time, applied pressure and temperature of the substrate can be adjusted. The stamps used by this printer are made of two elements: a polycarbonate scaffold and a patterned elastomeric diaphragm (fig. 18.b), usually PDMS. During the printing process the elastomeric diaphragm is bulged out by air pressure in order to be in a homogeneous contact with the substrate surface and resulting in a very even 1 cm^2 printed area. The fabrication of the stamps is described in the next two sections.

3.1.1 Preparation of PDMS stamps

The polymeric stamps with patterns in the micrometer range were fabricated using polydimethylsiloxane by replica molding. First PDMS prepolymer and curing agent (Sylgard 184 silicone elastomer kit) were mixed with a mass ratio of 9:1, vigorously stirred and then degassed for 20 min. A teflon-coated silicon master with the replica of the desired structure and a teflon spacer were placed on the casting station as shown in figure 18.c.

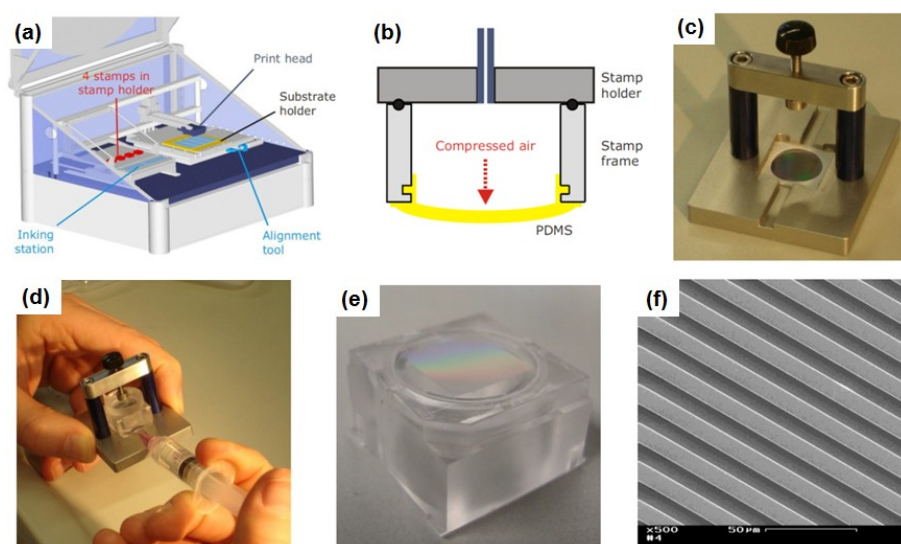


Fig. 18: (a) Illustration of the printer GeSiM μ -CP 3.0 and (b) a cross-section of the stamp used by the printer. (c) The casting station used to fabricate PDMS stamps. The Si master and the Teflon spacer are also visible. (d) Fabrication of a PDMS stamp by injection of the prepolymer in the polycarbonate frame. (e) A PDMS stamp after curing and releasing. On top the $1 \times 1 \text{ cm}^2$ patterned area is also visible. (f) A SEM image showing the micropatterns of a PDMS stamp.

The polycarbonate stamp scaffold was then placed on the silicon master and the PDMS was injected into the casting station through a small hole in the scaffold (fig. 18.d). Afterwards, the PDMS stamp was cured for 1 h at 80°C and then removed from the casting station. Figure 18.e shows a stamp after the curing process and ready to use, with the patterned PDMS diaphragm visible on top of the polycarbonate scaffold. A SEM image showing an enlargement of the patterned area, in this case lines with a width of 10 μm and a height of 5 μm , is shown in figure 18.f.

Six different PDMS stamp designs were used, as summarized in table 3: lines with approximately a width of 500 nm and 1 μm pitch, lines with a width of 10 μm and 20 μm pitch, lines with a width of 20 μm and 40 μm pitch, a regular grid of lines with a width of 5 μm , a 2D array of squares with a width of 5 μm and spaced 5 μm from each other, a 2D array of rings with an internal diameter of 10 μm , an external diameter of 20 μm and spaced 20 μm from each other. All the PDMS stamps have a patterned area of 1 cm^2 and all the structures have a height of 5 μm , except the first design which has a height of approximately 500 nm.

3.1.2 Preparation of PFPE stamps

The low stiffness of PDMS does not allow the accurate fabrication of structures with features in the nanometer range. Hence, perfluoropolyether (PFPE) was used instead of PDMS for the fabrication of stamps with features smaller than 500 nm. A similar fabrication procedure as with PDMS was used: perfluoropolyether prepolymer (Solvay Solexis Fomblin MD 700) and an ethanolic solution of 2,2-Dimethoxy-1,2-diphenylethan-1-one as photo initiator were mixed so that the initiator to PFPE weight ratio is 0.1 %, vigorously stirred and then degassed (figure 19). A teflon-coated silicon master with the replica of the desired structure and a teflon spacer were placed on the casting station. The polycarbonate stamp scaffold was then placed on the silicon master and the PFPE was injected into the casting station through a small hole in the scaffold. Afterwards, the PFPE stamp was cured for 30 min by UV radiation and then removed from the casting station. One PFPE mold design was used, consisting of a 2D array

of squares with a width of approximately 1 μm , a pitch of 1.2 μm , a height of about 500 nm and an area of 1 cm^2 .

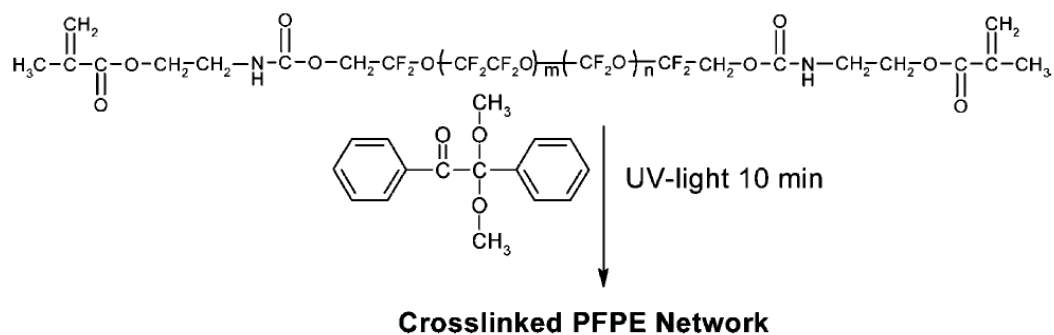


Fig. 19: Mechanism of PFPE cross-linking: methacryloyl functionalized PFPE is mixed with a photoinitiator (2,2-Dimethoxy-1,2-diphenylethane-1-one) and photocured by exposing the material to UV radiation, allowing the cross-linking of PFPE. Modified after Rolland *et al.* [147].

Table 3: List of the stamp designs, along with the SEM images of the silicon master and of the final stamp. All SEM pictures in this table are provided by the microcontact printer producer (Gesim).

Pattern	Material	Master (SEM)	Stamp (SEM)
10 μm lines	PDMS		
20 μm lines	PDMS		

Pattern	Material	Master (SEM)	Stamp (SEM)
5 μm grid	PDMS		
5 μm squares	PDMS		
20 μm donuts	PDMS		
500 nm lines	PDMS		
1/0.2 μm squares	PFPE		

3.2 Fabrication of silver structures by micro-contact printing of 3-mercaptopropyltriethoxysilane and electroless plating

A $5 \cdot 10^{-3}$ M solution of MP TES in commercial grade ethanol was used as ink. Several other organic solvents are used in literature for the deposition of silanes, such as benzene [148] and toluene [149], but considering that none of these solvent has any reported significant advantage, ethanol was used since it is easy to handle, less harmful and less expensive. Water is generally not used as a solvent with silanes because of its role in the hydrolysis reactions, and moreover it is problematic to use in soft lithography because it can not wet the hydrophobic PDMS stamps. Soda-lime glass microscope slides were used as substrates. Glass substrates were chosen for their low cost, transparency and because surface silanol groups, necessary for the condensation reaction with MP TES molecules, can be easily created on the glass surface by treatment with acids [150].

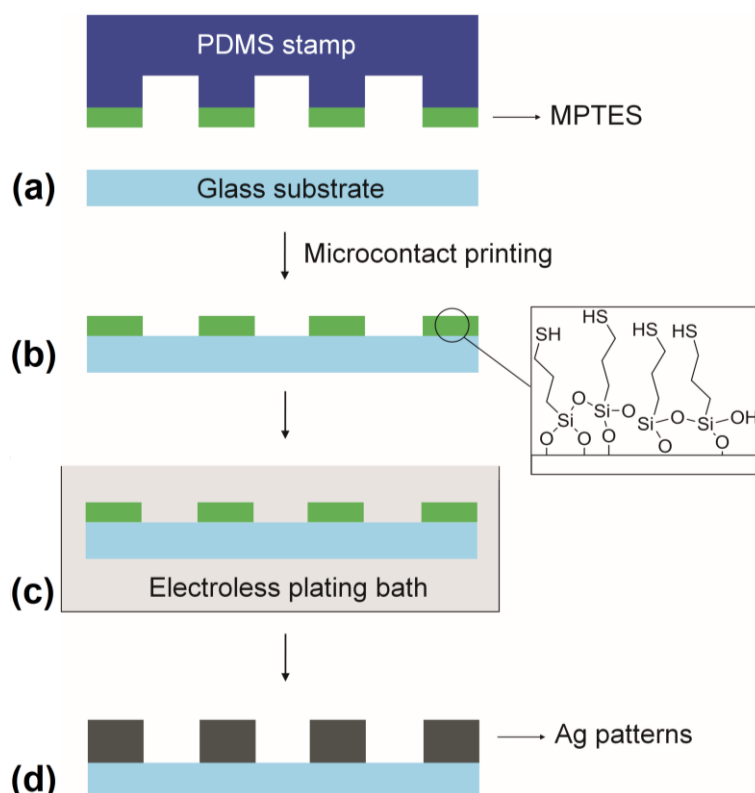


Fig. 20: Schematic illustration of the fabrication of silver structures by microcontact printing of MP TES and electroless plating. (a) A PDMS stamp is inked with MP TES and pressed against a glass substrate. (b) The glass substrate is selectively functionalized with MP TES. (c) Silver deposition by electroless plating. (d) Silver is selectively plated only on the MP TES functionalized areas [151].

After sonication for 15 min in a mixture of deionized water and acetone (v/v = 1:1) to remove organic contamination, the glass substrates were treated for 60 min with piranha solution (v/v = 7:3 mixture of 95 % H₂SO₄ and 30 % H₂O₂) in order to hydroxylate the glass surface, rinsed with deionized water and dried with an air stream. Prior to each printing process, the stamp is sonicated for 5 min in a mixture of water and ethanol (v/v = 1:1) to remove any dirt or residual ink molecules in order to avoid contamination.

The inking of the stamp was performed by placing a drop of ink on the structured area and letting the solvent dry. The printing process was carried out using the Gesim μ -CP 3.0 microcontact printer by gently pressing the inked stamp against the pretreated glass substrate for 500 s, as shown in figure 20. The substrate is then carefully rinsed with deionized water and ethanol to wash away any physisorbed MPTES molecules. The reaction of the MPTES with the glass surface takes place in two steps: first, the ethoxy groups of the MPTES molecules are hydrolyzed by the small amount of water contained in commercial ethanol (approximately 5 vol% H₂O), then the hydrolyzed MPTES molecules react with the hydroxyl groups of the hydroxylated substrate surface, forming a covalent bond between the MPTES and the substrate. The metal deposition on the printed structures was carried out in an aqueous solution containing 1.5 g/l AgNO₃ as silver source, 4.5 ml/l ethylenediamine as complexing agent, 0.1 g/l 3,5-diiodo-L-tyrosine dehydrate as stabilizer and 4.0 g/l potassium sodium tartrate as reducing agent. The pH was raised to 12.0 by adding NaOH and the temperature was set to 35°C. The printed glass substrates were immersed in the plating bath, then the reducing agent was added. This triggered the reduction of silver ions and the selective silver plating of the MPTES printed areas. After a deposition time of about 300 s, the substrates were removed from the plating bath and thoroughly rinsed with deionized water and ethanol [151].

3.3 Fabrication of silver structures by capillary force lithography of PMMA and electroless plating

Soda-lime microscope slides were used as substrates. After sonication for about 15 min in a mixture of deionized water and acetone (v/v = 1:1) to remove organic contamination and dirt, the glass substrates were immersed for 40 min in an aqueous solution containing 18.0 g/l SnCl₂ in order to create a thin SnO₂ layer on its surface. The role of this SnO₂ layer is to

promote the adsorption of silver ions during the subsequent silver electroless plating process [152]. The pretreated substrate is then rinsed with deionized water and dried with an air stream. For the patterning process, a 5 wt% solution of commercial grade PMMA in acetone was used. The use of a low PMMA concentration ensures a very fast capillary rise due to the low viscosity of the solution. This also allows the total conformity of the stamp to the substrate, i.e. the absence of a residual layer between the stamp and the substrate and hence the exposure of the substrate surface without a posttreatment process such as reactive-ion etching. In addition, acetone evaporates very quickly due to its high volatility, significantly lowering the patterning time. A concentration of 5 wt% PMMA in acetone was found to be the ideal concentration since a solution with a higher wt% leaves a residual layer in the printed areas, while a solution with lower PMMA concentration leads to defective and inhomogeneous patterns.

The patterning process was performed using the Gesim μ -CP 3.0 microcontact printer by placing a small drop (approximately 10 μ l) of PMMA solution on a pretreated glass substrate and promptly pressing it with a stamp as shown in figure 21.

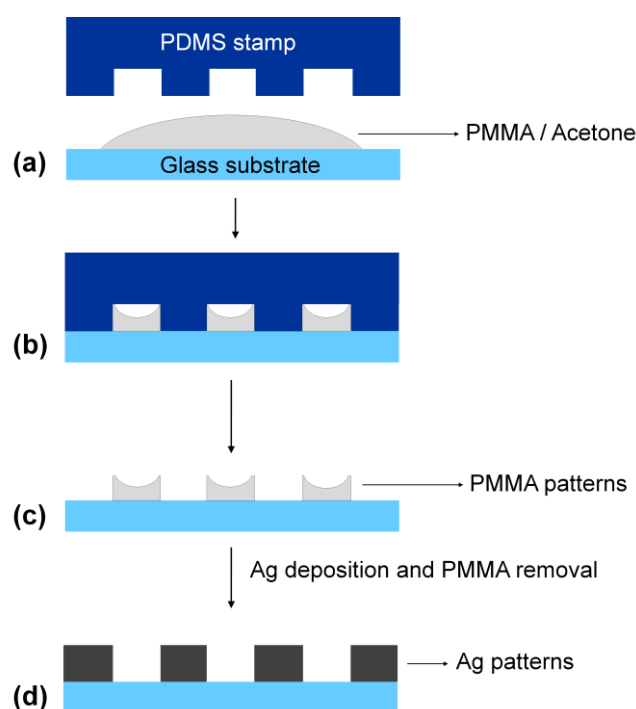


Fig. 21: Illustration of the fabrication of Ag structures by CFL of a 5 wt% PMMA solution in acetone followed by EP. (a) A small drop of PMMA solution is placed on a pretreated substrate and (b) immediately pressed with a stamp, allowing the solution to rise through the channels via capillary force. (c) The solvent evaporates and the mold is removed. (d) Ag is deposited on the exposed substrate surface, while the PMMA structures prevent the deposition on the covered areas. The PMMA structures are then removed with acetone [22].

After 10 – 100 s, depending on the structures size, the stamp was slowly lifted to avoid any damage to the PMMA structures and the substrate was carefully rinsed with deionized water and ethanol. The patterning of structures with sizes in the micrometer range takes approximately 100 s, whereas the patterning of structures in the submicrometer range is almost instantaneous, since only about 10 s are needed. For comparison, the fabrication of submicrometer polymeric structures by CFL requires a time of at least 1000 s [119], but patterning time of one or more hours are frequently reported in literature [120,153].

The silver deposition was carried out at room temperature in an aqueous solution containing 6.0 g/l AgNO₃ as silver source, 4.0 g/l NaOH and 20 ml/l ammonium hydroxide solution (ca. 25 % NH₃). The glass substrates with PMMA structures were immersed in the plating bath, then 4.5 g/l glucose as reducing agent was added. This triggered the reduction of silver ions and the silver deposition on the exposed areas of the substrates, while the PMMA structures prevent the silver deposition on the covered areas. After a deposition time of about 60 s, the substrates were removed from the plating bath and thoroughly rinsed with acetone to remove the sacrificial PMMA structures [22].

4. Characterization methods

4.1 Transmission electron microscopy (TEM)

Transmission electron microscopy images were taken with a JEOL JEM-2010F with spherical aberration (Cs) corrected objective lens and condenser lens system. The TEM was operated at an acceleration voltage of 80 kV.

4.2 Scanning electron microscopy (SEM) and Energy-dispersive X-ray spectroscopy (EDX)

Scanning electron microscopy images were acquired with two different microscopes: a Zeiss DSM-982 Gemini and a FEI NanoSEM 450. The same two microscopes were also used to

perform Energy-dispersive X-ray microscopy. The measurements were performed by Susanne Goldberg, Marcel Haft, Michael Kohl and Jan Brückner.

4.3 Atomic force microscopy (AFM)

Atomic force microscopy analysis was performed using a Veeco Dimension 3100 atomic force microscope with a Veeco Nanoscope IV SPM controller. The microscope was operated in tapping mode and using a Tap 150-G silicon tip (BudgetSensors) with a resonant frequency of 150 kHz, a force constant of 5 N/m and a tip radius < 10 nm. The measurements were performed by Benjamin Schumm.

4.4 Fourier transform infrared spectroscopy (FTIR)

Fourier transform infrared spectra were collected with a Bruker Vertex 70 (32 scans, 2 cm⁻¹ resolution, KBr plates). The measurements were performed by Florian Wisser.

4.5 Thermal gravimetric analysis (TGA)

Thermogravimetric analysis was performed with a Netzsch STA 409 PC/PG analyzer in synthetic air atmosphere and using a heating rate of 5 °C/min. The measurements were performed by Ilka Kunert.

4.6 X-Ray Diffraction (XRD)

X-ray diffractograms were acquired using a Panalytical X'Pert Pro diffractometer in Bragg–Brentano geometry with Cu K_{α1} radiation.

5. List of used chemicals

In the following table the used chemicals are listed. All the chemicals were used without further purification.

Table 4: List of used chemicals, with chemical formula, CAS number, purity grade and manufacturer.

Chemical	Formula	CAS Number	Purity [%]	Manufacturer
2,2-Dimethoxy-1,2-diphenylethan-1-one	$C_{16}H_{16}O_3$	24650-42-8	99	Acros
3,5-diiodo-L-tyrosine dihydrate	$C_9H_9I_2NO_3 \cdot 2H_2O$	18835-59-1	> 98	Sigma-Aldrich
3-aminopropylphosphonic acid	$H_2N(CH_2)_3PO(OH)_2$	13138-33-5	98	Sigma-Aldrich
3-mercaptopropyltriethoxysilane	$HS(CH_2)_3Si(OCH_2CH_3)_3$	14814-09-6	> 80	Sigma-Aldrich
Acetone	$(CH_3)_2CO$	67-64-1	99.9	BCD Chemie
Alumina nanoparticles (13 nm)	$\delta-Al_2O_3$	1344-28-1	99.8	Sigma-Aldrich
Alumina microparticles ($\leq 10 \mu m$ avg. part. size)	$\alpha-Al_2O_3$	1344-28-1	99.5	Sigma-Aldrich
Ammonium hydroxide solution	NH_4OH	1336-21-6	25	Sigma-Aldrich
Ammonium chloride	NH_4Cl	12125-02-9	99.5	Sigma-Aldrich
Borosilicate glass microscope slides	-	-	-	VWR
Cobalt(II) chloride hexahydrate	$CoCl_2 \cdot 6H_2O$	7791-13-1	98	Sigma-Aldrich
Copper(II) sulfate pentahydrate	$CuSO_4 \cdot 5H_2O$	7758-99-8	> 99	Sigma-Aldrich
Dopamine hydrochloride	$(HO)_2C_6H_3(CH_2)_2NH_2 \cdot HCl$	62-31-7	-	Sigma-Aldrich
Ethanol	CH_3CH_2OH	64-17-5	-	-
Ethylenediamine	$NH_2(CH_2)_2NH_2$	107-15-3	> 99	Sigma-Aldrich
Ethylenediaminetetraacetic acid (EDTA)	$(HO_2CCH_2)_2NCH_2CH_2N(CH_2CO_2H)_2$	60-00-4	> 99	Sigma-Aldrich
Fomblin MD-700 (PFPE)	-	9002-84-0	-	Solvay
D-(+)-Glucose	$C_6H_{12}O_6$	50-99-7	> 99.5	Sigma-Aldrich
Hydrazine hydrate solution (78-82%)	$NH_2NH_2 \cdot H_2O$	10217-52-4	-	Sigma-Aldrich
Nickel(II) chloride hexahydrate	$NiCl_2 \cdot 6H_2O$	7791-20-0	> 98	Sigma-Aldrich
Polymethylmethacrylate (PMMA)	$(C_5O_2H_8)_n$	9011-14-7	-	Sigma-Aldrich

Chemical	Formula	CAS Number	Purity [%]	Manufacturer
Potassium sodium tartrate tetrahydrate	$\text{KNaC}_4\text{H}_4\text{O}_6 \cdot 4\text{H}_2\text{O}$	6381-59-5	99	Sigma-Aldrich
Silicon dioxide nanoparticles (10 - 20 nm)	SiO_2	7631-86-9	99.5	Sigma-Aldrich
Silver nitrate	AgNO_3	7761-88-8	99.5	Grüssing
Sodium borohydride	NaBH_4	16940-66-2	98	Sigma-Aldrich
Sodium hydroxide	NaOH	1310-73-2	98.5	Sigma-Aldrich
Sodium hypophosphite monohydrate	$\text{NaPO}_2\text{H}_2 \cdot \text{H}_2\text{O}$	10039-56-2	> 99	Sigma-Aldrich
Sylgard 184	-	-	-	Dow Corning
Tin(II) chloride	SnCl_2	7772-99-8	98	Sigma-Aldrich
Tris(hydroxymethyl) – aminomethane–HCl (Tris–HCl)	$\text{NH}_2\text{C}(\text{CH}_2\text{OH})_3 \cdot \text{HCl}$	1185-53-1	> 99	Sigma-Aldrich
Trisodium citrate dihydrate	$\text{Na}_3\text{C}_6\text{H}_5\text{O}_7$	6132-04-3	-	Sigma-Aldrich
Tungsten carbide microparticles (0.5 - 2 μm)	WC	12070-12-1	-	H.C. Starck
Tungsten carbide nanoparticles (50 nm)	WC	12070-12-1	-	H.C. Starck

IV Results and discussion

In the first part of this chapter the results regarding the functionalization of particles with MPTES, 3-APP and polydopamine is discussed, followed by the electroless metal deposition of Cu, Ag, Ni and Co on the functionalized particles. In the second part the results concerning the selective functionalization of glass substrates with MPTES, the selective fabrication of PMMA sacrificial layers and the subsequent metallization by EP are discussed.

1. Functionalized particles

1.1 Particle characterization (as received)

In this part the characterization of the as received uncoated particles used in this work are shown in order to better evaluate the characteristics of the functionalized and metal coated particles. TEM images, SEM images, XRD diffractograms and TGA analysis are reported.

1.1.1 Al₂O₃ nanoparticles

Alumina nanoparticles were purchased from Sigma Aldrich. According to the manufacturer the particles have a primary particle size of 13 nm, which is verified by high resolution TEM characterization (fig.22). Figure 22.a shows a SEM image of the Al₂O₃ nanoparticles, while figures 22.b-d show TEM images with different magnifications. The nanoparticles are received in a dry state and hence have some degree of agglomeration. In addition, the lattice fringes can be seen in the high resolution TEM pictures, indicating the crystallinity of the particles. Figure 23.a shows the XRD diffraction pattern of the alumina nanoparticles, confirming their crystallinity and size in the nanometer range, since peak broadening can be seen. The XRD diffractogram also indicates that the Al₂O₃ nanoparticles are the δ -phase (JCPDS 4-877). Figure 23.b shows the TGA analysis, in which a mass loss of about 4.5 % can be seen. This mass loss is due to the removal of the water bound on the Al-OH groups of the particle surface [154,155].

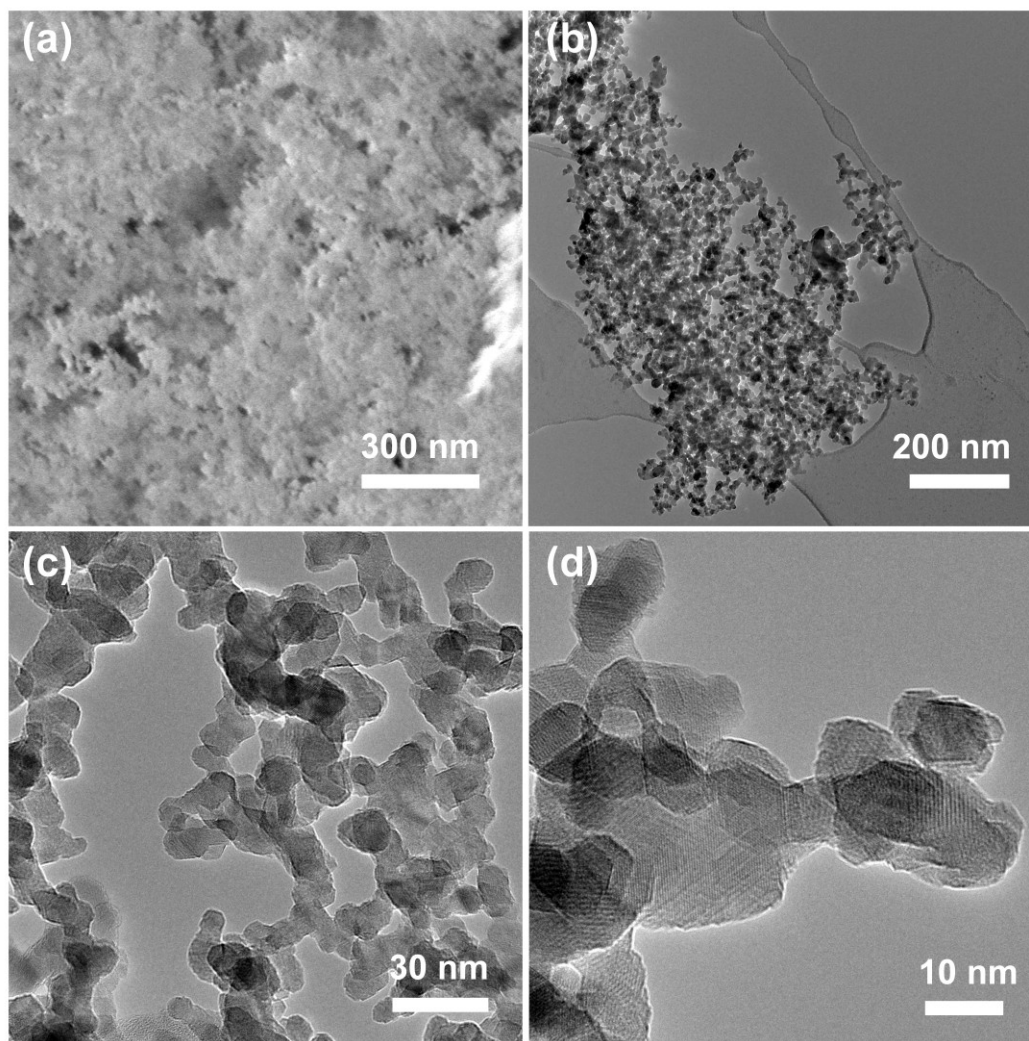


Fig. 22: (a) SEM image and (b-d) TEM images of the Al₂O₃ nanoparticles (as received) used in this work.

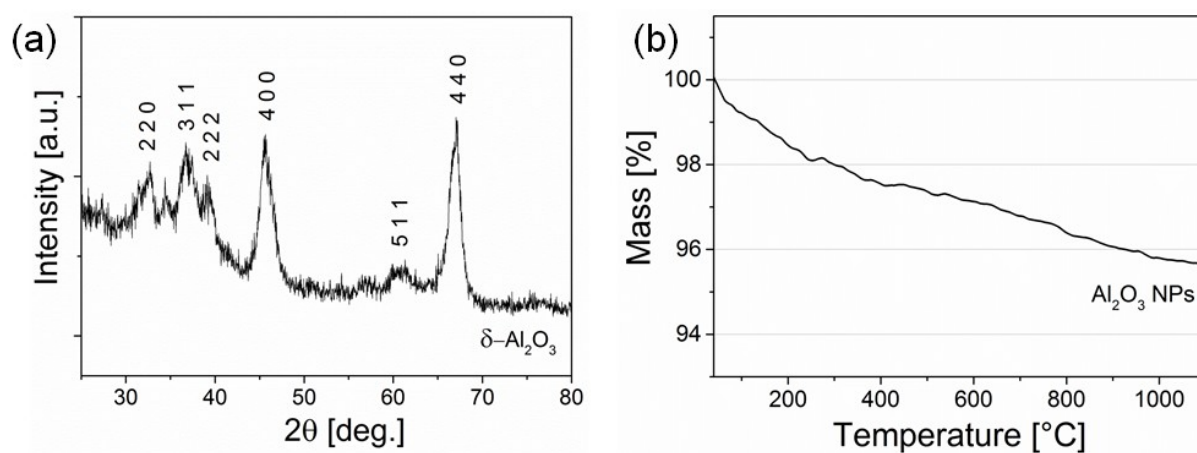


Fig. 23: (a) XRD diffractogram and (b) TGA analysis of the Al₂O₃ nanoparticles (as received) used in this work.

1.1.2 Al₂O₃ microparticles

Alumina microparticles were purchased from Sigma Aldrich. According to the manufacturer the particles have an average particles size $\leq 10 \mu\text{m}$. Figures 24.a-c show SEM images of the as received alumina microparticles with different magnifications. The particles have an irregular shape and sizes in the 4 – 10 μm range. Figure 25.a shows the XRD diffraction pattern of the alumina microparticles, confirming their crystallinity and indicating that the particles are the α -phase (JCPDS 10-173). Figure 25.b shows the TGA analysis up to 1000°C, in which a mass loss of about 0.5 % can be seen. As for the nanoscaled particles, this mass loss is due to the removal of the water bound on the Al-OH groups of the particle surface [154,155]. The higher content of water bound to the δ -alumina nanoparticles surface (4.5 %) as compared with the α -alumina microparticles (0.5 %) is partially related to the different surface properties of δ - and α -alumina [154], but is in this case mainly due to the higher specific surface area of the nanoparticles, i.e. higher surface to volume ratio and hence a higher concentration of Al-OH groups.

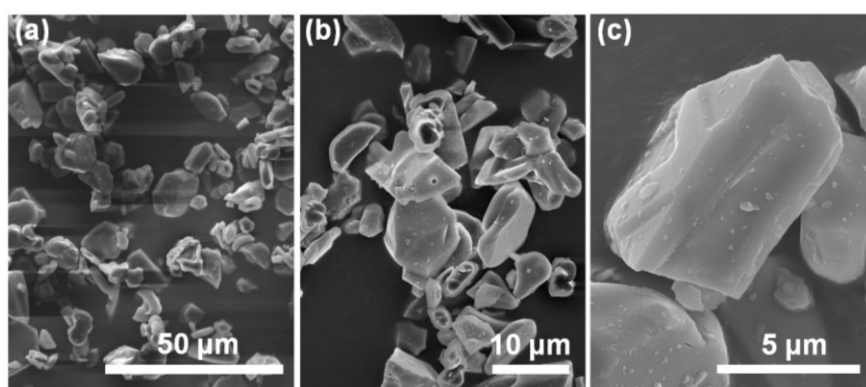


Fig. 24: SEM images of the Al₂O₃ microparticles (as received) used in this work.

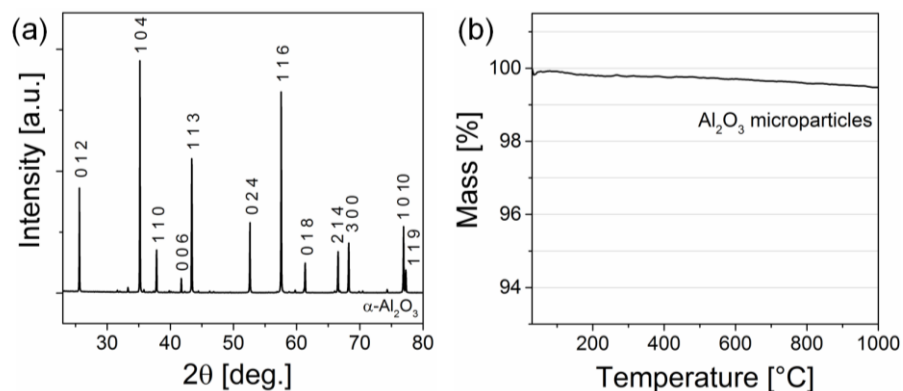


Fig. 25: (a) XRD and (b) TGA analysis of the Al₂O₃ microparticles (as received) used in this work.

1.1.3 SiO₂ nanoparticles

Silica nanoparticles were purchased from Sigma Aldrich. According to the manufacturer the particles have a particle size in the 10 – 20 nm range (determined by BET analysis), which is verified by high resolution TEM characterization (fig. 26). Figure 26.a shows a SEM image of the silica nanoparticles, while figures 26.b,c show TEM images with different magnifications. In this case, the nanoparticles are amorphous and hence no lattice fringes can be seen in the TEM images. Moreover, the nanoparticles are received in a dry state and hence show some degree of agglomeration. Figure 26.d shows the XRD diffraction pattern of the SiO₂ nanoparticles, confirming their amorphous nature.

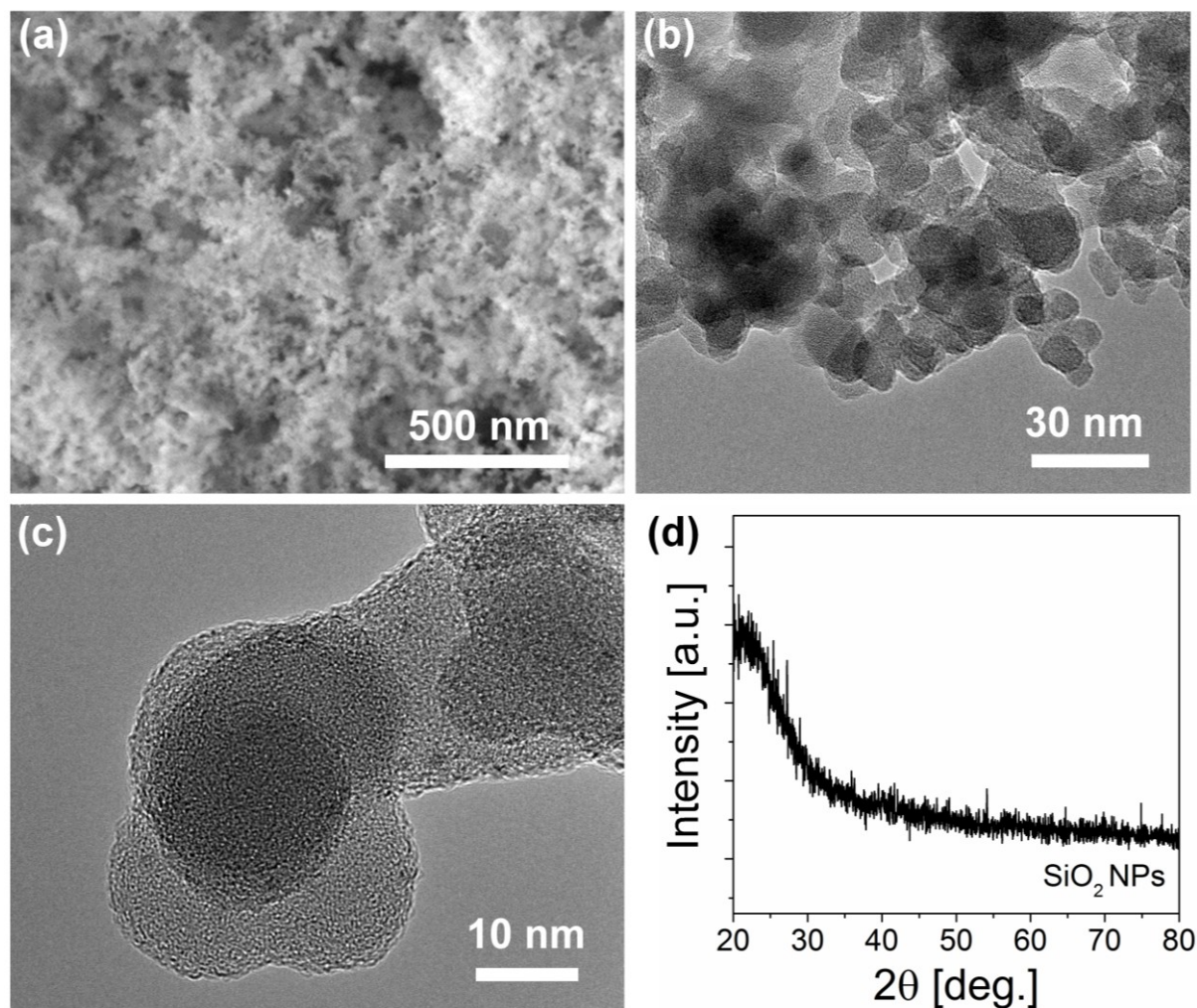


Fig. 26: (a) SEM image, (b,c) TEM images and (d) XRD diffraction pattern of the SiO₂ nanoparticles (as received) used in this work.

1.1.4 WC nanoparticles

Tungsten carbide nanoparticles were obtained from the company H.C. Starck. Figure 27 show TEM images with different magnifications. The particles have some degree of aggregation and a particle size of approximately 50 nm. Figure 28.a shows the XRD diffractogram of the WC nanoparticles, indicating their crystallinity (JCPDS 25-1047) and size in the nanometer range, since peak broadening can be seen. Figure 28.b shows the thermogravimetric analysis performed in air, in which a mass gain of about 18 % due to the oxidation of WC to WO_3 can be seen [156]. The oxidation process starts at 400°C and stops at around 650°C.

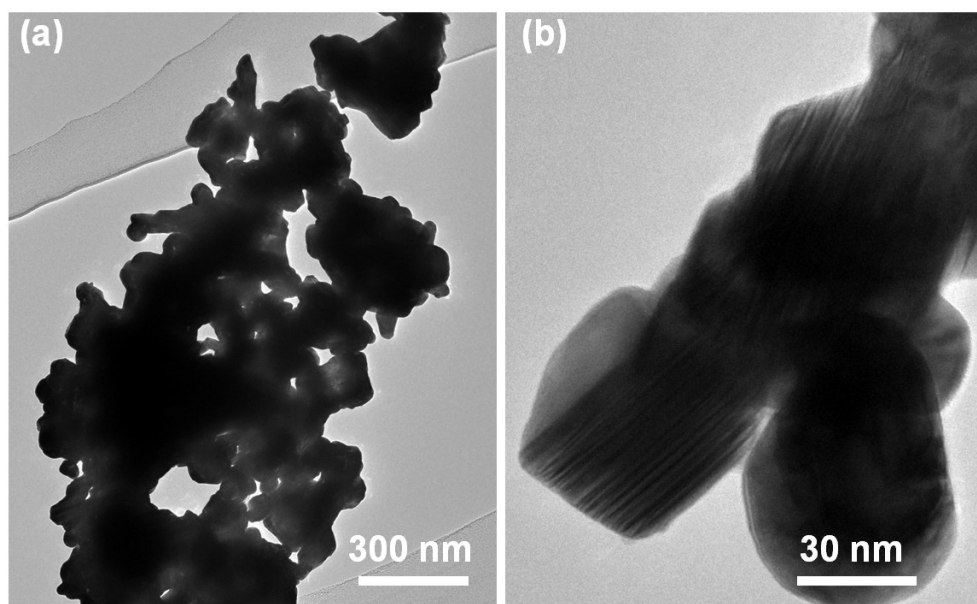


Fig. 27: (a,b) TEM images of the tungsten carbide nanoparticles (as received) used in this work.

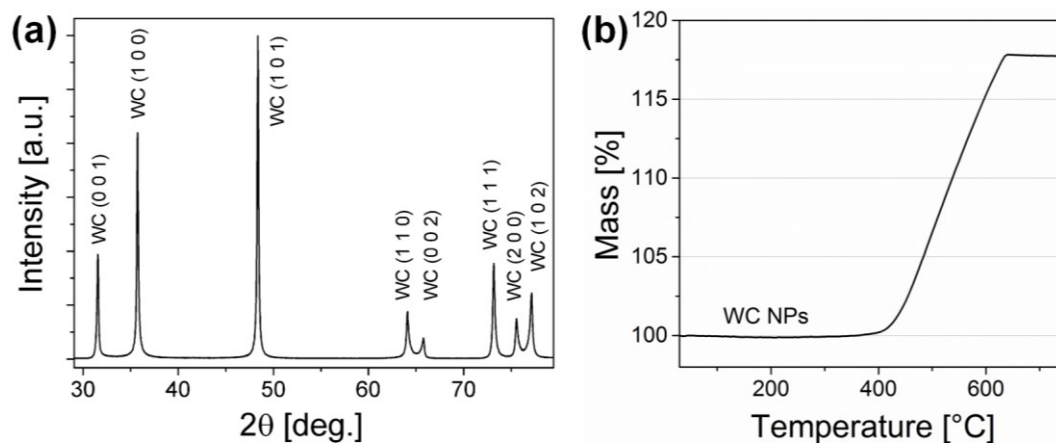


Fig. 28: (a) XRD diffraction pattern and (b) TGA analysis (in air) of the tungsten carbide nanoparticles (as received) used in this work.

1.1.5 WC microparticles

Tungsten carbide microparticles were obtained from the company H.C. Starck. Figure 29 shows SEM images with different magnifications. The particles have sizes in the 0.5 – 2 μm range, are irregular in shape and show a faceted surface with flat areas and sharp edges. Figure 30.a shows the XRD diffraction pattern of the WC microparticles (JCPDS 25-1047), with peaks slightly sharper than the peaks of the WC nanoparticles from figure 28.a because of the bigger particle size. Figure 30.b shows the thermogravimetric analysis performed in air, in which a mass gain of about 18 % due to the oxidation of WC to WO_3 can be seen [156]. The oxidation process starts at 400°C and stops at around 850°C.

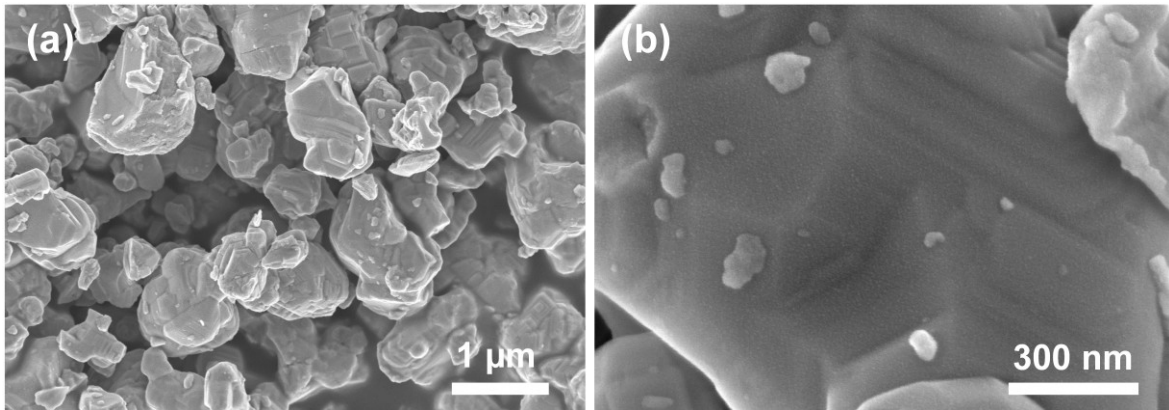


Fig. 29: (a,b) SEM images of the tungsten carbide microparticles (as received) used in this work.

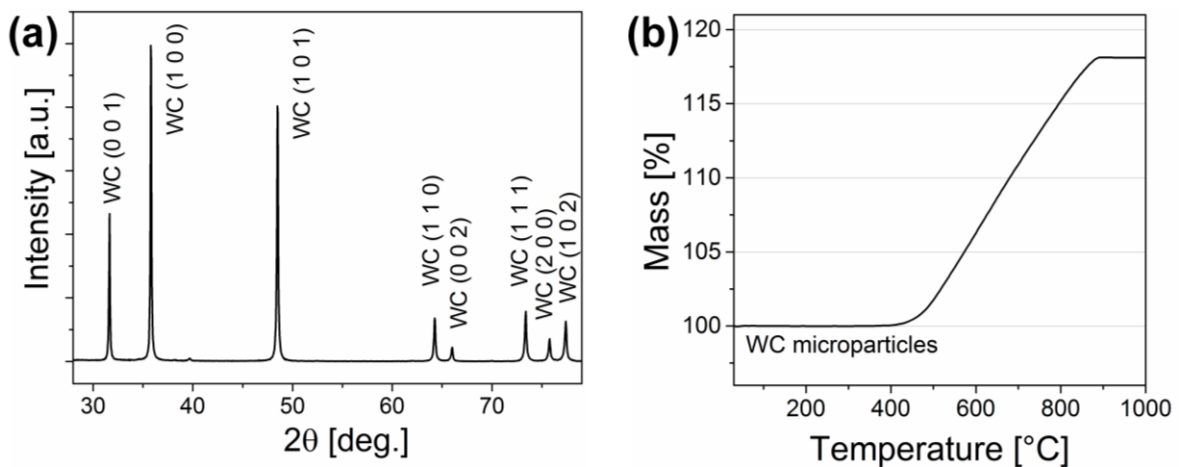


Fig. 30: (a) XRD diffraction pattern and (b) TGA analysis (in air) of the tungsten carbide microparticles (as received) used in this work.

1.2 Particle functionalization with 3-mercaptopropyltriethoxysilane

In this section, the results of the functionalization of silica and alumina particles with MPTES are shown. In particular, the reaction of MPTES with the particle surface is verified by TEM and IR analysis.

1.2.1 MPTES@Al₂O₃ nanoparticles

TEM images of Al₂O₃ nanoparticles before and after the functionalization with MPTES are shown in figure 31. An amorphous coating can be seen on the surface of the alumina particles, with an irregular thickness ranging from 1 to 4 nm. According to the literature, the thickness of an MPTES monolayer is about 0.7 nm [148], suggesting that the coating on the surface of the particles in figure 31.d is made of both monolayers and thicker disordered agglomerates.

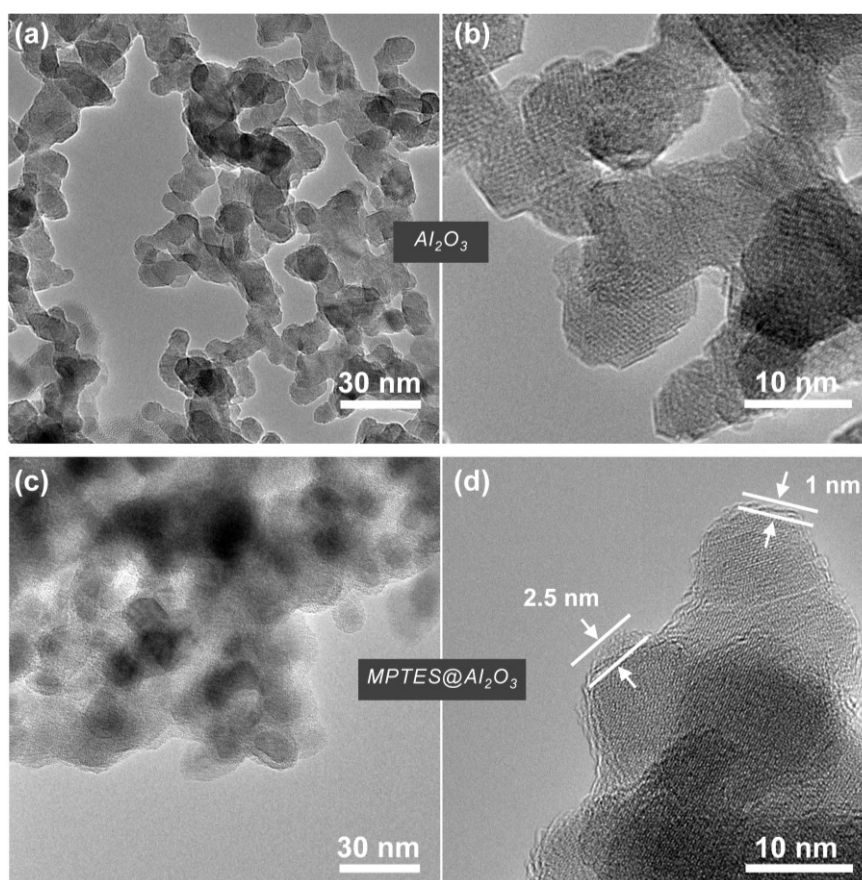


Fig. 31: TEM images of alumina nanoparticle (a,b) before and (c,d) after the functionalization with 3-mercaptopropyltriethoxysilane. An amorphous coating can be seen on the surface of the crystalline alumina nanoparticles, with a thickness ranging from 1 to 4 nm.

The condensation reaction of MPTES with the particle surface is in competition with the self-polymerization of MPTES in solution, leading to the formation of oligomers, as shown in figure 32 [148]. These oligomers also undergo condensation reactions with the particle surface and are responsible for the thicker agglomerates of the coating. As indicated by Hu *et al.*, the thiol groups in such MPTES oligomers are not densely packed and well ordered as in a monolayer, but they still show the capacity to promote metal deposition [148].

The alumina nanoparticles coated with MPTES were also analyzed with FTIR spectroscopy. The FTIR spectra of MPTES-coated alumina nanoparticles, pristine alumina nanoparticles and pure condensed MPTES (as reference) are shown in figure 33. In the FTIR spectrum of MPTES-coated alumina nanoparticles, several absorption bands in the 2850 – 3000 cm^{-1} and 1000 – 1500 cm^{-1} spectral regions can be seen, indicating the presence of MPTES on the Al_2O_3 particles [157,158]. The broad absorption bands in the 950 – 1250 cm^{-1} spectral region are typical absorption features of the polysiloxanes [157,158]. Among them, the two strong absorption bands at 1090 cm^{-1} and 1020 cm^{-1} are assigned to the stretching of the Si–O–Si bond, indicating the condensation of adjacent MPTES on the alumina particles surface and demonstrating that a part of the MPTES molecules have undergone self-polymerization, resulting in the formation of oligomers [159,160]. Interestingly, the absorption band at 1090 cm^{-1} is shifted to lower wavelengths in comparison to the MPTES reference, where the band is at 1120 cm^{-1} . This band is characteristic of the type of the Si second neighbor atom and a shift to lower wavelengths indicates the formation of Si–O–Al bonds [161,162].

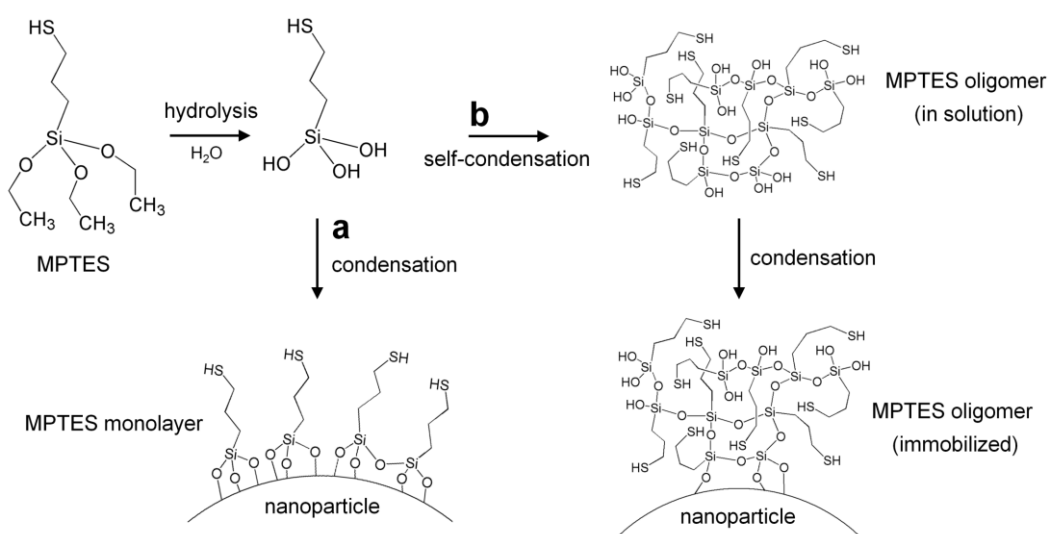


Fig. 32: Schematic illustration of the condensation reactions involving MPTES. Route a: hydrolysis and condensation of MPTES molecules leading to the formation of a monolayer. Route b: hydrolysis and self-condensation of MPTES molecules in solution leading to the formation of an oligomer.

The results show that the alumina nanoparticles were successfully coated with MPTES. Moreover, FTIR spectroscopy analysis suggests the presence of Si–O–Al bonds, indicating that MPTES is covalently bound to the particle surface.

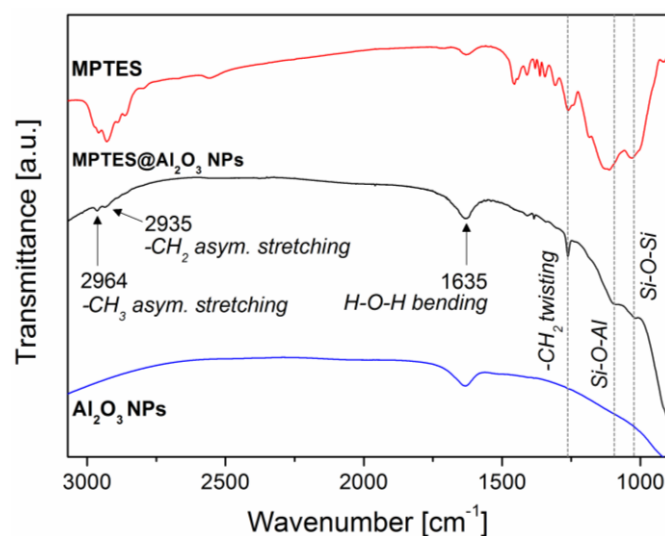


Fig. 33: FTIR spectra of alumina nanoparticles (blue line), condensed MPTES as a reference (red line) and alumina nanoparticles coated with MPTES (black line).

1.2.2 MPTES@ SiO_2 nanoparticles

In the case of alumina nanoparticles, the amorphous MPTES coating is clearly distinguishable from the crystalline alumina particle in the TEM images, but in the case of silica nanoparticles TEM analysis is not helpful because the particles and also the MPTES coating are amorphous and based on silica, hence, no contrast difference or lattice fringes can be seen. The MPTES coated silica nanoparticles were therefore investigated with FTIR spectroscopy. The FTIR spectra of MPTES coated SiO_2 nanoparticles, pristine SiO_2 nanoparticles and pure condensed MPTES (as reference) are shown in figure 34. In the FTIR spectrum of MPTES coated silica nanoparticles, the absorption bands of the $-\text{CH}_2$ and $-\text{CH}_3$ asymmetric stretching modes can be seen in the 2800 – 3000 cm^{-1} spectral region, demonstrating the presence of the organic MPTES coating. The absorption band at 1455 cm^{-1} is assigned to the $-\text{CH}_2$ scissoring mode [163], whereas at lower wavelengths a strong and broad absorption band of silica covers the other peaks. The functionalization with MPTES is suitable for oxide particles, but does not work with carbides. For this reason, the method using 3-APP was developed and the results are shown in the next section.

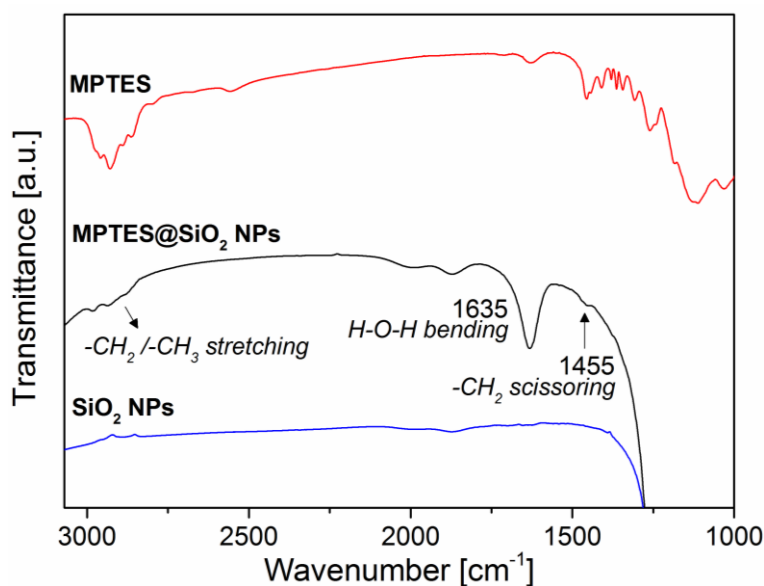


Fig. 34: FTIR spectra of silica nanoparticles (blue line), condensed MPTES as a reference (red line) and silica nanoparticles coated with MPTES (black line).

1.3 Particle functionalization with 3-aminopropylphosphonic acid

In this section the results of the functionalization of tungsten carbide particles with 3-aminopropylphosphonic acid are reported. The main advantage of this method is that it can be used to activate carbides, which are notoriously chemically inert. Moreover, phosphonic acids are able to form only monolayers on the substrate surface, contrary to MPTES which can also form thicker oligomers. On the other hand, 3-aminopropylphosphonic acid is very expensive as compared to other functional molecules, with 1 g from around 200 € (laboratory scale price).

1.3.1 3-APP@WC microparticles

TEM images of a tungsten carbide microparticle before and after the functionalization with 3-aminopropylphosphonic acid are shown in figure 35. A monolayer with a thickness of about 0.6 nm can be seen on the surface of the functionalized WC microparticle, in good agreement with the thicknesses of similar phosphonic acids measured with AFM [164,165].

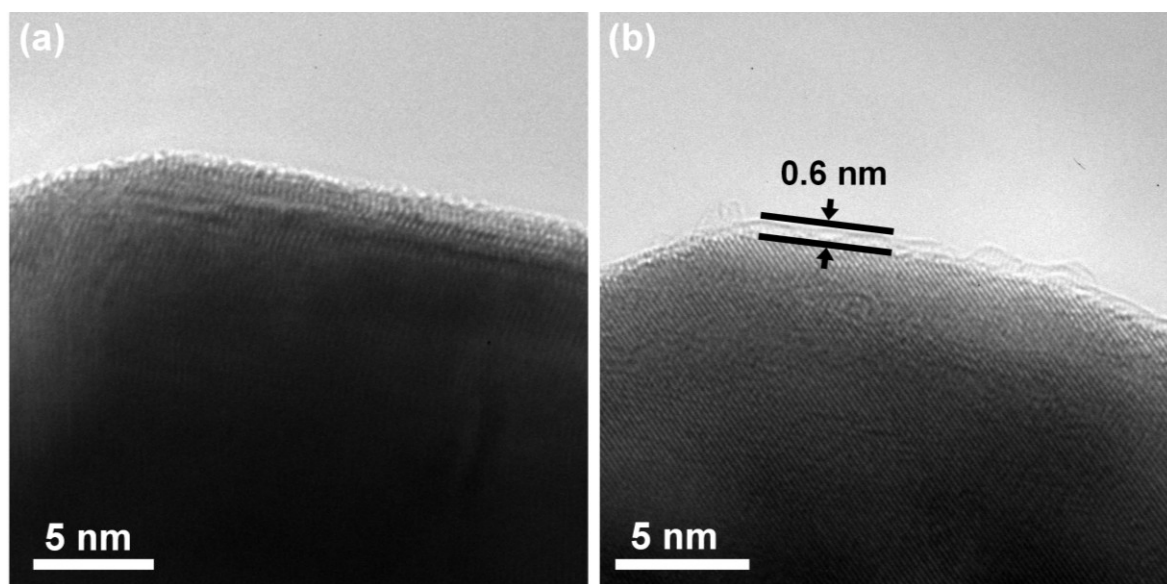


Fig. 35: TEM images of (a) an untreated WC microparticle and (b) a WC microparticle functionalized with 3-APP. A monolayer of 3-APP is visible on the particle surface.

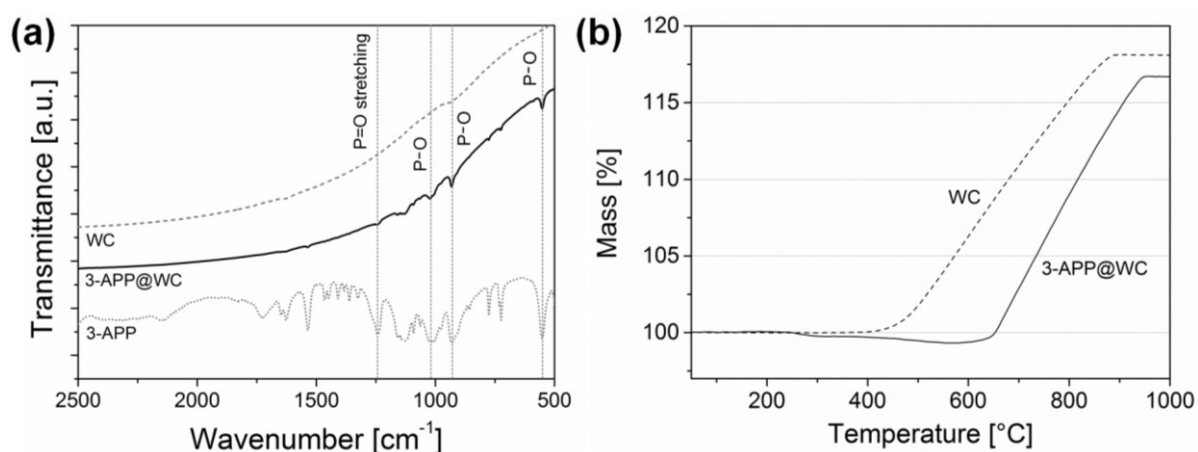


Fig. 36: (a) FTIR spectra of pristine tungsten carbide microparticles, 3-APP functionalized tungsten carbide microparticles and pure 3-APP as a reference. (b) Thermogravimetric analysis of the 3-APP functionalized WC microparticles and pristine WC microparticles as a reference.

The tungsten carbide microparticles functionalized with 3-APP were also investigated with FTIR spectroscopy and thermogravimetric analysis. Figure 36.a shows FTIR spectra of pristine tungsten carbide microparticles, 3-aminopropylphosphonic acid functionalized tungsten carbide microparticles and pure 3-aminopropylphosphonic acid as a reference. In the FTIR spectrum of the 3-APP functionalized WC microparticles, several broad absorption bands can be seen in the spectral region between 850 cm^{-1} and 1200 cm^{-1} , as in the 3-APP reference spectrum. These bands are assigned to the P–O stretching modes, while the weak absorption band at 1242 cm^{-1} is assigned to the P=O stretching vibration modes [166,167].

The decrease in intensity of the P=O band as compared to the P–O bands suggests that the bonding mode of the phosphonic acid on the WC particles surface involves the P=O group.

Figure 36.b shows the thermogravimetric analysis of the 3-APP functionalized WC microparticles and pristine WC microparticles as a reference. Pristine tungsten carbide microparticles are stable up to 400°C, when the oxidation of WC to WO₃ begins and a mass gain of about 18 % is observed [156], while tungsten carbide microparticles functionalized with 3-aminopropylphosphonic acid show also a mass loss of about 1.3 %. The mass loss starts at lower temperatures due to the decomposition of the organic 3-APP monolayer and continues in parallel with the WC oxidation up to 600°C, when the latter becomes dominant.

1.4 Functionalization with polydopamine

In this part, the results of the coating with polydopamine of alumina micro- and nanoparticles as well as tungsten carbide micro- and nanoparticles are shown. In contrast to 3-APP that forms monolayers and MPTES that forms both monolayers and small oligomers, polydopamine growth on a substrate surface up to several tens of nanometers in thickness. The polydopamine coating thickness for different polymerization times is systematically investigated with TEM and thermogravimetric analysis.

1.4.1 Polydopamine@Al₂O₃ nanoparticles

TEM images of Al₂O₃ nanoparticles before and after the functionalization with polydopamine are shown in figure 37. A thin and amorphous polydopamine coating can be seen on the surface of the crystalline Al₂O₃ nanoparticles, with a thickness of about 2 nm after 1 h of polymerization time, in good agreement with the expected thickness according to the data of Lee *et al.* [60]. The alumina nanoparticles coated with polydopamine were also investigated with FTIR spectroscopy. The FTIR spectra of the polydopamine coated alumina nanoparticles, pristine alumina nanoparticles and pure polydopamine (as reference) are shown in figure 38.a. In the FTIR spectrum of the polydopamine coated alumina nanoparticles, several absorption peaks can be seen in the spectral region between 1200 cm⁻¹ and 1600 cm⁻¹, as in the polydopamine reference.

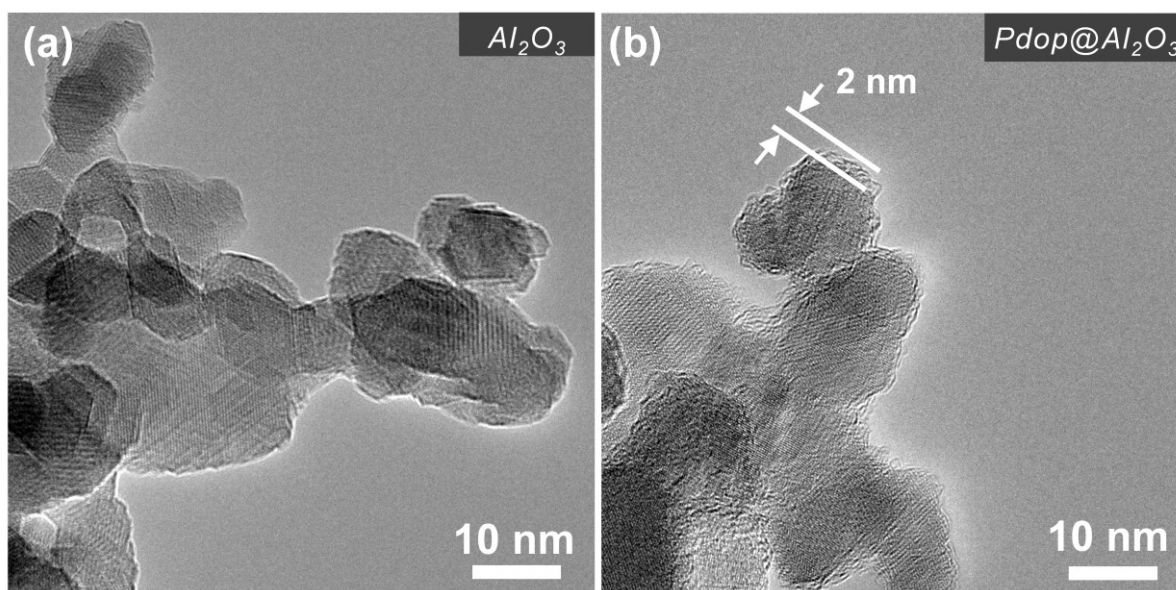


Fig. 37: TEM images of alumina nanoparticle (a) before and (b) after the coating with polydopamine. An amorphous polydopamine coating ca. 2 nm thick can be seen on the surface of the crystalline alumina nanoparticles after 1 h polymerization time.

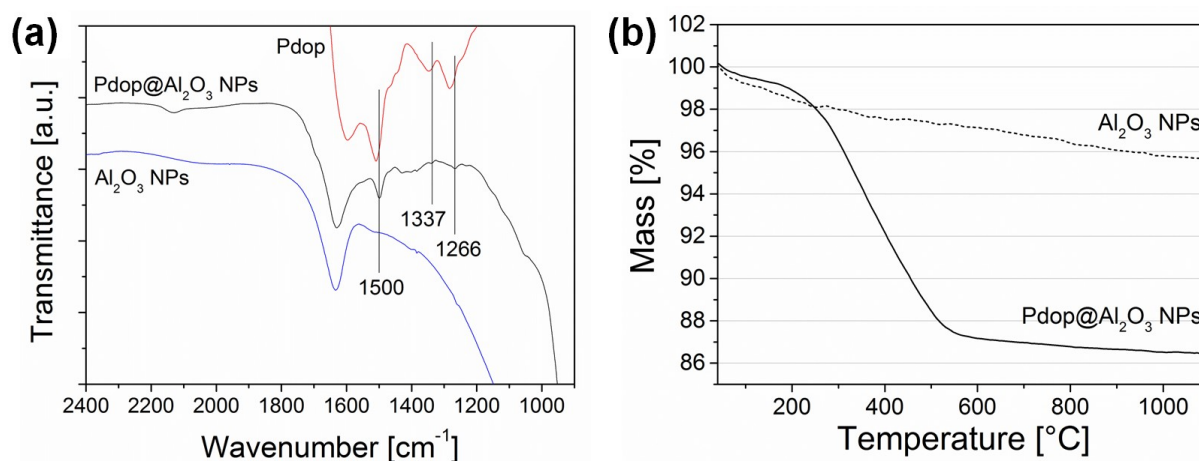


Fig. 38: (a) FTIR spectra of uncoated alumina nanoparticles, polydopamine coated alumina nanoparticles (1 h polymerization time) and pure polydopamine as a reference. (b) Thermogravimetric analysis of polydopamine coated alumina nanoparticles and uncoated alumina nanoparticles as a reference.

In particular, the strong absorption band at 1500 cm^{-1} is assigned to the shearing vibrations of the amino groups, while other peaks are partially covered by the broad absorption band of the Al_2O_3 nanoparticles. Interestingly, the absorptions bands of the polydopamine coated particles are slightly shifted to lower wavelengths as compared to pure polydopamine, suggesting a strong interaction of the polydopamine coating with the alumina particles surface, probably due to the high reactivity of the oxide nanoparticles.

Figure 38.b shows the thermogravimetric analysis of polydopamine coated alumina nanoparticles and uncoated alumina nanoparticles as a reference. Uncoated alumina nanoparticles show a mass loss of about 4.5 % due to the water bound on the Al-OH groups of the particle surface [154,155], whereas the coated alumina nanoparticles show a more substantial weight loss of about 13.5 % due to the decomposition of the polydopamine layer, at first at a slow rate followed by a higher rate up to 600°C, a trend also described in other works [80,81].

1.4.2 Polydopamine@Al₂O₃ microparticles

The coating of alumina microparticles with polydopamine was investigated by TEM and thermogravimetric analysis. TEM images showing the thickness of the polydopamine layer for different polymerization times are depicted in figure 39. The thickness increases linearly at about 6 nm/h until 5 h polymerization time, then the thickness increases at a much slower rate.

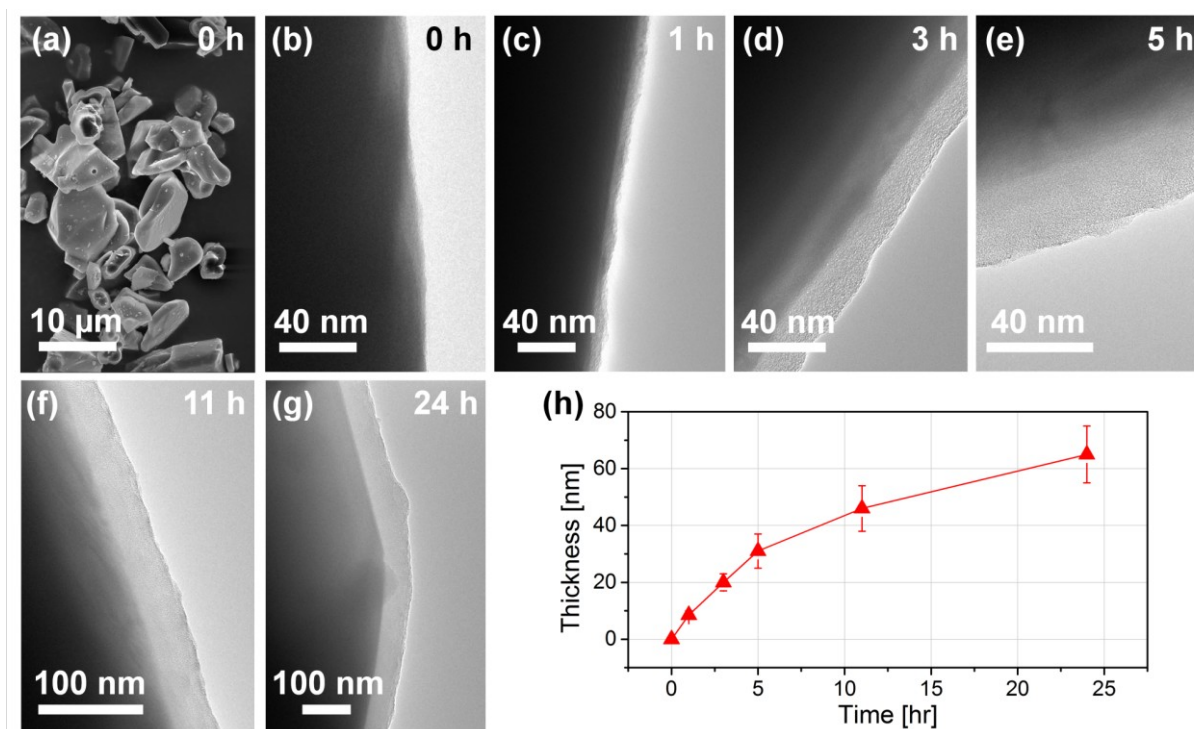


Fig. 39: (a) SEM image of uncoated alumina microparticles. (b-g) TEM images of the polydopamine coated alumina microparticles after 0 h, 1 h, 3h, 5 h, 11 h and 24 h polymerization time, respectively. (h) Thickness of the polydopamine coating (measured from the TEM pictures) against polymerization time.

This trend is in agreement with the data reported by Lee *et al.* [60], but a higher deposition rate is observed in the case of alumina microparticles, where a thickness of 65 ± 10 nm is reached after 24 h polymerization time, while only about 50 nm is reported by Lee *et al.* after the same polymerization time.

Figure 40.a shows the thermogravimetric analysis of polydopamine coated alumina microparticles for the different polymerization times. Uncoated alumina nanoparticles (0 h polymerization time) show a small mass loss of about 0.5 % due to the water bound on the Al-OH groups of the particle surface [154,155], while the polydopamine coated alumina microparticles show an increasing weight loss with increasing polymerization time, up to 6 %. This is due to the decomposition of the polydopamine coating, which takes place with a characteristic two-step trend: first a slow rate mass loss up to 250°C followed by a higher rate mass loss up to 600°C, as shown with polydopamine coated alumina nanoparticles and as reported in literature [80,81]. The polydopamine mass deposited on the alumina microparticles for different polymerization times was reported in figure 40.b. The deposited polydopamine mass was calculated as the difference between the mass loss of the polydopamine coated alumina particles and the uncoated alumina particles from figure 40.a. The results are in good agreement with the TEM analysis, i.e. the thicker the polydopamine coating the greater is the polydopamine mass deposited on the particles. Moreover, the polydopamine mass grow almost linearly at a rate of about 0.25 %/h. The results show that also the alumina microparticles can be coated with a uniform polydopamine layer and, in addition, the thickness of this layer can be accurately tuned from a few nanometers up to 65 ± 10 nm by changing the polymerization time.

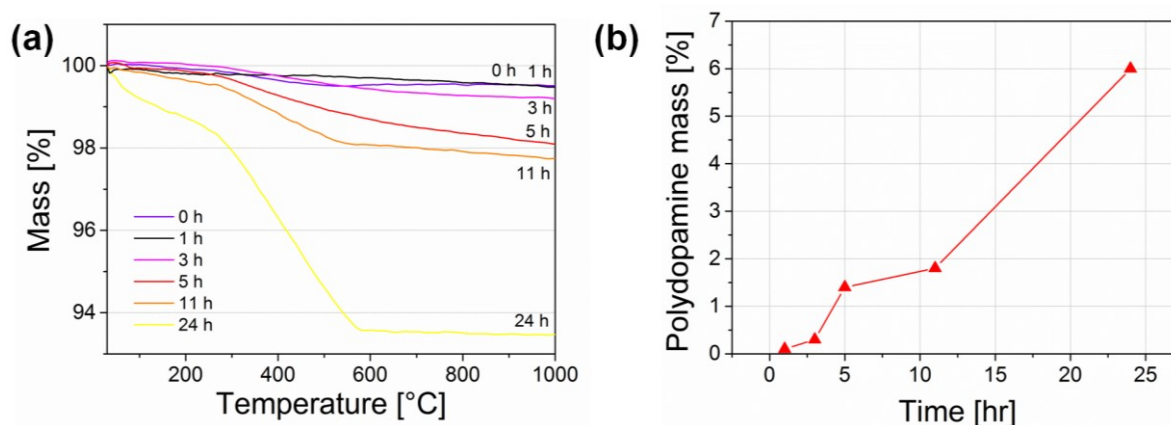


Fig. 40: (a) TGA curves of the uncoated (0 h) and the polydopamine coated alumina microparticles after 1 h, 3h, 5 h, 11 h and 24 h polymerization time. (b) Mass of the coated polydopamine on the alumina microparticles after different polymerization times, calculated from the TGA analysis in figure (a).

1.4.3 Polydopamine@WC nanoparticles

TEM images showing the thickness of the polydopamine layer for different polymerization times up to 24 h are shown in figure 41. The thickness increases almost linearly at about 1.4 nm/h over the whole polymerization time range investigated, unlike the coating of alumina microparticles where the thickness increases with a varying rate. This trend is not in agreement with the data reported by Lee *et al.* about the kinetics of dopamine polymerization [60], suggesting that at a nanoscale level another model is necessary to describe the polydopamine coating process.

Figure 42.a shows the thermogravimetric analysis of polydopamine coated WC nanoparticles for different polymerization times together with uncoated particles as reference (0 h polymerization time). Uncoated tungsten carbide nanoparticles are stable up to 400°C, when the oxidation of WC to WO₃ begins and a mass gain of about 18 % is observed [156]. On the other hand, polydopamine coated tungsten carbide nanoparticles exhibit also a mass loss at lower temperatures due to the decomposition of the organic polydopamine coating, with an increasing mass loss as the polymerization time increases.

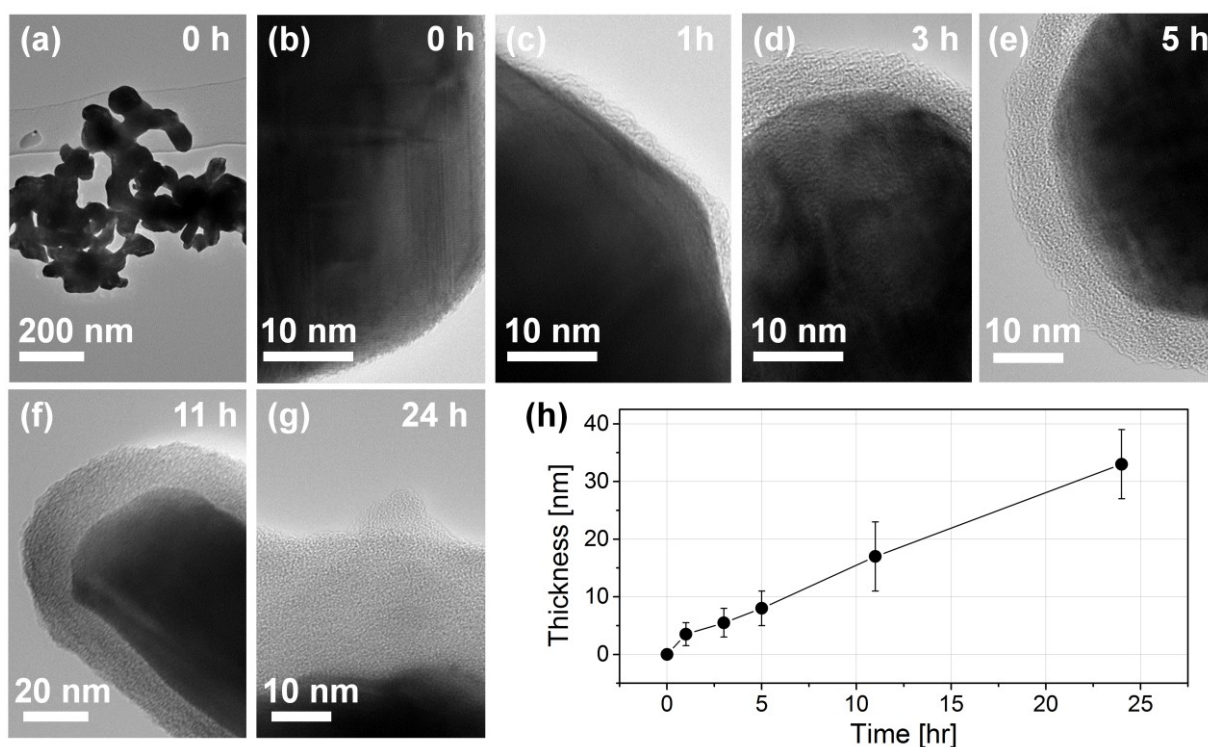


Fig. 41: (a,b) TEM images of uncoated tungsten carbide nanoparticles. (c-g) TEM images of the polydopamine coated tungsten carbide nanoparticles after 1 h, 3h, 5 h, 11 h and 24 h polymerization time, respectively. (h) Thickness of the polydopamine coating (measured from the TEM pictures) against polymerization time.

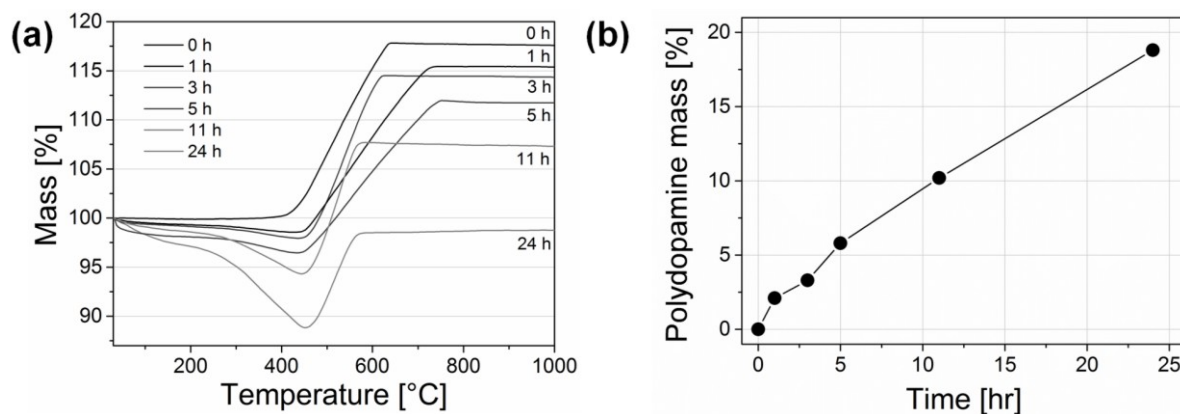


Fig. 42: (a) TGA curves of the uncoated (0 h) and the polydopamine coated tungsten carbide nanoparticles after 1 h, 3h, 5 h, 11 h and 24 h polymerization time. (b) Mass of the coated polydopamine on the tungsten carbide nanoparticles after different polymerization times, calculated from the TGA analysis in figure (a).

Also in this case, the characteristic two-step decomposition trend of polydopamine decomposition can be seen, with a slow rate mass loss up to 250°C followed by a higher rate mass loss that is partially covered in this case by the WC oxidation reaction. The mass increase due to WC oxidation to WO_3 stops for different samples at different temperatures. This is related to the different average particle size of the investigated samples: particles with a smaller average size oxidize faster than particles with a bigger average size [168]. Since all the WC samples used in this work come from the same batch, the difference in average particle size was probably produced by washing and centrifuging the different samples with slightly different procedures.

The mass of the polydopamine deposited on the tungsten carbide nanoparticles for different polymerization times is reported in figure 42.b. The deposited polydopamine mass was again calculated as the difference between the mass loss of the polydopamine coated WC nanoparticles and the mass loss of the uncoated WC nanoparticles from figure 42.a. The results are in good agreement with the TEM analysis, i.e. the thicker the polydopamine coating the greater is the polydopamine mass deposited on the WC nanoparticles. In addition, the deposited polydopamine mass grows almost linearly at a rate of 0.8 %/h up to 19 % after 24 h polymerization time. The results show that also the tungsten carbide nanoparticles can be coated with a uniform polydopamine layer of tunable thickness from a few nanometers up to 33 ± 6 nm. Surprisingly, dopamine grows at a slower rate on WC nanoparticles as on Al_2O_3 microparticles and with a different growth trend. This is probably due to the fact that WC is more chemically inert than alumina.

1.4.4 Polydopamine@WC microparticles

TEM images showing the thickness of the polydopamine layer for different polymerization times from 1 h up to 24 h are depicted in figure 43. The thickness increases linearly at about 1.5 nm/h until 5 h polymerization time, then the thickness increases at a much slower rate. This trend is in agreement with the polydopamine growth on alumina microparticles and the data reported by Lee et al. [60], however, a much slower deposition rate is observed in the case of tungsten carbide microparticles, where a thickness of 18 ± 4 nm is reached after 24 h polymerization time, while 50 nm is reported by Lee et al. and a thickness of 65 ± 10 nm is reached in the case of alumina microparticles.

Figure 44.a shows the thermogravimetric analysis of polydopamine coated tungsten carbide microparticles for different polymerization times together with uncoated particles as reference (0 h polymerization time). Uncoated tungsten carbide microparticles are stable up to 400°C, when the oxidation of WC to WO_3 begins and a mass gain of about 18 % is observed [156]. Polydopamine coated tungsten carbide microparticles show also a mass loss at lower temperatures due to the decomposition of the organic polydopamine coating, with an increasing mass loss as the polymerization time increases, similar to the case of WC nanoparticles.

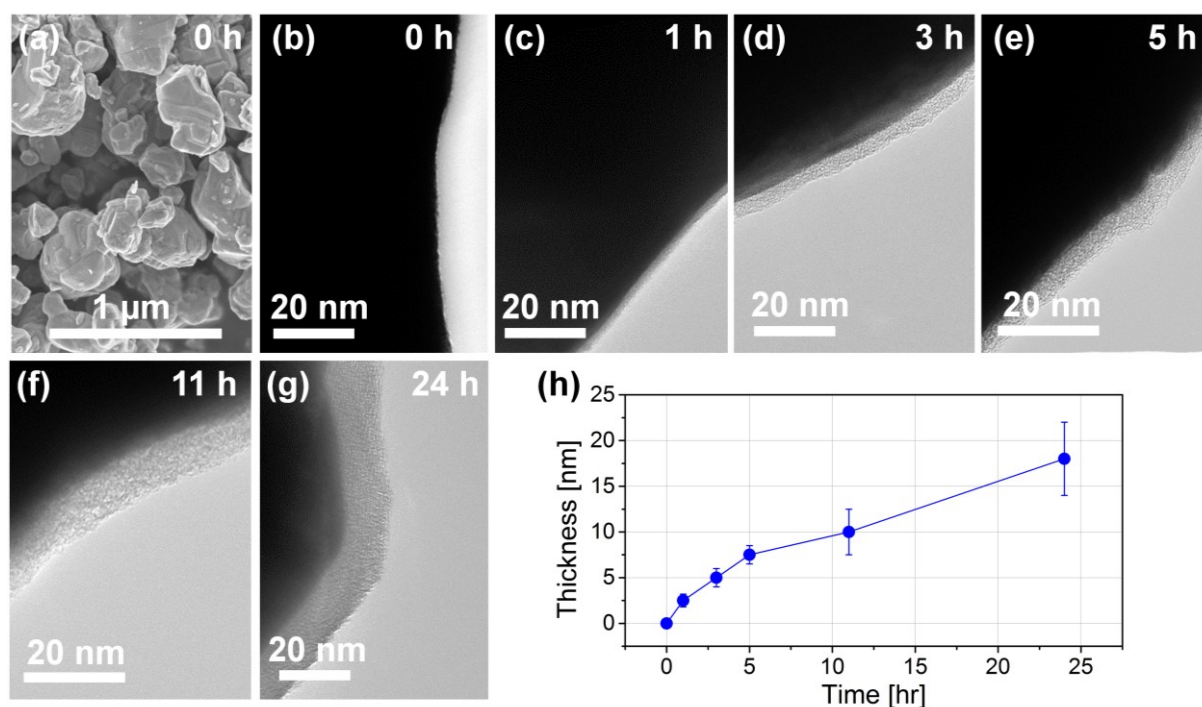


Fig. 43: (a) SEM image of uncoated tungsten carbide microparticles. (b-g) TEM images of the polydopamine coated tungsten carbide microparticles after 0 h, 1 h, 3h, 5 h, 11 h and 24 h polymerization time, respectively. (h) Thickness of the polydopamine coating (measured from the TEM pictures) against polymerization time.

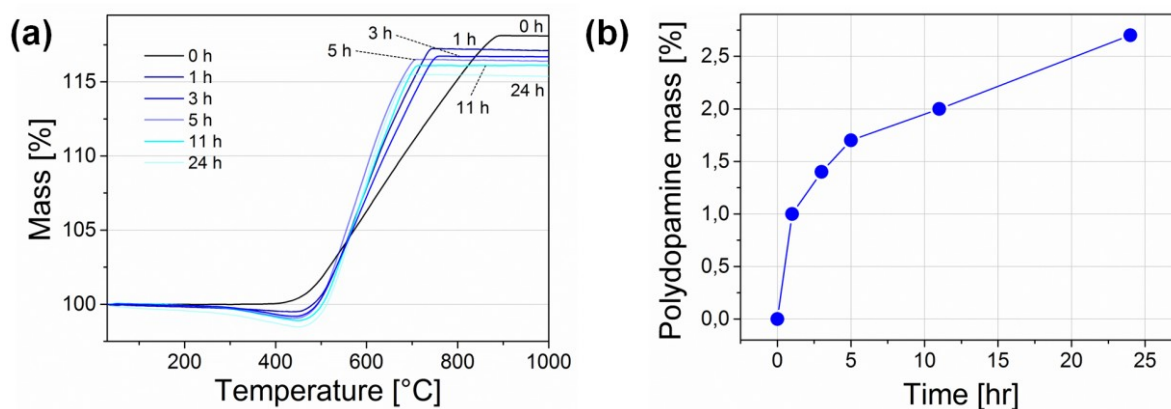


Fig. 44: (a) TGA curves of the uncoated (0 h) and the polydopamine coated tungsten carbide microparticles after 1 h, 3h, 5 h, 11 h and 24 h polymerization time. (b) Mass of the coated polydopamine on the tungsten carbide microparticles after different polymerization times, calculated from the TGA analysis in figure (a).

Again, the characteristic two-step decomposition trend of polydopamine can be seen, with a slow rate mass loss up to 250°C followed by a higher rate mass loss that is partially covered by the WC oxidation reaction. As in the case of the WC nanoparticles, the mass increase due to WC oxidation to WO_3 stops for different samples at different temperatures because of a different average particle size between the samples, probably produced by washing and centrifuging the different particles with slightly different procedures. The mass of the polydopamine deposited on the tungsten carbide microparticles for different polymerization times is shown in figure 44.b. The results are in good agreement with the TEM analysis, i.e. the thicker the polydopamine coating the higher is the polydopamine mass deposited on the WC microparticles. In this case, the deposited polydopamine mass grow non-linearly, i.e. at first a sharp increase in the polydopamine mass content takes place, followed by a much slower increase.

Polydopamine coated WC microparticles were also characterized with SEM. Unlike the Al_2O_3 particles, they show very flat and clean surfaces which are optimal to study the morphology of the polydopamine coating. Figures 45.a and b show uncoated WC particles, characterized by flat surfaces and sharp edges, while figures 45.c and d show polydopamine coated WC microparticles with 24 h polymerization time. The coated particles have smoothed edges and corners, and the surface shows a fine granularity, as reported in other works in the literature [77,85]. The tungsten carbide microparticles coated with polydopamine were also investigated with FTIR spectroscopy. The FTIR spectra of the polydopamine coated WC microparticles, pristine WC microparticles and pure polydopamine (as reference) are shown in figure 46. In the FTIR spectrum of the polydopamine coated WC microparticles, several absorption peaks can be seen in the spectral region between 1000 cm^{-1} and 1600 cm^{-1} , as in

the polydopamine reference spectrum. The absorption bands at 1518 cm^{-1} , 1336 cm^{-1} and 1078 cm^{-1} are assigned to the N–H shearing vibrations mode, aromatic rings absorption and stretching vibrations mode of C–OH groups, respectively [80,169,170]. Moreover, dopamine has several strong IR absorption bands at wavelengths higher than 1600 cm^{-1} , but none of them are observed in figure 46, suggesting that all dopamine molecules were removed or effectively polymerized [65,80].

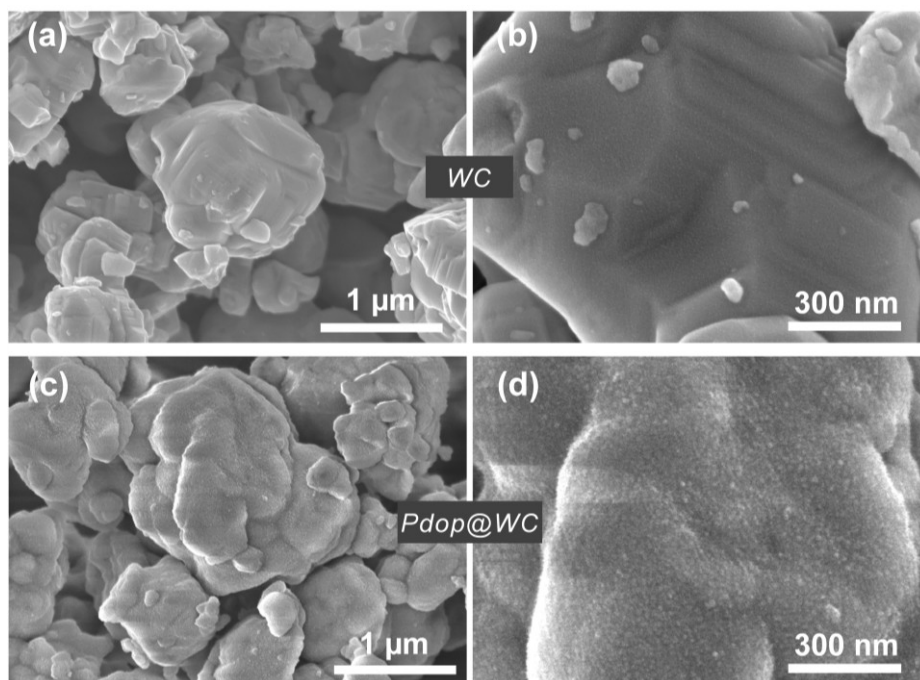


Fig. 45: SEM images of (a,b) uncoated WC microparticles and (c,d) polydopamine coated WC microparticles with 24 h polymerization time.

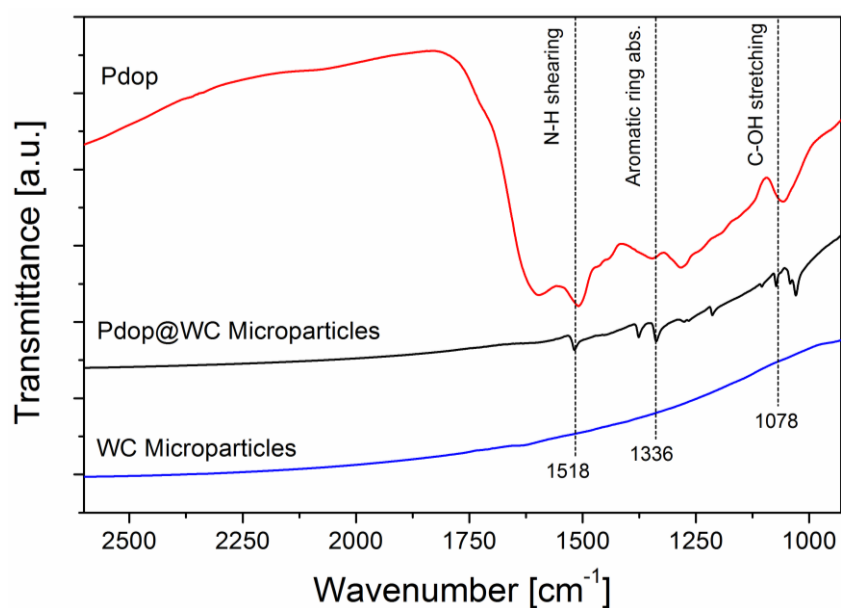


Fig. 46: FTIR spectra of polydopamine coated WC microparticles, uncoated WC particles and pure polydopamine as a reference.

In figure 47 all the results regarding the polydopamine coating process are summarized, together with the model introduced by Lee *et al.* Given a similar size of the substrate, these results indicate that in the same conditions polydopamine deposits three times faster on alumina microparticles than on tungsten carbide microparticles, suggesting that the thickness of polydopamine coatings is not substrate independent as reported by Lee *et al.* [60]. Moreover, for the same material, in this case tungsten carbide, a thicker polydopamine layer is observed on nanoparticles as on microparticles, suggesting that also the size of the substrate play an important role, so far not explored in the literature. In addition, the polydopamine growth trend for alumina and WC microparticles is the same as the one reported by Lee *et al.*, while in the case of WC nanoparticles a different growth trend is observed, suggesting that at a nanoscale level another model is necessary to describe the polydopamine coating process. An explanation may be that different materials induce a different orientation of the first polydopamine oligomers that adhere on the particle surface, which in turn influence the orientation and hence the growth of the subsequent polydopamine layer. Also the catalytic activity of alumina, due to Lewis acidity of surface aluminium ions, might influence the process [171].

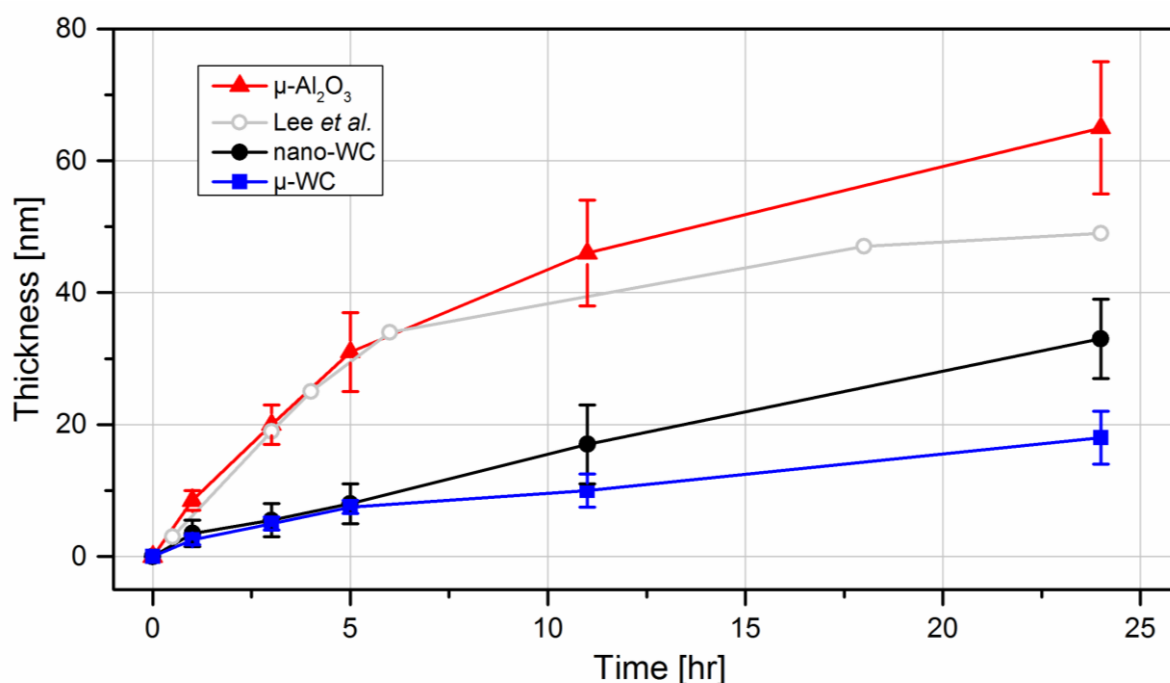


Fig. 47: Thickness of the polydopamine coating (measured from the TEM pictures) against polymerization time for the different substrates investigated in this work: alumina microparticles, tungsten carbide microparticles and nanoparticles. Also the data from the model introduced by Lee *et al.* are reported [60].

2. Metal plated particles

2.1 Silver coated particles

2.1.1 Ag@Pdop@WC microparticles

SEM images of the silver coated WC microparticles, pre-functionalized with polydopamine (24 h polymerization time), are shown in figure 48. The surface of the metal coated microparticles is much rougher than the pristine microparticles. Moreover, the WC microparticles are completely plated with a coarse metal coating, which has a granular morphology consisting of coalesced metal grains, distinctive of metal coatings deposited by electroless plating and other solution based processes [22,59,172,173]. The silver coated WC microparticles were also characterized by XRD. The thickness determination of the metal coating is not straightforward: the particles are too thick to be investigated with TEM and from SEM images only an approximate conjecture can be made. By comparing the SEM images before and after the plating process, it can be seen that the Ag coating has a relatively thin thickness (< 50 nm).

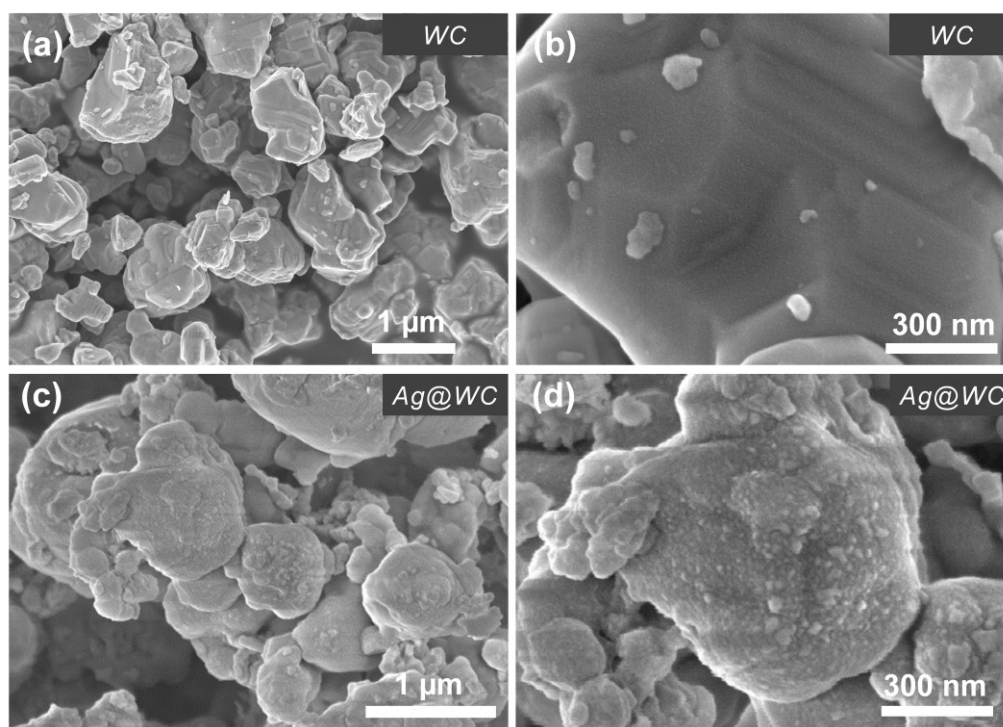


Fig. 48: (a,b) Pristine WC and (c,d) Ag coated WC microparticles, formerly functionalized with polydopamine.

Figure 49 shows the diffraction patterns of the pristine WC microparticles, polydopamine coated WC microparticles and Ag coated WC microparticles. The diffractogram of the Ag coated WC microparticles shows the diffraction peaks of WC along with four more peaks at 38.2° , 44.3° , 64.5° and 77.5° which correspond to the (111), (200), (220) and (311) lattice planes of silver (JCPDS 4-783), respectively. These results show that polydopamine functionalized WC microparticles can be coated with a coarse silver layer by electroless plating, however, the exact thickness of the silver layer can not be easily determined. SEM images indicate that the deposited silver coating has a relatively thin and irregular thickness.

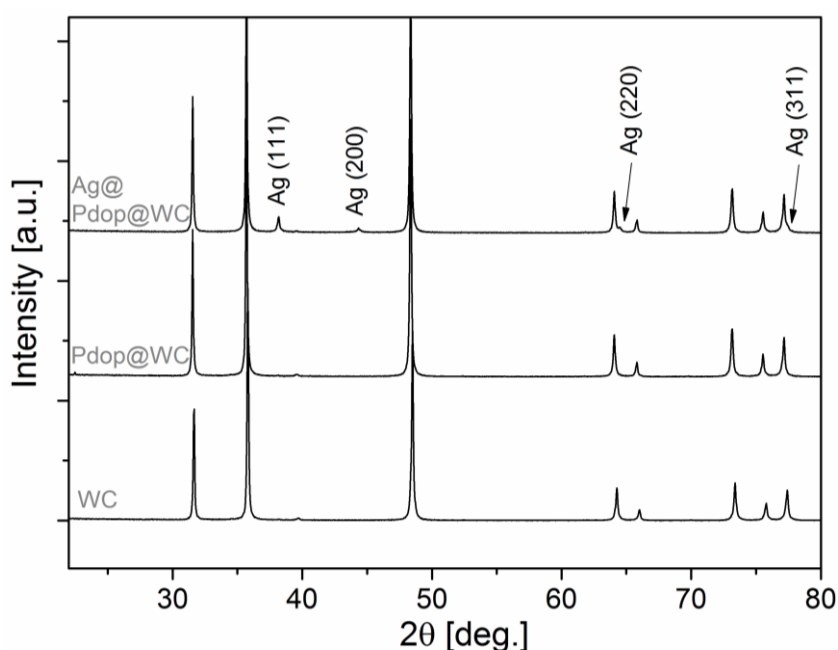


Fig. 49: XRD diffractograms of the pristine WC microparticles, polydopamine coated WC microparticles and silver coated WC microparticles.

2.2 Copper coated particles

2.2.1 Cu@MPTES@Al₂O₃ and Cu@MPTES@SiO₂ nanoparticles

SEM images of the uncoated and copper coated silica nanoparticles and alumina nanoparticles are shown in figures 50.a-d. An increase of the nanoparticle size after the copper plating is clearly visible.

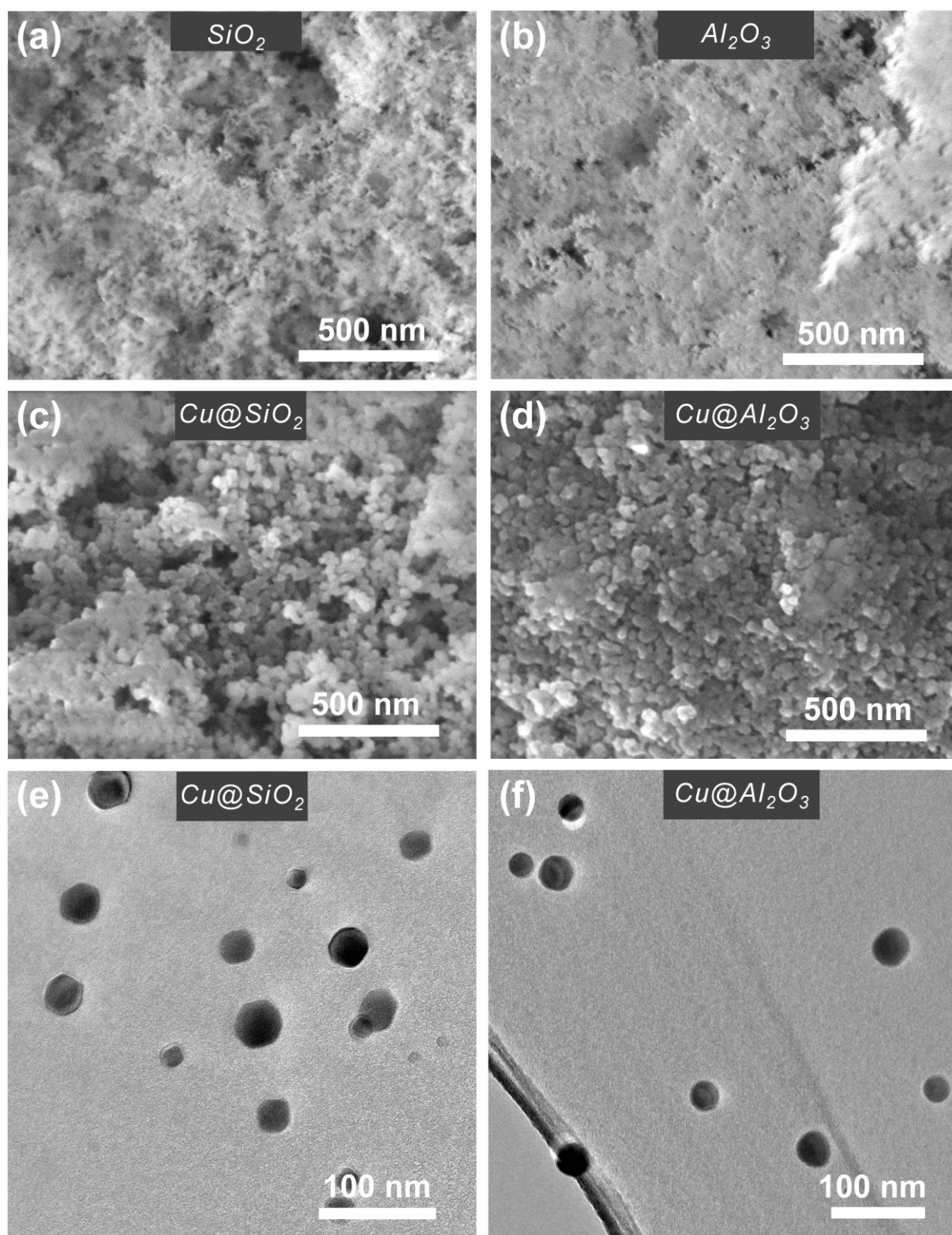


Fig. 50: SEM images of (a) pristine silica nanoparticles, (b) pristine alumina nanoparticles, (c) copper coated silica nanoparticles and (d) copper coated alumina nanoparticles. (e,f) TEM images of the copper plated silica nanoparticles and copper plated alumina nanoparticles, respectively. Both alumina and silica copper plated particles were pre-functionalized with MPTES.

Figure 50.e-f show TEM images of the copper plated silica nanoparticles and alumina nanoparticles, respectively. The plated nanoparticles have a size in the 30 – 50 nm range and a slightly irregular spherical shape. In addition, a weight increase of about 80 % after the copper electroless deposition process was observed. In figure 51.a and b are depicted SEM images with the respective EDX mapping for copper plated silica nanoparticles and copper plated alumina nanoparticles, respectively. From the EDX mapping images it can be seen that the copper (in green) and silicon (in cyan) from figure 51.a as well as copper and aluminum (in red) from figure 51.b are uniformly distributed, indicating that the nanoparticles are homogeneously coated with copper.

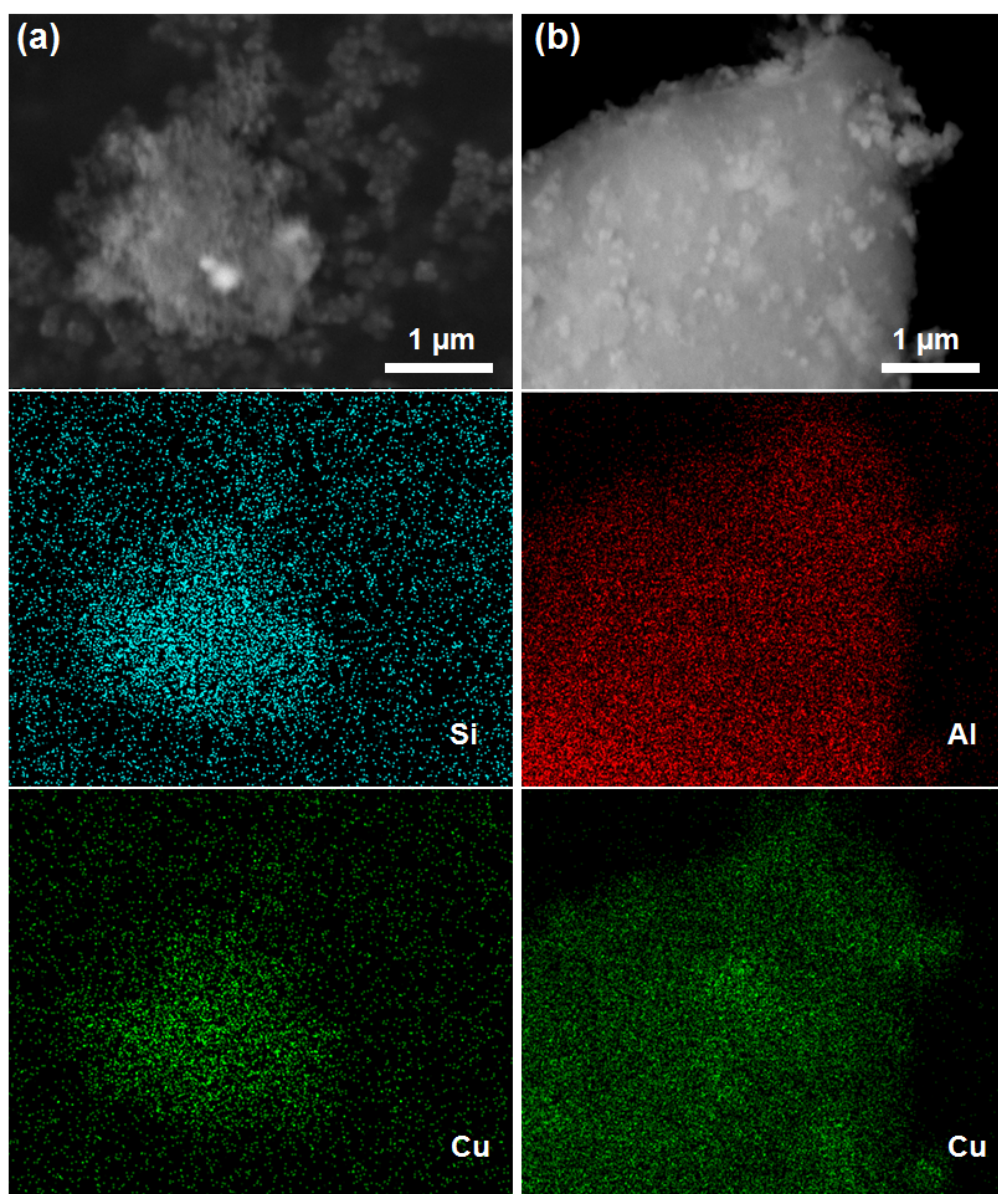


Fig. 51: SEM image and the respective EDX mapping for (a) copper coated silica nanoparticles and (b) copper coated alumina nanoparticles.

The copper coated Al_2O_3 and SiO_2 nanoparticles were also characterized by X-ray diffraction. Figure 52.a shows the diffractograms of pristine and copper coated silica nanoparticles. In the diffractogram of pristine silica nanoparticles, only the characteristic broad peak of amorphous SiO_2 at low angles can be seen, whereas the diffractogram of the copper coated silica nanoparticles shows also three diffraction peaks at 43.3° , 50.5° and 74.2° , which are assigned to the (111), (200) and (220) lattice planes of copper (JCPDS 4-836), respectively. Similarly, figure 52.b shows the diffractograms of pristine and copper coated alumina nanoparticles. In the diffractogram of pristine alumina nanoparticles only the diffraction peaks of $\delta\text{-Al}_2\text{O}_3$ can be seen, whereas the diffractogram of the copper coated alumina nanoparticles shows also the three copper diffraction peaks at 43.4° , 50.6° and 74.3° . These results reveal that silica and alumina nanoparticles functionalized with MPTES can be coated with a copper layer by electroless plating with a thickness of about 10-25 nm [145].

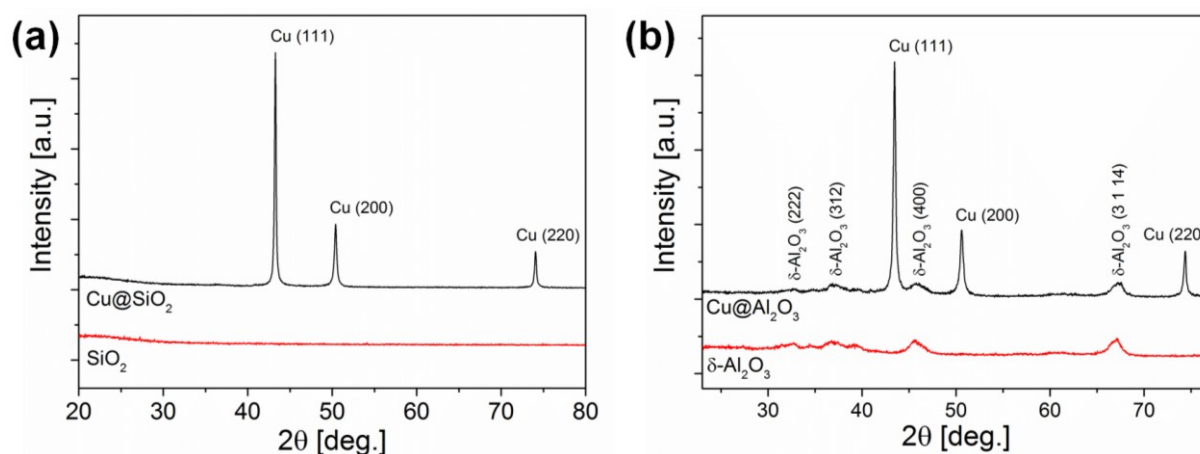


Fig. 52: (a) XRD diffractograms of the pristine silica nanoparticles and copper coated silica nanoparticles, pre-functionalized with MPTES. (b) XRD diffractograms of the pristine alumina nanoparticles and copper coated alumina nanoparticles, pre-functionalized with MPTES.

2.2.2 Cu@3-APP@WC microparticles

SEM images of the copper coated tungsten carbide microparticles are shown in figure 53. The metal coated tungsten carbide microparticles are plated with a grainy copper coating, which has a rough morphology consisting of coalesced metal grains, peculiar of metal coatings deposited by electroless plating and other solution based processes [22,59,172,173]. The copper coated WC microparticles were additionally characterized by X-ray diffraction.

Figure 54 shows the diffraction patterns of copper coated WC microparticles. The diffraction peaks of tungsten carbide (JCPDS 25-1047) at 48.4° , 64.0° , 65.8° , 73.0° , 75.5° and 77.0° can be seen along with the copper (JCPDS 4-836) diffraction peaks at 43.3° , 50.4° and 74.1° , indicating a successful deposition process. These results show that 3-aminopropylphosphonic acid functionalized WC microparticles can be coated with a rough copper layer by electroless plating, however, as in the case of silver plated WC microparticles, the exact thickness of the metal can not be easily determined: the particles are too thick to be analyzed with TEM and from SEM images only an approximate conjecture can be made. By comparing the SEM images before and after the plating process, it can be seen that the deposited copper coating has a relatively thin and irregular thickness of about 50 nm.

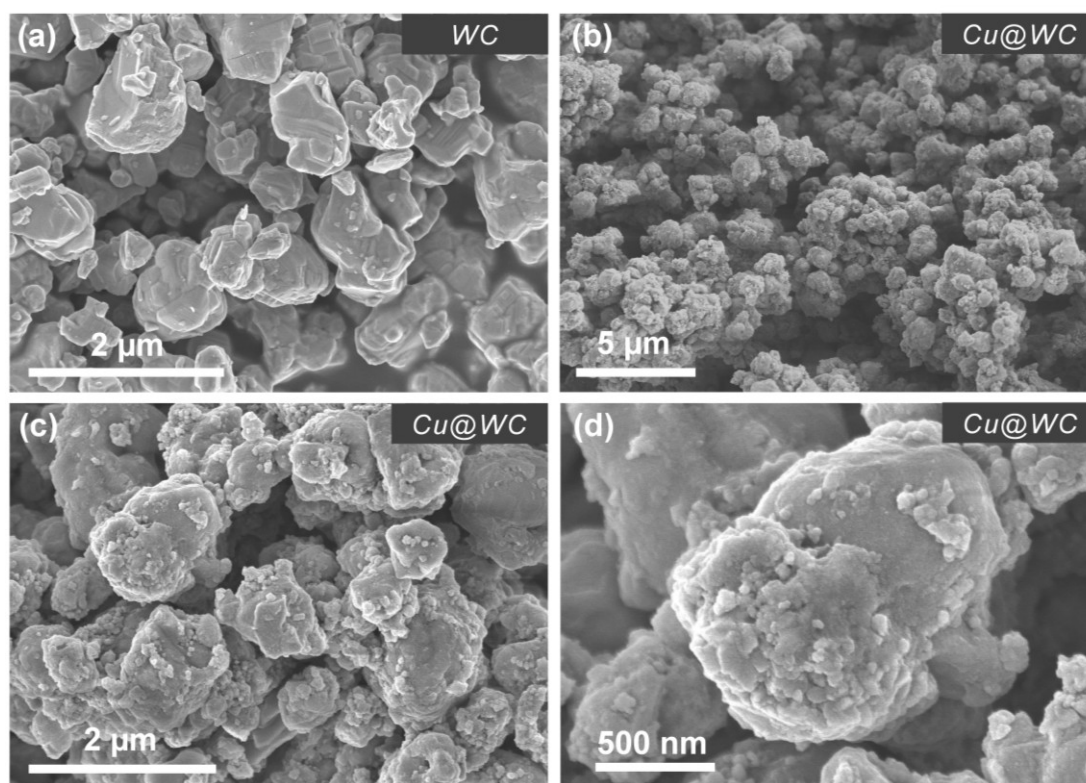


Fig. 53: SEM images of (a) pristine tungsten carbide microparticles. (b-d) Copper coated tungsten carbide microparticles, pre-functionalized with 3-APP.

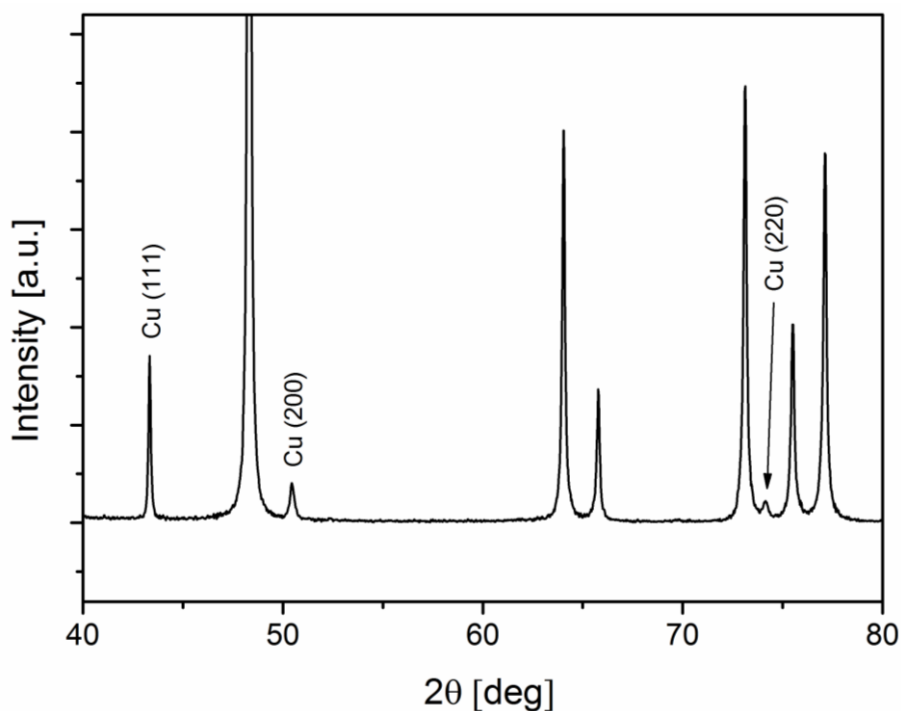


Fig. 54: XRD diffractogram of the copper coated WC microparticles, pre-functionalized with 3-APP.

2.2.3 Cu@Pdop@Al₂O₃ nanoparticles

SEM images of the uncoated and copper coated alumina nanoparticles are shown in figure 55.a und 55.b, respectively. An increase of the nanoparticles size up to around 30-40 nm after the copper plating is clearly visible. Figure 55.c shows a TEM image of the copper plated alumina nanoparticles, while in figure 55.d the related particle size distribution histogram for a population of 40 nanoparticles is shown. The coated nanoparticles have an irregular spherical shape and a size in the 20-40 nm range, in agreement with the average particle size observed in the SEM image from figure 55.b. In figure 56 is depicted a SEM image with the respective EDX mapping for of the copper plated alumina nanoparticles. It can be seen that the copper (in cyan) and aluminum (in red) are uniformly distributed, indicating that the nanoparticles are uniformly coated with copper.

The copper coated alumina nanoparticles were also characterized by X-ray diffraction. Figure 57 shows the diffraction patterns of the pristine Al₂O₃ nanoparticles, polydopamine coated Al₂O₃ nanoparticles and copper plated Al₂O₃ nanoparticles. The diffractogram of copper coated alumina nanoparticles shows the broad diffraction peaks of δ -Al₂O₃ (JCPDS 4-877) along with three more peaks at 43.3°, 50.4° and 74.1° which correspond to the (111), (200) and (220) lattice planes of copper (JCPDS 4-836), respectively, demonstrating the successful

copper coating. These results show that alumina nanoparticles functionalized with polydopamine can be uniformly plated by electroless plating with a copper coating with an average thickness of about 10-20 nm [146].

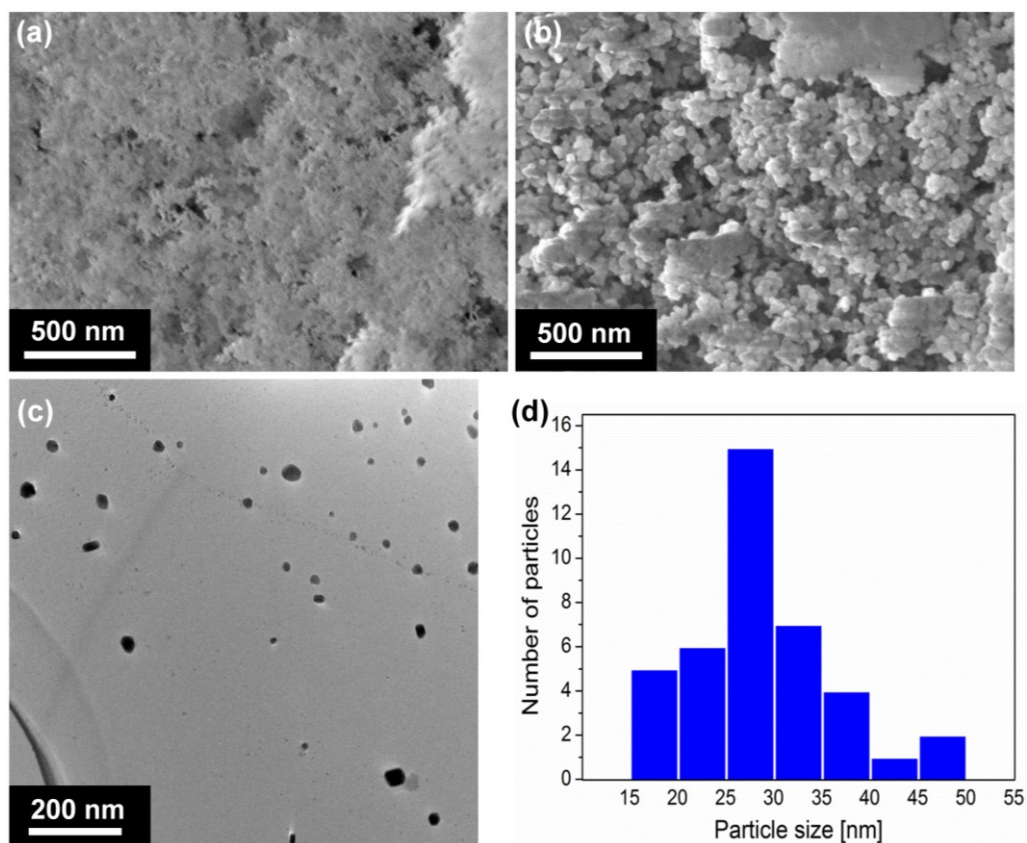


Fig. 55: SEM images of (a) pristine alumina nanoparticles and (b) copper coated alumina nanoparticles, pre-functionalized with polydopamine. (c) TEM image of the copper coated alumina nanoparticles and (d) the related particle size distribution histogram (for a population of 40 nanoparticles).

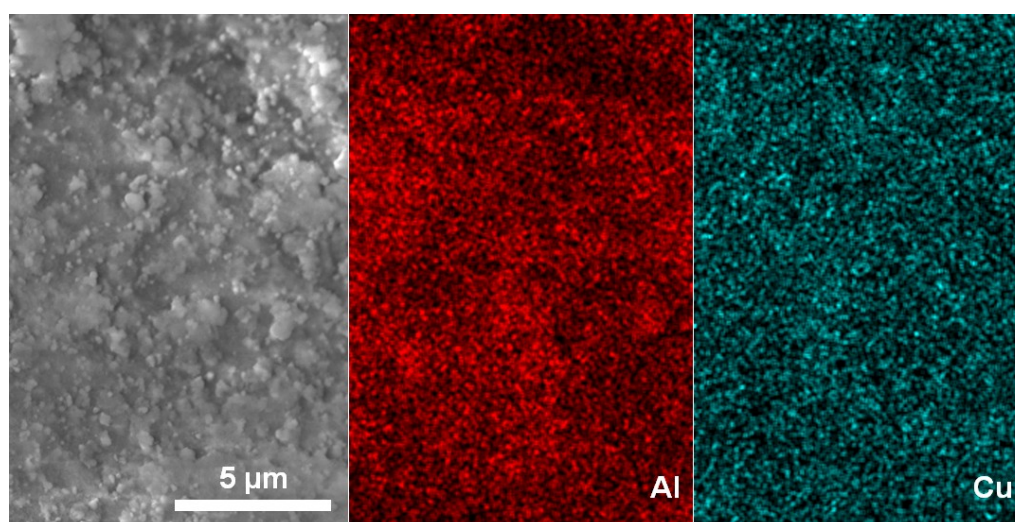


Fig. 56: SEM and the respective EDX mapping images for copper coated alumina nanoparticles, pre-functionalized with polydopamine.

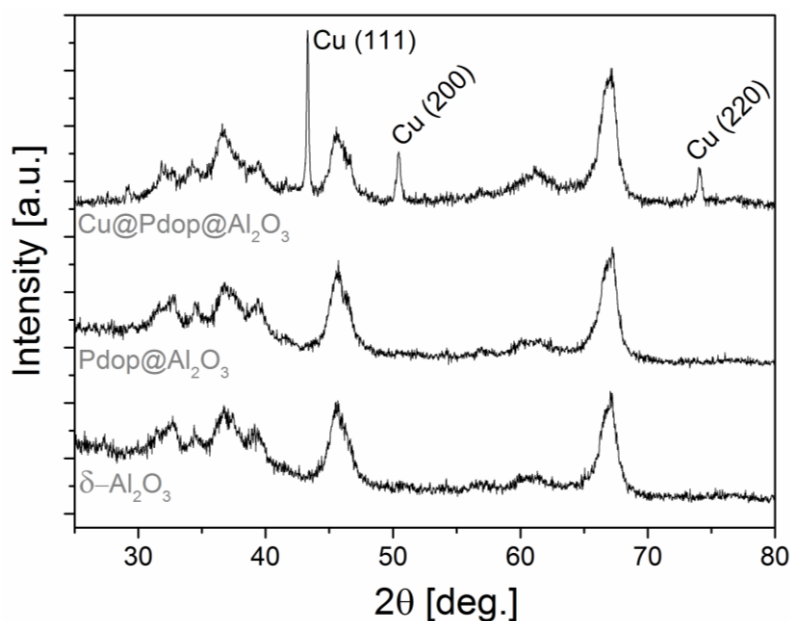


Fig. 57: X-ray diffractograms of the pristine Al_2O_3 nanoparticles, polydopamine coated Al_2O_3 nanoparticles and copper coated Al_2O_3 nanoparticles.

2.2.4 Cu@Pdop@WC microparticles

Figure 58 show SEM images of the uncoated tungsten carbide microparticles and copper coated tungsten carbide microparticles pre-functionalized with polydopamine (24 h polymerization time). After the electroless deposition process the tungsten carbide microparticles are entirely plated with a grainy copper coating, which has a very rough morphology consisting of coalesced metal grains, characteristic of metal coatings deposited by electroless plating and other solution based processes [22,59,172,173]. The copper coated WC microparticles were also characterized by X-ray diffraction. Figure 59 shows the diffraction patterns of pristine WC microparticles, polydopamine functionalized WC microparticles and copper coated WC microparticles. In all diffraction patterns, the diffraction peaks of tungsten carbide (JCPDS 25-1047) at 31.5° , 35.7° , 48.4° , 64.0° , 65.8° , 73.0° , 75.5° and 77.0° can be seen. In the copper coated WC microparticles also three more peaks at 43.3° , 50.4° , and 74.1° are present, corresponding to the (111), (200), and (220) lattice planes of copper (JCPDS 4-836), indicating a successful deposition process. These results show that polydopamine functionalized tungsten carbide microparticles can be coated with a coarse and grainy copper layer by electroless plating, however, as in the case of silver plated WC microparticles, the exact thickness of the metal can not be easily determined. SEM images

indicate that the deposited silver coating has a relatively thin and irregular thickness of about 50 nm.

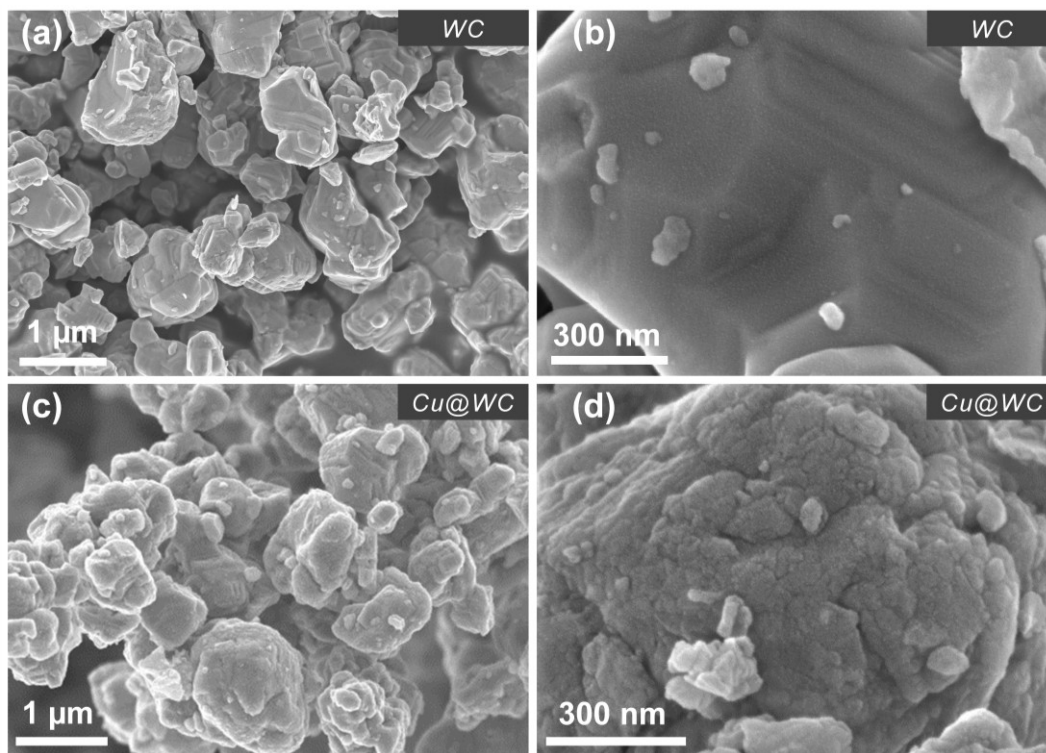


Fig. 58: SEM images of (a,b) pristine tungsten carbide microparticles and (c,d) copper coated tungsten carbide microparticles, pre-functionalized with polydopamine.

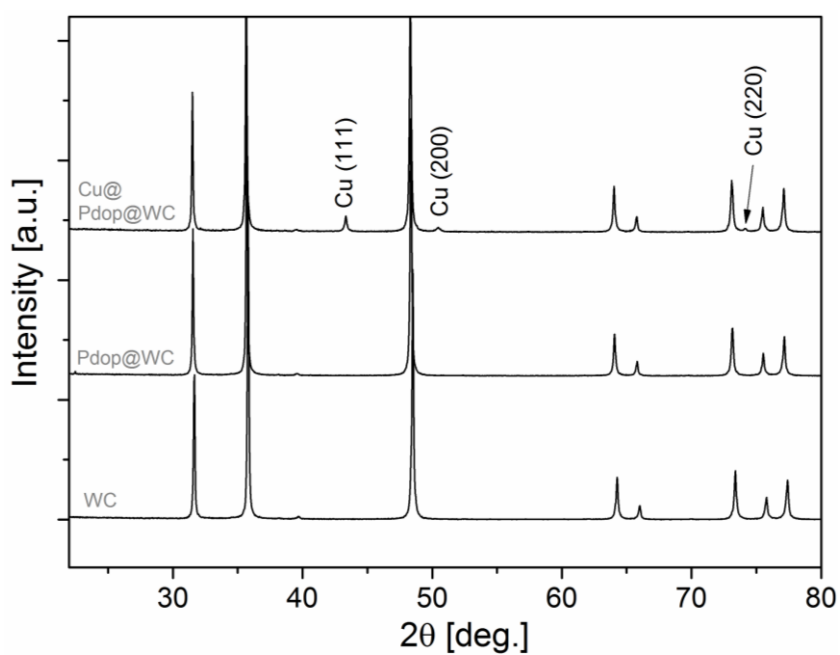


Fig. 59: XRD diffraction patterns of the pristine WC microparticles, polydopamine coated WC microparticles and copper coated WC microparticles.

2.3 Nickel coated particles

2.3.1 Ni@3-APP@WC microparticles

SEM images of the uncoated and nickel coated tungsten carbide microparticles are shown in figure 60. The plated WC microparticles are entirely covered with a grainy nickel coating, which has a rough morphology consisting of coalesced metal grains. Such metal coatings are peculiar of coatings deposited by electroless plating and other solution based processes [22,59,172,173], but in this case, the metal grains are smaller compared to the copper grains in the coatings shown in the previous chapters. EDX analysis shows a nickel content of 20 % in element weight percentage, but X-ray diffraction shows only the diffraction peaks of tungsten carbide. Nevertheless, the coated microparticles are magnetic, as shown in figure 60.d, demonstrating that a conformal nickel coating was achieved, since all the powder responded to the magnet. This indicates that the tungsten carbide particles are actually coated with nickel, which is amorphous because of the high boron content from the reducing agent NaBH_4 [2]. These results show that 3-aminopropylphosphonic acid functionalized WC microparticles can be coated with a conformal, noncrystalline and magnetic nickel layer made of coalesced fine particles.

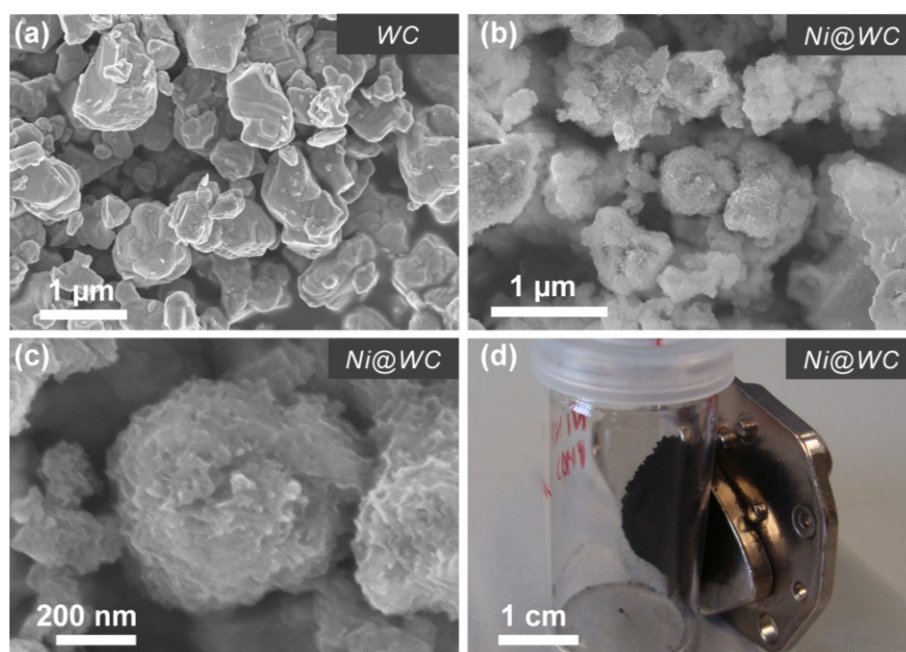


Fig. 60: SEM images of (a) pristine tungsten carbide microparticles and (b-c) nickel coated tungsten carbide microparticles, pre-functionalized with a monolayer of 3-APP. (d) A picture showing the magnetic properties of the nickel coated WC particles.

2.4 Cobalt-coated particles

2.4.1 Co@3-APP@WC microparticles

Figure 61 shows SEM images of the uncoated and cobalt coated tungsten carbide microparticles. The plated WC microparticles are entirely covered with a rough cobalt coating, which has a coarse grainy morphology consisting of coalesced metal grains, peculiar of metal coatings deposited by electroless plating and other solution based processes [22,59,172,173]. EDX analysis shows Co content of 14 % in element weight percentage, but X-ray diffraction shows only the peaks of WC, as in the case of nickel coated WC microparticles. The coated particles are however magnetic, as shown in figure 61.c, demonstrating that a conformal cobalt coating was achieved. The reason for the non-crystallinity is a high boron content coming from the reducing agent NaBH_4 , as in the nickel electroless plating process [2]. These results show that WC microparticles functionalized with 3-APP can be coated with a grainy cobalt layer made of coalesced fine particles. The cobalt coating is magnetic but noncrystalline probably because of the relatively high boron content.

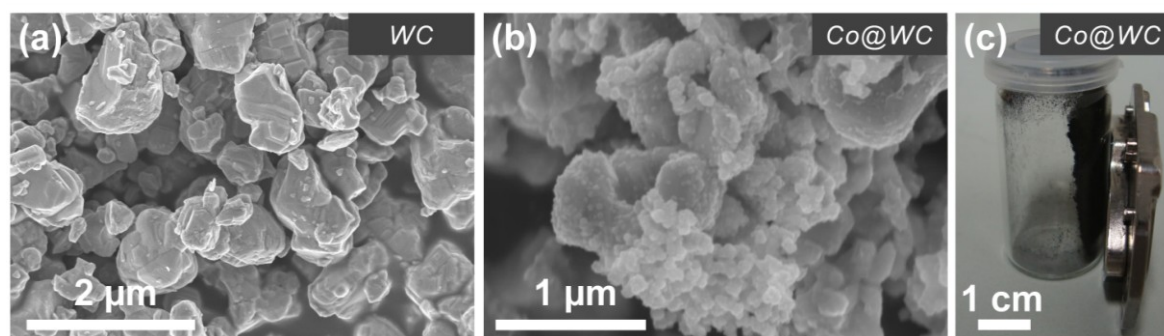


Fig. 61: SEM images of (a) pristine tungsten carbide microparticles and (b) cobalt coated tungsten carbide microparticles, pre-functionalized with a monolayer of 3-APP. (c) A picture showing the magnetic properties of the synthesized cobalt coated WC particles.

2.4.2 Co@Pdop@WC microparticles

Figure 62 show SEM images of the uncoated tungsten carbide microparticles and cobalt coated tungsten carbide microparticles pre-functionalized with polydopamine. After the electroless deposition process the tungsten carbide microparticles are covered with a thick and

coarse cobalt coating, which has a very grainy morphology consisting of coalesced metal grains, as the cobalt coated WC particles functionalized with 3-aminopropylphosphonic acid. Also in this case, EDX analysis shows a cobalt content of approximately 15 % in element weight percentage and X-ray diffraction shows only the diffraction peaks of tungsten carbide. The plated particles are nonetheless magnetic, and the reason for the non-crystallinity is probably also in this case a high boron content coming from the reducing agent NaBH_4 , as in the nickel electroless plating process [2]. These results show that polydopamine functionalized tungsten carbide microparticles can be coated with a rough cobalt layer made of coalesced fine particles.

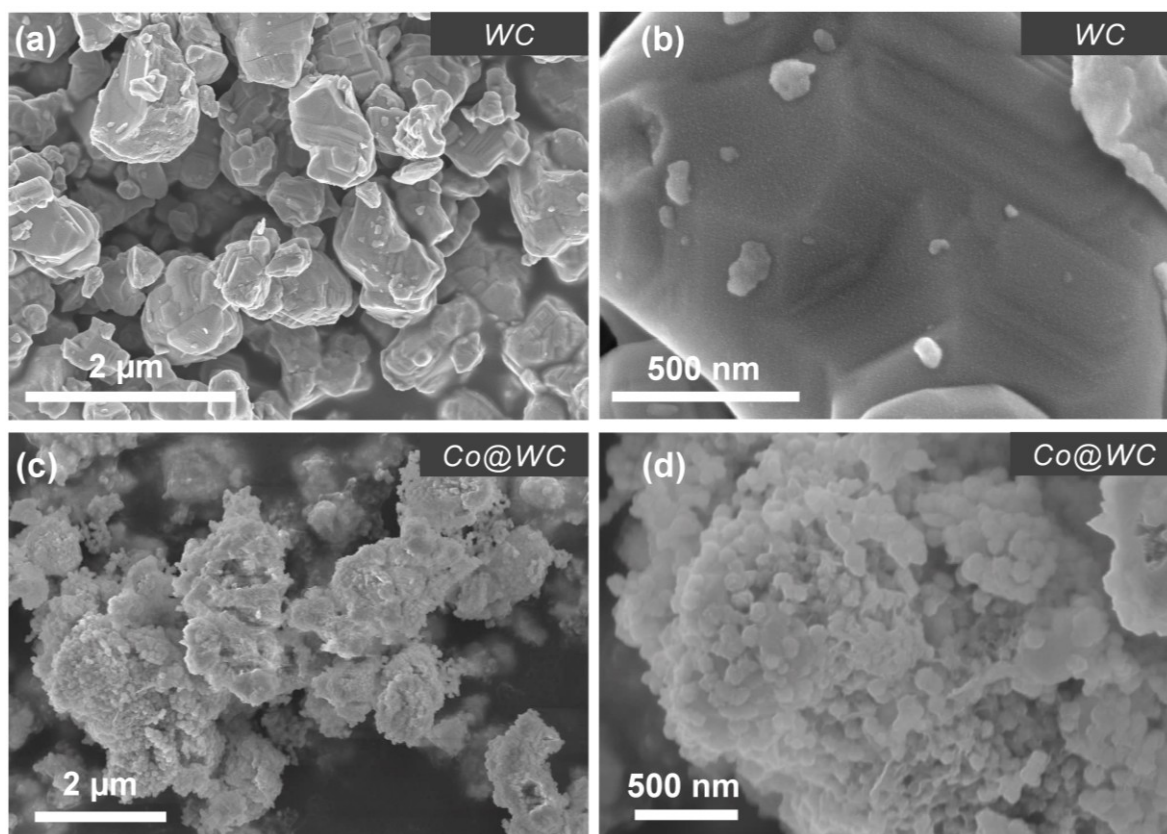


Fig. 62: SEM images of (a,b) pristine tungsten carbide microparticles and (c,d) cobalt coated tungsten carbide microparticles, pre-functionalized with polydopamine.

3. Metal matrix composites fabricated by powder metallurgy

3.1 Cu composites reinforced with Cu@Al₂O₃ nanoparticles

Copper matrix composites incorporating 1 wt% of copper plated alumina nanoparticles were successfully fabricated by powder metallurgy. The copper plated alumina nanoparticles were synthesized as described in chapter III.1.4.2 by using the MPTES functionalization method followed by electroless plating, while the composite fabrication was performed by CEP-Compound Extrusion Products GmbH and the Institute of joining technology and assembly of the Technical University of Dresden. In figure 63 are depicted SEM images with different magnification of a polished cross-section of the copper matrix composite reinforced with 1 wt% copper plated alumina nanoparticles. The nanoparticles (white spots) are well dispersed with some agglomerates in the submicron range, but the samples show also some degree of porosity, especially on the macroscopic level (black spots in fig. 63.a). Porosity, which is highly undesired since it drastically reduces the mechanical properties of the composite, probably originates from inaccurately dried nanoparticles or residual chemicals which evaporates during the extrusion process.

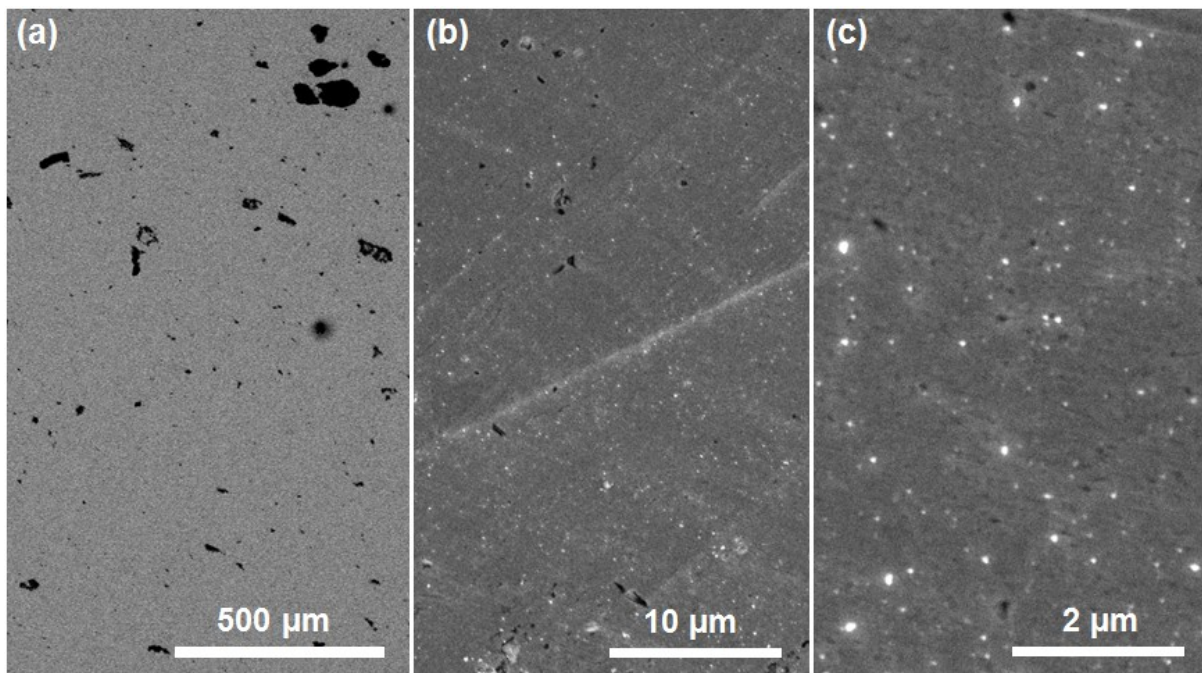


Fig. 63: SEM images of a polished cross-section of a copper matrix composite rod reinforced with 1 wt% copper plated alumina nanoparticles. Courtesy of C. Großmann, J. Zschetsche, U. Füssel (Institute of joining technology and assembly of the TU of Dresden).

3.2 Cu composites reinforced with Cu@WC microparticles

Copper matrix composites incorporating 1 wt% of copper plated tungsten carbide microparticles were successfully fabricated by powder metallurgy. The copper plated WC microparticles were synthesized as described in chapter III.1.4.2 by using the 3-APP functionalization method followed by electroless plating, while the composite fabrication was performed by the Institute of joining technology and assembly of the Technical University of Dresden. Figure 64 shows SEM images with different magnification of a polished cross-section of the copper matrix composite reinforced with 1 wt% copper plated tungsten carbide microparticles. The WC microparticles (white spots) are very well dispersed, however some black spots can also be seen. In this case it is not due to porosity, but simply to the detachment of WC particles during the polishing of the composite rods for SEM analysis.

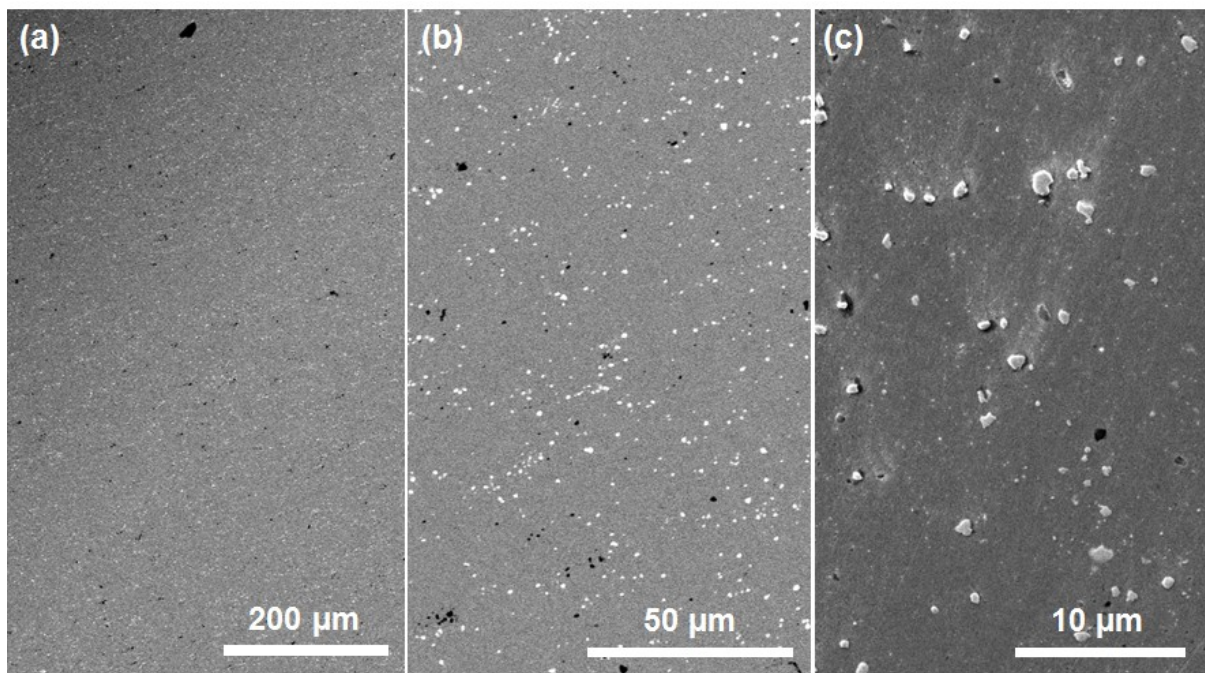


Fig. 64: SEM images of a polished cross-section of a copper matrix composite rod reinforced with 1 wt% copper plated tungsten carbide microparticles. Courtesy of C. Großmann, J. Zschetzsche, U. Füssel (Institute of joining technology and assembly of the TU of Dresden).

4. Silver structures by soft lithography

4.1 Microcontact printed 3-mercaptopropyltriethoxysilane

An AFM image of printed MPTES lines on a glass substrate using a stamp with 20 μm wide lines and 40 μm pitch is shown in figure 65, together with the respective cross-section taken along the white dotted line. The wide band crossing the picture from the lower left corner to the upper right corner is the unprinted glass substrate, while the MPTES printed regions are clearly visible in the bottom-right and top-left parts of the image. The unprinted region has a width of $20.0 \pm 0.1 \mu\text{m}$, in good agreement with the nominal width of 20 μm of the silicon master patterns. Moreover, the MPTES printed regions are very well delineated and distinguishable from the unprinted region in the middle of the picture. They show a roughness of $R_q = 3.5 \pm 0.6 \text{ nm}$ and $R_a = 1.3 \pm 0.4 \text{ nm}$, while the unprinted glass substrate has a roughness of $R_q = 0.6 \pm 0.1 \text{ nm}$ and $R_a = 0.5 \pm 0.1 \text{ nm}$. This implies the MPTES patterns printed by microcontact printing are not a well ordered monolayer.

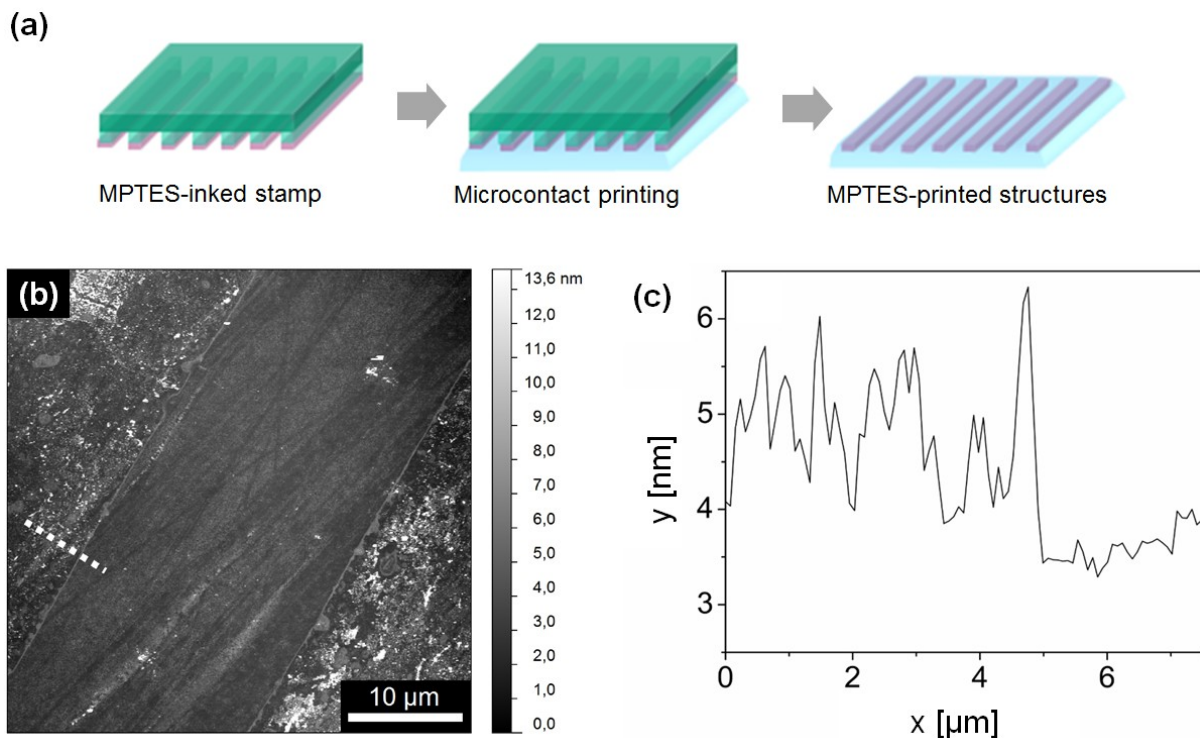


Fig. 65: (a) Schematic illustration of the MPTES microcontact printing process. (b) AFM image of a printed MPTES pattern (in this case lines with a width of 20 μm and a pitch of 40 μm) and (c) the cross-section profile along the white dotted line.

The higher roughness of the MPTES printed areas as compared with the glass substrate can be explained with the presence of both MPTES monolayer and MPTES aggregates of different sizes. As in the case of the MPTES functionalized nanoparticles, such aggregates with heights up to several nanometers are oligomers made of condensed MPTES molecules.

Since the ink is freshly prepared before each printing process, the presence of such aggregates is related to the ability of the microcontact printing method to promote chemical reactions and to simplify the formation of new chemical bonds, i.e. its ability to lower the kinetic barrier of a reaction [174]. In this case, the microcontact printing process promoted the condensation of single MPTES molecules into oligomers as a side effect of the MPTES patterning process, even though the contact time was only 500 s. These results show that MPTES molecules are well suited to be printed with a PDMS stamp by soft lithography, probably because of its good interaction with the polymeric stamp. The MPTES pattern is well defined and both regions where MPTES is printed as a monolayer as well as oligomers are present.

4.2 Ag structures on printed 3-mercaptopropyltriethoxysilane patterns

Figure 66 shows optical microscope images of the silver microstructures (dark-colored) fabricated by selective electroless plating on the previously printed MPTES patterns, i.e. lines with a width of 20 μm and a pitch of 40 μm , a regular grid of lines with a width of 5 μm and a 2D array of rings with an internal diameter of 10 μm , an external diameter of 20 μm and spaced 20 μm from each other. All the structures are well defined, uniform over large areas and there are no major defects like overgrowing or undesired interconnections of the structures. Moreover, the silver structures were plated over a relatively large area of 1 cm^2 .

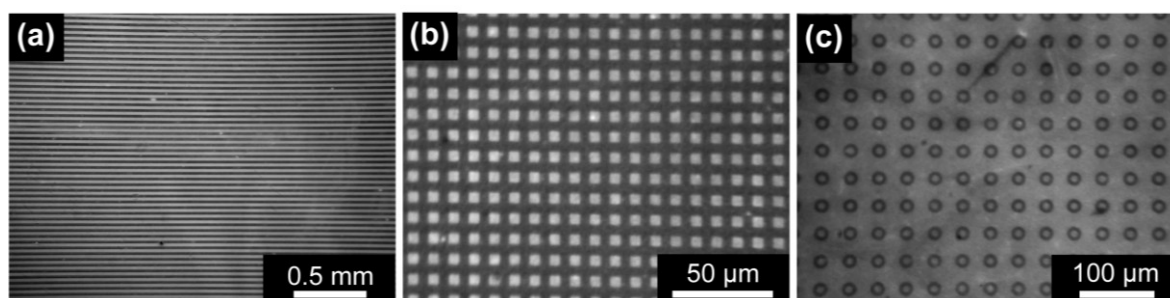


Fig. 66: Optical images of the silver structures (dark-colored) fabricated by electroless plating on the MPTES-printed glass substrates. (a) lines with a width of 20 μm and 40 μm pitch, (b) a regular grid of lines with a width of 5 μm , (c) a 2D array of rings with an internal diameter of 10 μm , an external diameter of 20 μm and spaced 20 μm from each other.

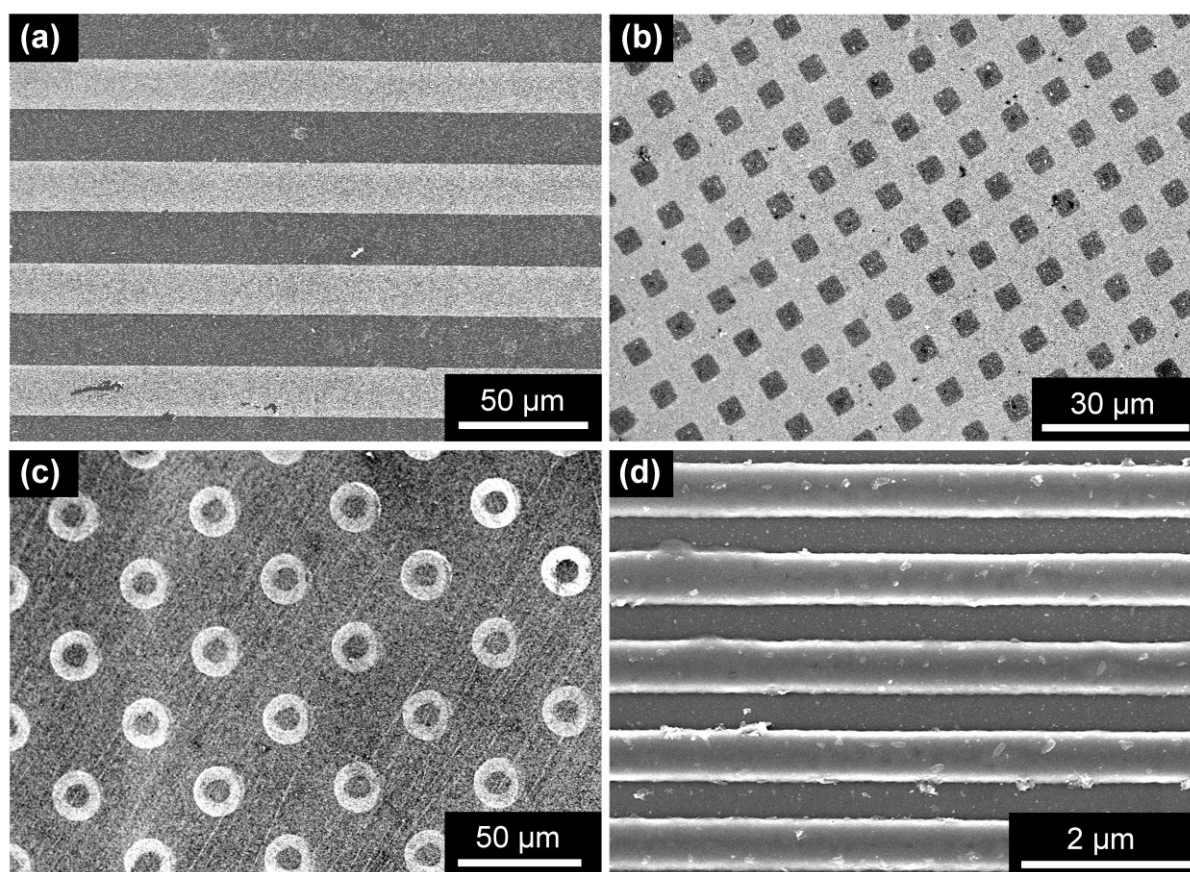


Fig. 67: SEM images of the silver structures (light-colored) fabricated by electroless plating on the MP TES-printed glass substrates. (a) lines with a width of 20 μm and 40 μm pitch, (b) a regular grid of lines with a width of 5 μm , (c) a 2D array of rings with an internal diameter of 10 μm , an external diameter of 20 μm and spaced 20 μm from each other, (d) lines with approximately a width of 500 nm and 1 μm pitch.

Figure 67.a-c shows SEM images of the same silver microstructures (colored in white). The patterns are continuous, well delineated over the entire printed area and in agreement with the stamps specifications. Small silver particles can be seen also on the glass substrates in the MP TES-free regions between the silver structures, evidencing a selectivity problem. On these regions the MP TES molecules were not printed and consequently no silver should be found there. The presence of silver particles on the MP TES-free regions is probably due to ink diffusion during the printing process or deposition of Ag particles formed in the plating bath. Figure 67.d shows a SEM image of silver structures fabricated with a PDMS stamp with a width of 500 nm and a pitch of 1 μm . These are the smallest silver structures made with this method, however a miniaturization into linewidths in the 0.1 – 0.5 μm range seems straightforward.

Figure 68.a is a high magnification SEM image of the structure from figure 67.a showing the morphology of the electroless plated silver. The surface appears very grainy and rough, and consists of coalesced silver particles, typical of the metal structures fabricated by electroless

deposition [4]. The size of the coalesced silver particles is 50 – 200 nm in width, whereas the thickness cannot be exactly estimated from the SEM images. The quality of the plated silver is confirmed by the X-ray diffraction pattern shown in figure 68.b, which shows the diffraction peaks of silver (JCPDS 4-783). AFM measurements show an irregular thickness ranging from 10 nm up to 50 nm due to the high roughness of the patterns, but also depending on the plating time and pattern size.

In addition, the silver structures are conductive and show a resistance of about 1 k Ω (measured with a two-point method, with contacts 1 cm apart). By comparison, a standard ITO-coated glass shows a sheet resistance of around 10 Ω /sq [132,182]. Such a high resistance value is probably explained by the high density of grain boundaries due to the granular silver structures. The selective deposition of silver structures by electroless plating shows that the thiol group of the printed MPTES molecules is effectively acting as a deposition catalyst, promoting the plating of silver only on the MPTES-printed regions and showing that silver micro- and submicron structures can be fabricated via direct electroless plating without further activation steps.

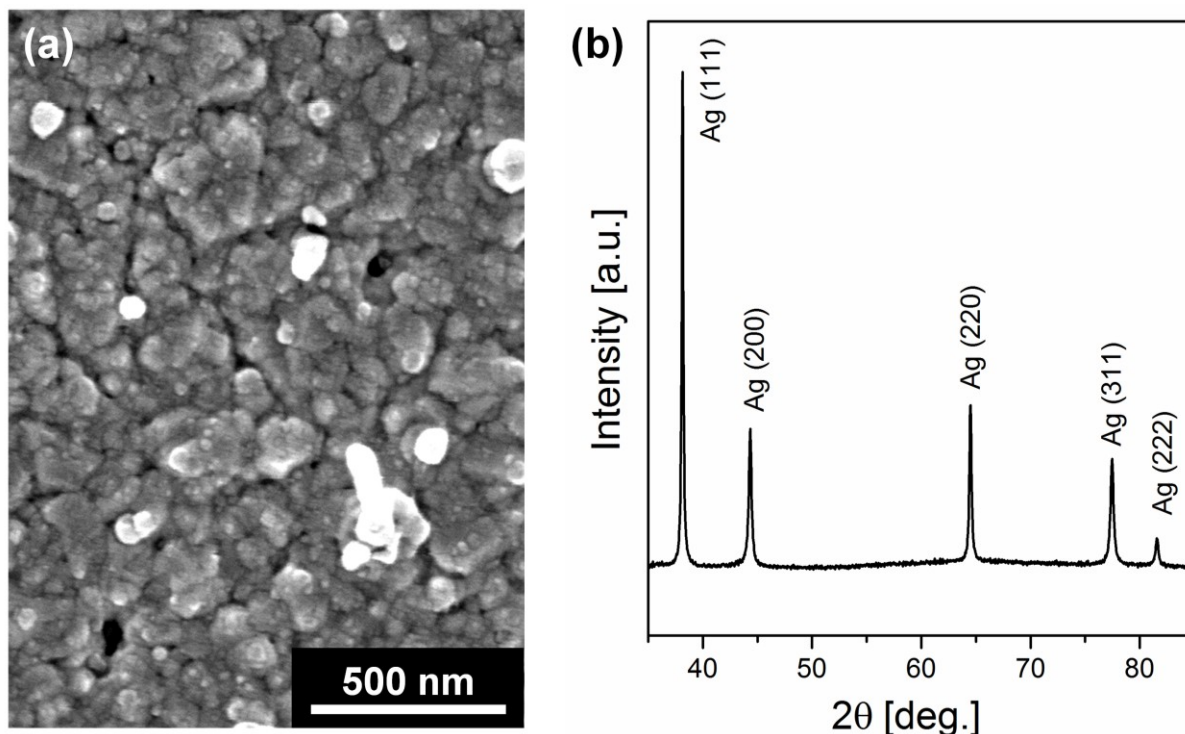


Fig. 68: (a) SEM image showing the grainy morphology of the silver structures fabricated by electroless plating on a MPTES-printed glass substrate (high magnification image taken from the structures shown in fig.67.a). (b) Diffraction pattern of the silver structures deposited by electroless plating on a MPTES-printed glass substrate (diffractogram taken using the sample shown in fig.67.a).

The suggested mechanism is that in the alkaline plating bath the thiol groups are deprotonated ($-S^-$) and help initiating the silver nucleation process by binding Ag^+ and establishing activated regions with a high density of Ag^+ complexes. These regions with $(-S^-)Ag^+$ complexes act as nucleation sites, opposed to the unfunctionalized glass surface which is not activated and cannot promote the silver deposition process. The silver patterns fabricated with this method are well defined over large areas (up to 1 cm^2) and the dimensions are in agreement with the stamps specifications. The structures are made of small coalesced silver grains and show a resistance of about $1\text{ k}\Omega$.

4.3 PMMA resist structures by Capillary Force Lithography

The PMMA structures were investigated with AFM and SEM analysis, shown in figure 70 and 71, respectively. In particular, figure 71.d shows the SEM image of the PMMA grid structure from figure 71.c after it was peeled off of the glass substrate, demonstrating the lack of any residual layer after the printing process and the overall stability of the PMMA patterns. All the PMMA structures are extremely uniform, defect-free and show a great edge definition. Notably, figures 70.g and 71.e show donuts-like structures, showing the ability of this technique to fabricate curvaceous and non-trivial patterns.

It is in theory possible to fabricate each planar pattern by choosing the right polymeric stamp, but in practice the choice is limited because of issues related to the capillary effect and the polymeric stamps: in large channels the capillary force is negligible and therefore the fabrication of large structures is more demanding, whereas the fabrication of nanometric structures is problematic because stamps with small features are challenging to manufacture and, secondly, the PMMA structures are easily torn apart during the peeling process [13].

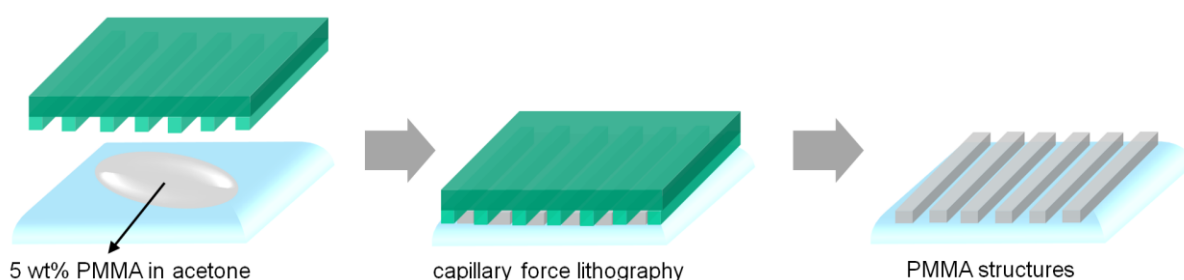


Fig. 69: Schematic illustration of the capillary force lithography process, used to fabricate PMMA structures as sacrificial layer for the manufacture of silver structures.

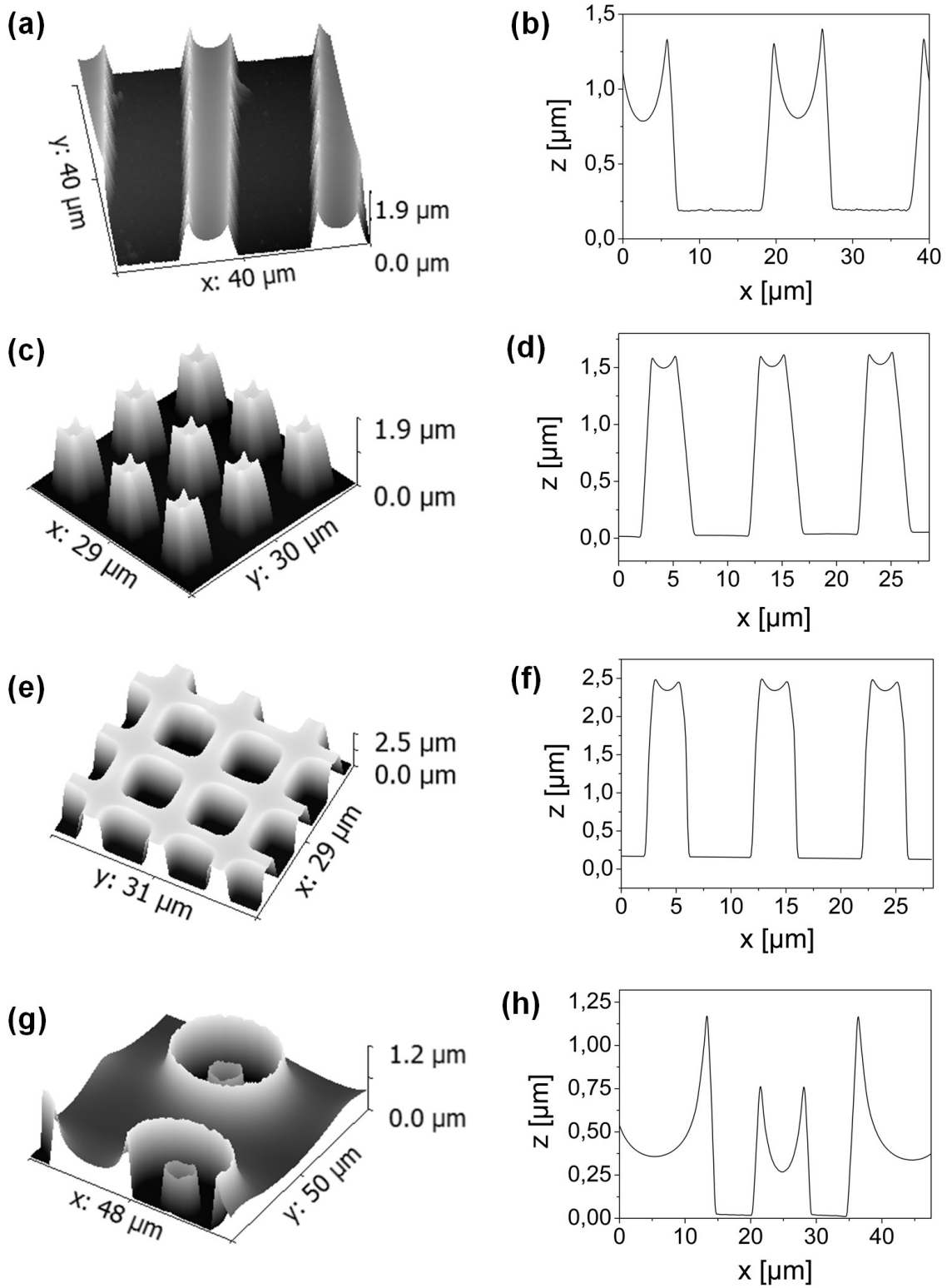


Fig. 70: AFM images and the respective cross-sections of the PMMA structures fabricated by the modified capillary force lithography method using a 5 wt% solution of PMMA in acetone. (a,b) lines with a width of 10 μm and 20 μm pitch, (c,d) a 2D array of squares with a width of 5 μm and spaced 5 μm from each other, (e,f) a regular grid of lines with a width of 5 μm, (g,h) a 2D array of rings with an internal diameter of 10 μm, an external diameter of 20 μm and spaced 20 μm from each other.

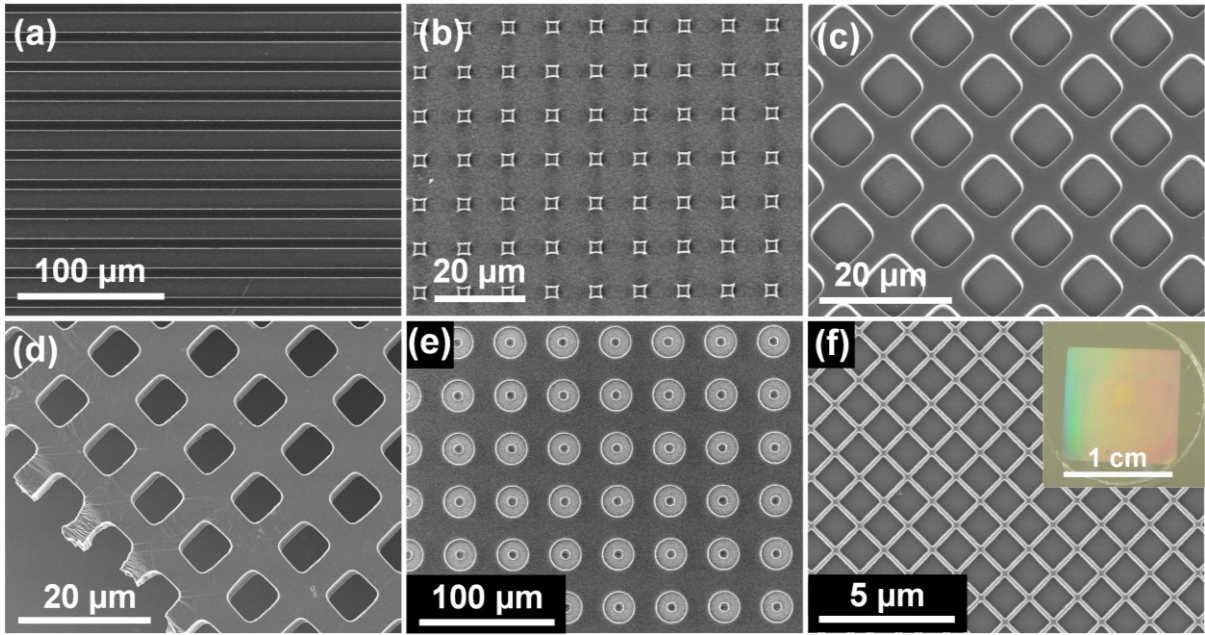


Fig. 71: SEM images of the PMMA structures fabricated by the modified capillary force lithography method using a 5 wt% solution of PMMA in acetone. (a) lines with a width of 10 μm and 20 μm pitch, (b) a 2D array of squares with a width of 5 μm and spaced 5 μm from each other, (c) a regular grid of lines with a width of 5 μm , (d) a peeled off regular grid of lines with a width of 5 μm , (e) a 2D array of rings with an internal diameter of 10 μm , an external diameter of 20 μm and spaced 20 μm from each other, (f) a grid of lines with a width of approximately 200 nm and spaced approximately 1 μm from each other. The inset shows a glass substrate covered with a PMMA patterned area of 1 cm^2 .

Therefore, the capillary force lithography method introduced in this work is best suited for the printing of PMMA structures in the submicrometer and micrometer range, with linear, angled and curved shapes. Moreover, regions as large as 1 cm^2 were uniformly and defect-free patterned, as shown in the inset of figure 71.f.

Due to the capillary rise during the molding process, a meniscus is observed at the summit of the PMMA structures. According to the capillary rise equation, the maximum height h a fluid can rise through a narrow channel is:

$$h = 2\gamma\cos\theta / \rho gr \quad (3)$$

where γ is the surface tension at the interface between liquid and air, θ is the contact angle, ρ is the density of the liquid, g is the gravitational constant, and r is the radius of the channel [175]. The maximum height h a liquid can rise through a narrow channel is hence inversely proportional to the channel radius and this explains why the larger structures, i.e. 10 μm -wide lines and donuts, have a lower capillary rise than smaller patterns, i.e. 5 μm -wide squares and grid. In addition, a certain extent of lateral shrinkage takes place. It is interesting to note that

this swelling is anisotropic along the vertical direction: the lateral shrinkage of the PMMA structures is 5 % in the bottom part, while it becomes more significant at the top, with shrinkage of approximately 20 % for the 10 μm -wide structures and up to 40 % for the 5 μm -wide structures. Such trapezoid-shaped structures can be better seen in the cross sections in figure 70. Such shape can be partly explained by the AFM tip shape effect, considering that all regular structures measured with AFM appear trapezoid-shaped to some extent. However, in this case the anisotropic shrinkage of the polymeric structures is remarkable and is probably related to two other factors: the PDMS stamp deformation during the stamping process and the swelling effect of acetone of PDMS structures which are not in a free swelling regime. The first one is related to the low stiffness of PDMS, which in turn causes deformation of the stamp because of its own weight and the applied pressure during the soft lithography process [176,177]. The second factor is related to the fact that the elastomeric PDMS mold is not in a free swelling regime during the printing process because its weight and the applied pressure are keeping it tightly against the substrate and, in addition, the solvent is not absorbed from the bottom surface of the PDMS stamp. According to the literature, in this regime an anisotropic deformation of the mold takes place [178,179]. Given a swelling ratio of PDMS in acetone of 1.06 [178], the former factor is probably the one giving the bigger contribution.

The molding process by capillary force lithography is made of two distinct steps: the capillary rise of the PMMA solution in acetone in the stamp channels, and the subsequent evaporation of the solvent through the PDMS mold. The fast capillary rise of the PMMA solution due to the low viscosity of acetone is essential in this fabrication method, but it can be shown that the limiting step is the solvent evaporation phase. The time t a fluid needs to rise through a channel by capillary force is given by:

$$t = 2\eta z^2 / R\gamma\cos\theta \quad (4)$$

where η is the viscosity of the fluid, z is the channel length, R is the hydraulic radius, which is approximately one half of the width of the channel, γ is the surface tension at the interface between air and fluid, and θ is the contact angle [180]. Hence, for a channel with a width of 10 μm and a length of 1 μm , using the surface tension of acetone in air $\gamma = 25 \text{ dyn cm}^{-1}$, a contact angle of about 30° (estimated from the AFM images) and $\eta = 0.3 \text{ mPa s}$ [181], a time of approximately 5 ms is calculated. This implies that the PMMA solution in acetone rise through the channels of the stamp and fills them almost instantly. Since it can be observed

that the molding process takes about 100 s using micrometer structures and about 10 s using submicrometer structures, it follows that the evaporation of the solvent, i.e. the time the acetone needs to diffuse from the bulk to the surface of the PMMA structures and then leave through the PDMS stamp, is very slow if compared to the speed the solution need to rise through and fill the channels, and hence is the actual limiting step. In addition, structures in the micrometer range need a much longer molding time than structures in the submicron range because the solvent has to move through a greater distance before reaching the PMMA surface.

This modified capillary force lithography method is extremely fast and versatile since virtually any planar pattern in the micrometer and submicrometer range can be fabricated in 10 – 100 s on areas up to 1 cm². Some degree of anisotropic lateral shrinkage due to the stamp deformation during molding is unavoidable but irrelevant since the PMMA structures are used as sacrificial resist in the fabrication of metallic patterns. Moreover, it was demonstrated that the PMMA solution in acetone rise through the channels almost instantly, while the limiting step is the evaporation of the solvent.

4.4 Silver structures from patterned PMMA resist

Figure 72 shows SEM images of the silver microstructures (light-colored) fabricated by electroless plating followed by the removal of the PMMA resist structures with acetone. The stamps used to fabricate the Ag structures are (a,b) lines with a width of 10 μm and a pitch of 20 μm , (c,d) a regular grid of lines with a width of 5 μm , (e,f) a 2D array of squares with a width of 5 μm and spaced 5 μm from each other and (g,h) a 2D array of squares with a width of approximately 1 μm and a pitch of 1.2 μm . The silver patterns are very well defined and uniform over large areas, with the patterns shown in figures 72.e-h in agreement with the stamps specifications, while the patterns shown in figures 72.a-d are slightly larger, probably because of the more pronounced lateral shrinkage of the PMMA resist structures during the molding process. Compared with the silver structures fabricated by selective EP of the printed MPTES patterns, much less silver particles can be seen on the glass substrates, indicating the better selectivity of this method. Because of the inherent growth mechanism of electroless plating, the silver patterns show a granular and rough morphology.

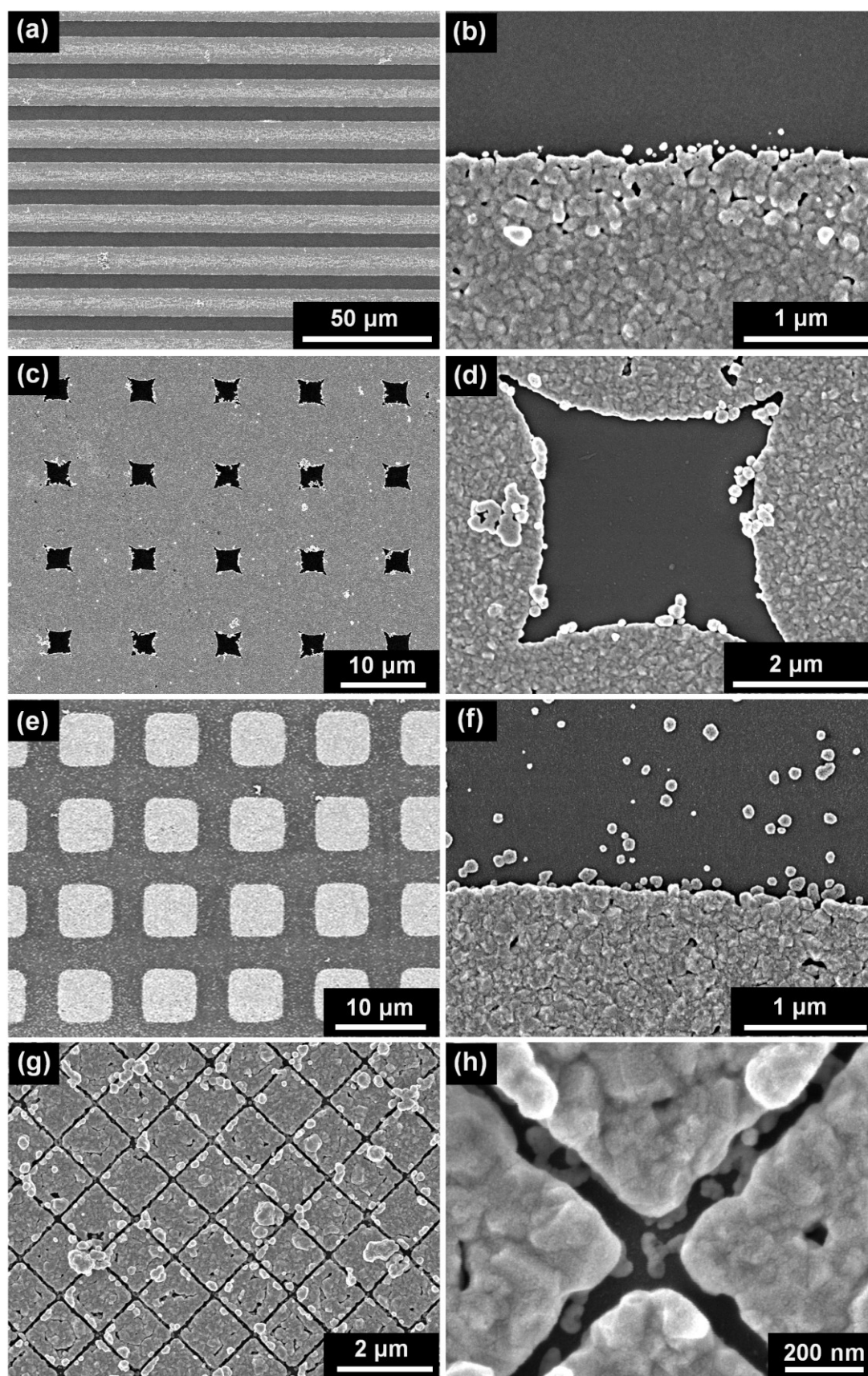


Fig. 72: SEM images of the silver structures (light-colored) fabricated by electroless plating followed by the removal of the PMMA resist structures with acetone. (a,b) lines with a width of 10 μm and a pitch of 20 μm, (c,d) a regular grid of lines with a width of 5 μm, (e,f) a 2D array of squares with a width of 5 μm and spaced 5 μm from each other, and (g,h) a 2D array of squares with a width of approximately 1 μm and a pitch of 1.2 μm.

The structures are made of coalesced particles with sizes in the 50 – 200 nm range, however they are robust and well defined, as shown by EDX analysis in figure 73. The thickness of the silver structures was measured with AFM and is around 60 nm, hence slightly thicker as the structures fabricated with the EP of printed MPTES (fig. 73.b). In addition, the silver grid shown in figure 73 has a sheet resistance of $1.0 \pm 0.1 \Omega/\text{sq}$ (measured with a four-point probes method) and a transmittance of 9.8% at $\lambda = 500 \text{ nm}$, making it suitable for electronic applications, e.g. in the fabrication of semitransparent electrodes. Considering a filling factor of 82 %, i.e. the area of the substrate which is covered with silver and hence not transparent to light, the transmittance value of 9.8% is very promising and can be increased by using a different stamp pattern, leading to a smaller filling factor. The quality of the electroless deposited silver is confirmed by the diffractogram shown in figure 74, which shows the diffraction peaks of silver (JCPDS 4-783).

These results show that the structures fabricated by capillary force lithography are of better quality than the structures fabricated with the plating of the printed MPTES patterns, in particular they are thicker, more defined and show a higher conductivity. However, the size of the Ag grains can be a problem in the fabrication of smaller structures, particularly in the nanometer range.

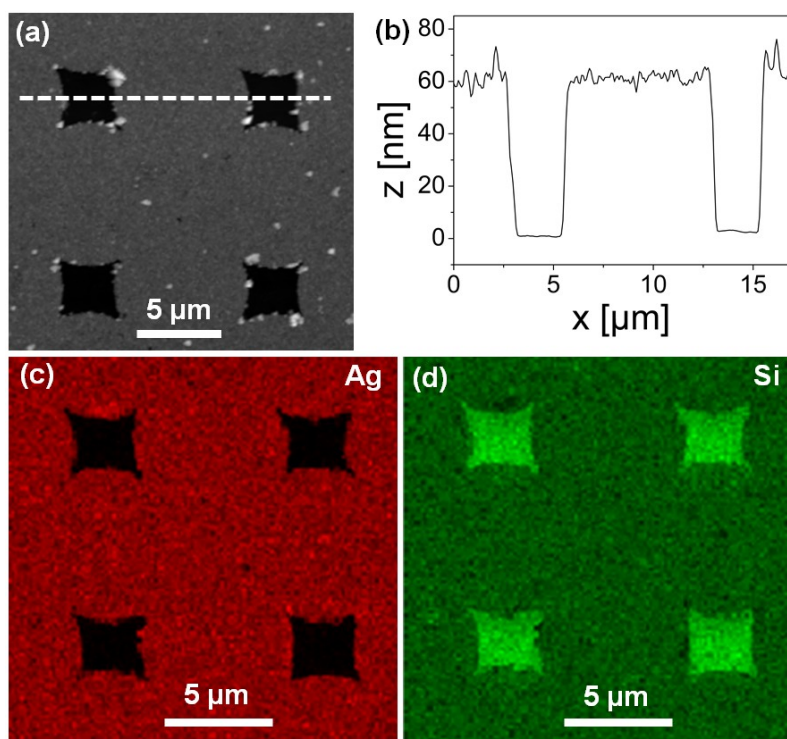


Fig. 73: (a) SEM image of a regular grid of silver lines with a width of 5 μm, and the respective (b) cross-section measured by AFM along the white dotted line, (c) EDX mapping for Ag and (d) EDX mapping for Si.

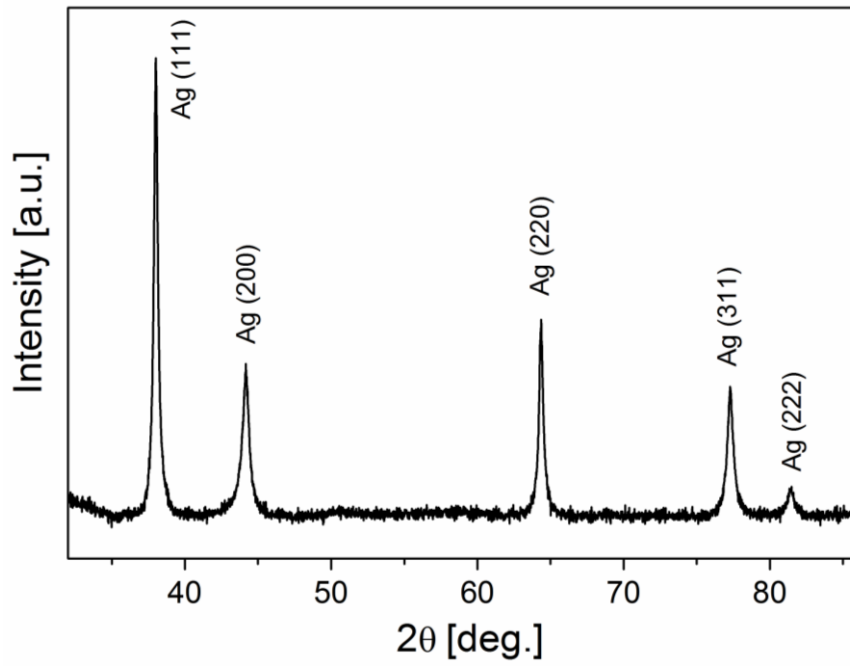


Fig. 74: XRD diffraction pattern of silver structures fabricated by electroless plating followed by the removal of the PMMA resist structures with acetone (diffractogram taken using the sample shown in fig.72.c).

V Conclusions and Outlook

In this work, new surface functionalization methods for electroless metal deposition processes were developed. In particular, the work is focused on the synthesis of metal coated particles regarding the application as reinforcement for metal matrix composites, and on the preparation of silver patterns on glass substrates for applications in the electronics and microelectronics industries, such as transparent electrodes. Three different particle functionalization methods were successfully developed, using three different systems: (3-mercaptopropyl)triethoxysilane for self-assembly layers in order to functionalize oxide particles, 3-aminopropylphosphonic acid forming monolayers to functionalize carbide particles and a substrate-independent method based on the bioinspired polymer coating made of polydopamine. All new methods are organic based and have significant advantages over the state of the art technique based on the substrate activation using Pd ions or nanoparticles, especially in terms of homogeneity of the coating, environmental aspects and efficiency.

The particle functionalization method using (3-mercaptopropyl)triethoxysilane was developed for the functionalization of oxide particles. Silica and alumina nanoparticles were successfully functionalized with (3-mercaptopropyl)triethoxysilane as verified by FTIR and TEM analysis. The key features of the (3-mercaptopropyl)triethoxysilane are the thiol and the three ethoxy groups: because of its high affinity toward metal ions the thiol group promotes the selective electroless metal deposition process, while the ethoxy groups can react with the hydroxyl groups of an oxide substrate, promoting the covalent bonding of the self-assembled monolayer. This MPTES layer on the particles surface has a thickness between 1 and 4 nm, suggesting that the coating is made of both monolayers and thicker disordered agglomerates. The condensation reaction of MPTES with the particle surface is in competition with the self-polymerization of MPTES in solution, leading to the formation of oligomers. These oligomers also undergo condensation reactions with the particle surface and are responsible for the thicker agglomerates of the coating. The MPTES functionalized silica and alumina nanoparticles were coated with copper by electroless plating. The copper coating has a thickness of about 10-25 nm and the plated particles maintain their spherical shape during the process.

The particle functionalization method involving the use of 3-aminopropylphosphonic acid was developed to functionalize carbide particles. The key features of the 3-aminopropylphosphonic acid are the phosphonate group and the amino group: because of its

high affinity toward metal ions, the amino group promotes the selective electroless metal deposition process, while the phosphonate group interacts with the metal ions of the carbide, promoting the adhesion of the molecule as a monolayer without any condensation. Tungsten carbide microparticles and nanoparticles were successfully functionalized with 3-aminopropylphosphonic acid as verified by FTIR, TGA and TEM images, from which a monolayer can be seen on the particles surface. In contrast to (3-mercaptopropyl)triethoxysilane, 3-aminopropylphosphonic acid does not react with itself, meaning that the deposition of oligomers is not possible. The tungsten carbide microparticles functionalized with 3-aminopropylphosphonic acid were coated with copper, nickel and cobalt by electroless plating. In the case of nickel and cobalt, specific plating baths were developed by modifying the plating baths used by Brenner and Riddell. All the metal coated tungsten carbide microparticles are entirely plated with a grainy metal coating, which has a rough morphology. These coatings consist of coalesced metal grains, peculiar of metal coatings deposited by electroless plating and other solution based processes. The exact thickness of the metal can not be easily determined. Comparing SEM images before and after the deposition process, the metal coating can be estimated as relatively thin with an average thickness of about 50 nm. The copper coating is crystalline, while nickel and cobalt coatings are amorphous because of the high boron content coming from the reducing agent NaBH_4 . In addition, the cobalt and nickel coatings are magnetic and EDX analysis show a cobalt content of 14 % in element weight percentage, whereas in the case of nickel a 20 % in element weight percentage is obtained.

The method using polydopamine was developed as a simple, bioinspired and substrate-independent functionalization process. The functionalization with polydopamine of alumina nanoparticles and microparticles as well as tungsten carbide nanoparticles and microparticles were systematically investigated with SEM, TEM, IR and TGA analysis. The method is extremely simple and versatile since a surface-adherent polydopamine coating with tunable thickness can be fabricated by simply immersing a substrate in an aqueous solution of dopamine buffered at pH 8.5. The longer the substrate stays in the solution, the thicker is the polydopamine layer. In this work, it was investigated how the thickness of the polydopamine coatings depends also on the substrate size and material type (such as carbide or oxide surfaces), whereas in the literature it is assumed that the dopamine polymerization reaction is substrate-independent. In the case of alumina microparticles a polydopamine thickness of 65 ± 10 nm was reached after 24 h of polymerization, while in the case of tungsten carbide nanoparticles and tungsten carbide microparticles a thickness of 33 ± 6 nm and 18 ± 4 nm was

reached after 24 h, respectively. Moreover, the polydopamine coating on WC microparticles can be examined by SEM. Uncoated WC microparticles are characterized by flat surfaces and sharp edges, while polydopamine coated WC microparticles have smoothed edges and corners, and the surface shows a fine granularity. This work is also the first in which such a systematic analysis of the dopamine polymerization process on different particle materials is performed and investigated. Due to the alkylamine and catechol functionalities of polydopamine, it can be used to promote the selective electroless metal deposition process because of the affinity of such functional groups toward metal ions. The process was used to fabricate copper coated tungsten carbide microparticles and alumina nanoparticles, as well as silver and cobalt coated tungsten carbide microparticles. The deposited metal shell is conformal and compact, with an estimated thickness of about 50 nm. The use of both micro- and nanoparticles, as well as a carbide and an oxide as particle materials, evidences the versatility of this technique.

The copper coated alumina nanoparticles synthesized as described in chapter III.1.4.2 by using the MPTES functionalization method followed by electroless plating, as well as the copper coated tungsten carbide microparticles synthesized as described in chapter III.1.4.2 by using the 3-APP functionalization method, were used to fabricate reinforced copper matrix composites. The composites contain 1 wt% of the plated particles and were successfully fabricated via powder metallurgy by the Institute of joining technology and assembly of the Technical University of Dresden. The nanoparticles are well dispersed with some agglomerates in the submicron range, but the samples also show some degree of porosity, while in the case of the WC microparticles a very homogeneous distribution and no porosity can be seen. These composites are under investigation for potential applications as reinforced electrodes for resistance spot welding, reinforced overhead wire and sliding contact for trains and other vehicles.

Moreover, two new processes for the fabrication of silver patterns on glass substrates were developed by selective functionalization via soft lithography combined with metal electroless deposition. In one approach (3-mercaptopropyl)-triethoxysilane is printed by microcontact printing on a glass substrate, followed by selective electroless metallization. In a second approach, PMMA structures are patterned by capillary force lithography as a sacrificial layer, followed by silver electroless plating and PMMA removal. These two patterning processes combine the advantages of both, soft lithography and electroless plating, leading to new, versatile and inexpensive patterning processes without the use of the conventional palladium-based sensitization, lithography and etching steps. This new fabrication methods offer unique

opportunities for the manufacture of micro- and submicrometer-sized silver structures. The selective functionalization of glass substrates with (3-mercaptopropyl)triethoxysilane by microcontact printing followed by silver electroless plating was developed as simple, cost effective alternative to the state of the art manufacture techniques of micro- and nanometer-sized metallic structures, such as photolithography and etching. All the structures are well defined, uniform over large areas and there are no major defects like overgrowing or undesired interconnections of the structures, however, some silver particles can be seen on the MPTES-free regions. This process is used to manufacture patterned silver layers on areas as large as 1 cm^2 , with thicknesses ranging from 10 nm up to 50 nm due to the high roughness of the patterns, depending on the plating time and pattern size. The structures show a grainy morphology made of coalesced silver particles.

The fabrication process of silver patterns on glass substrates based on capillary force lithography of a 5 wt% PMMA solution in acetone followed by silver electroless plating was developed to avoid the selectivity issues of the technique based on the printing of MPTES, previously described. The fabrication of several PMMA structures as resist by a very simple, cost-effective and versatile process using a new capillary soft lithography approach was investigated in this work. This single step patterning method is performed in only 10 – 100 s, depending on the structures size. This short patterning time is achieved due to an almost instant capillary rise of the low weight PMMA solution through the stamp channels, followed by solvent evaporation. This method was used to fabricate silver patterns of different shapes and sizes by silver deposition via electroless plating followed by PMMA removal. The silver patterns are very well defined, have a grainy morphology and a high uniformity over relatively large areas (1 cm^2), with the patterns in agreement with the stamps specifications. Compared with the silver structures fabricated by selective EP of the printed MPTES patterns, much less silver particles can be seen on the glass substrates, indicating the better selectivity of this method. This process is used to manufacture patterned silver layers with a thickness of approximately 60 nm. In addition, the silver grid made of $5 \text{ }\mu\text{m}$ -wide lines has a sheet resistance of $1.0 \pm 0.1 \text{ }\Omega/\text{sq}$ and a transmittance of 9.8% at $\lambda = 500 \text{ nm}$, making it suitable for electronic applications, e.g. in the fabrication of semitransparent electrodes.

All the developed processes combine organic functionalization with electroless plating, leading to innovative and simple coating and patterning techniques with potential to be scaled up quite efficiently. In future works, more derivatives of amino-phosphonic acids should be investigated for the activation of different particle materials. The use of the functionalization methods introduced in this work with other metals or alloys as coating and new substrate

materials should also be investigated, in particular other oxides and carbides particles. Additionally, the fabrication of composite materials reinforced with metal plated particles and the improvement of their properties should be studied in detail. In the case of the patterning methods, future works may be carried out to investigate the fabrication of smaller structures. A miniaturization into linewidths in the 0.1 – 0.5 μm range and an extension into larger patterned areas is straightforward, however, structures smaller than 0.2 μm can be challenging to fabricate because of the grain sizes of the silver structures fabricated by electroless plating. The conductivity of the silver patterns may be improved by using mild temperature treatments: an adequate thermal treatment is expected to improve the conductivity of the patterned silver layers by promoting the percolation of the grains, even though concerns regarding structure widening may arise.

VI References

- [1] P. Bindra, J.R. White, Fundamental aspects of electroless copper plating, in: G.O. Mallory, J.B. Hajdu (Eds.), *Electroless plating: fundamentals and applications*, W. Andrew Publisher, US, 1991, pp. 289–329
- [2] J. Sudagar, J. Lian, W. Sha, Electroless nickel, alloy, composite and nano coatings – A critical review, *J. Alloys Compd.* 571 (2013) 183
- [3] W.H. Safranek, Electroless cobalt and cobalt alloys, in: G.O. Mallory, J.B. Hajdu (Eds.), *Electroless plating: fundamentals and applications*, W. Andrew Publisher, US, 1991, pp. 463–509
- [4] S.S. Djokić, Electroless deposition of metals and alloys, in: B.E. Conway, R.E. White (Eds.), *Modern Aspects of Electrochemistry*, Vol. 35, Springer, US, 2002, pp. 51–133
- [5] J.E. Mahan, *Physical Vapor Deposition of Thin Films*, John Wiley & Sons, US, 2000
- [6] C.A. Leon, R.A.L. Drew, Preparation of nickel-coated powders as precursors to reinforce MMCs, *J. Mater. Sci.* 35 (2000) 4763
- [7] G. Zou, M. Cao, H. Lin, H. Jin, Y. Kang, Y. Chen, Nickel layer deposition on SiC nanoparticles by simple electroless plating and its dielectric behaviors, *Powder Technol.* 168 (2006) 84
- [8] R. Sharma, R.C. Agarwala, V. Agarwala, Development of copper coatings on ceramic powder by electroless technique, *Appl. Surf. Sci.* 252 (2006) 8487
- [9] H. Wang, J. Jia, H. Song, X. Hu, H. Sun, D. Yang, The preparation of Cu-coated Al₂O₃ composite powders by electroless plating, *Ceram. Int.* 37 (2011) 2182
- [10] P.C. Hidber, W. Helbig, E. Kim, G.M. Whitesides, Microcontact printing of palladium colloids: Micron-scale patterning by electroless deposition of copper, *Langmuir* 12 (1996) 1375
- [11] T.B. Carmichael, S.J. Vella, A. Afzali, Selective electroless metal deposition using microcontact printing of phosphine-phosphonic acid inks, *Langmuir* 20 (2004) 5593
- [12] A.A. Mewe, E.S. Kooij, B. Poelsema, Seeded-growth approach to selective metallization of microcontact-printed patterns, *Langmuir* 22 (2006) 5584

-
- [13] B.D. Gates, Q. Xu, M. Stewart, D. Ryan, C.G. Willson, G.M. Whitesides, New approaches to nanofabrication: Molding, printing, and other techniques, *Chem. Rev.* 105 (2005) 1171
- [14] F. Bessueille, S. Gout, S. Cotte, Y. Goepfert, D. Leonard, M. Romand, Selective metal pattern fabrication through micro-contact or ink-jet printing and electroless plating onto polymer surfaces chemically modified by plasma treatments, *J. Adhesion* 85 (2009) 690
- [15] B.J. Jankiewicz, D. Jamiola, J. Choma, M. Jaroniec, Silica-metal core-shell nanostructures, *Adv. Colloid Interface Sci.* 170 (2012) 28
- [16] M. Stroumbouli, P. Gyftou, E.A. Pavlatou, N. Spyrellis, Codeposition of ultrafine WC particles in Ni matrix composite electrocoatings, *Surf. Coat. Technol.* 195 (2005) 325
- [17] J. Michalski, K. Konopka, M. Trzaska, Description of Al₂O₃ powders coated by Ni-P particles obtained through an electroless chemical reaction and possibilities to obtain an Al₂O₃/Ni-P composite, *Mater. Chem. Phys.* 81 (2003) 407
- [18] S.C. Tjong, Novel nanoparticle-reinforced metal matrix composites with enhanced mechanical properties, *Adv. Eng. Mater.* 9 (2007) 639
- [19] A. Brenner, G.E. Riddell, Nickel plating on steel by chemical reduction, *J. Res. Nat. Bur. Stand.* 37 (1946) 31
- [20] A. Brenner, G.E. Riddell, Deposition of nickel and cobalt by chemical reduction, *J. Res. Nat. Bur. Stand.* 39 (1947) 385
- [21] V.M. Dubin, S.D. Lopatin, V.G. Sokolov, Selective electroless Ni deposition onto Pd-activated Si for integrated circuit fabrication, *Thin Solid Films* 226 (1993) 94
- [22] G. Mondin, B. Schumm, J. Fritsch, R. Hensel, J. Grothe, S. Kaskel, Fast patterning of poly(methyl methacrylate) by a novel soft molding approach and its application to the fabrication of silver structures, *Mater. Chem. Phys.* 137 (2013) 884
- [23] D. Zabetakis, W.J. Dressick, Selective electroless metallization of patterned polymeric films for lithography applications, *ACS Appl. Mater. Interfaces* 1 (2009) 4
- [24] L.G. Svendsen, T. Osaka, H. Sawai, Behavior of Pd/Sn and Pd catalysts for electroless plating on different substrates investigated by means of Rutherford backscattering, *J. Electrochem. Soc.* 130 (2000) 2252
- [25] Y. Lu, Electroless copper plating on 3-mercaptopropyltriethoxysilane modified PET fabric challenged by ultrasonic washing, *Appl. Surf. Sci.* 255 (2009) 8430

-
- [26] K. Miyoshi, Y. Aoki, T. Kunitake, S. Fujikawa, Facile fabrication of silver nanofin array via electroless plating, *Langmuir* 24 (2008) 4205
- [27] Y. Shacham-Diamand, V.M. Dubin, M. Angyal, Electroless copper deposition for ULSI, *Thin Solid Film* 262 (1995) 93
- [28] V.M. Dubin, Y. Shacham-Diamand, B. Zhao, P.K. Vasudev, C.H. Ting, Selective and Blanket Electroless Copper Deposition for Ultralarge Scale Integration, *J. Electrochem. Soc.* 44 (1997) 898
- [29] J.F. Rohan, G. O’Riordan, J. Boardman, Selective electroless nickel deposition on copper as a final barrier/bonding layer material for microelectronics applications, *Appl. Surf. Sci.* 185 (2002) 289
- [30] R. Haug, R. Behner, C.-P. Czaya, J. Hongquan, S.F. Kotthaus, R. Schuetz, C.P.O. Treutler, Low-cost direct chip attach: Comparison of SMD compatible FC soldering with anisotropically conductive adhesive FC bonding, *IEEE Trans. Electron. Pack. Manuf.* 23 (2000) 12
- [31] T. Osaka, M. Yoshino, New formation process of plating thin films on several substrates by means of self-assembled monolayer (SAM) process, *Electrochim. Acta* 53 (2007) 271
- [32] V. Tsakova, How to affect number, size, and location of metal particles deposited in conducting polymer layers, *J. Solid State Electrochem.* 12 (2008) 1421
- [33] M. Geissler, H. Kind, P. Schmidt, B. Michel, E. Delamarche, Direct patterning of NiB on glass substrates using microcontact printing and electroless deposition, *Langmuir* 19 (2003) 6283
- [34] A. Szasz, D.J. Fabian, Z. Paal, J. Kojnok, Chemical mechanisms in electroless deposition – A Study on the role of hydrogen in layer formation, *J. Non-Cryst. Solids* 103 (1988) 21
- [35] A. Hung, I. Ohno, Electrochemical study of hypophosphite-reduced electroless copper deposition, *J. Electrochem. Soc.* 137 (1990) 918
- [36] J. Dugasz, A. Szasz, Factors affecting the adhesion of electroless coatings, *Surface Coating Technol.* 58 (1993) 57
- [37] R.C. Bevington, H.J. Kim, Thermophysical properties of Ag-CdO composite materials, *IEEE Trans. Comp. Packag. Manufact. Technol.* 2 (1979) 46

- [38] J. Hajdu, Surface preparation for electroless nickel plating, in: G.O. Mallory, J.B. Hajdu (Eds.), *Electroless plating: fundamentals and applications*, W. Andrew Publisher, US, 1991, pp. 193–206
- [39] A. Rantell, A. Holtzman, Metallising of circuit boards using mixed $\text{SnCl}_2 / \text{PdCl}_2$ catalysts, *Circuit World* 2 (1976) 30
- [40] N. Feldstein, M. Schlesinger, N.E. Hedgecock, S.L. Chow, Electron-microscope investigation of mixed stannous chloride-palladium chloride catalysts for plating dielectric substrates, *J. Electrochem. Soc.* 121 (1974) 738
- [41] Z. Deng, M. Chen, L. Wu, Novel method to fabricate SiO_2/Ag composite spheres and their catalytic, surface-enhanced Raman scattering properties, *J. Phys. Chem. C* 111 (2007) 11692
- [42] R.L. Cohen, K.W. West, Generative and stabilizing processes in tin-palladium sols and palladium sol sensitizers, *J. Electrochem. Soc.* 120 (1973) 502
- [43] N. Koura, Electroless plating of silver, in: G.O. Mallory, J.B. Hajdu (Eds.), *Electroless plating: fundamentals and applications*, W. Andrew Publisher, US, 1991, pp. 441–462
- [44] J. Liebig, Über die Producte der oxydation des alkohols, *Annalen der Pharmacie* 14 (1835) 133
- [45] J. Liebig, Über versilberung und vergoldung von glas, Sonderdruck aus den Berichten der technischen Commission der königl. Academie der Wissenschaften in München (1857) 132
- [46] H. Chang, C.H. Pitt, G.B. Alexander, Electroless silver plating of oxide particles in aqueous-solution, *J. Mater. Sci.* 28 (1993) 5207
- [47] S.G. Warriar, R.Y. Lin, Silver coating on carbon and SiC fibers, *J. Mater. Sci.* 28 (1993) 4868
- [48] C.M. Friend, The effect of matrix properties on reinforcement in short alumina fibre-aluminium metal matrix composites, *J. Mater. Sci.* 22 (1987) 3005
- [49] S.F. Moustafa, Z. Abdel-Hamid, A.M. Abd-Elhay, Copper matrix SiC and Al_2O_3 particulate composites by powder metallurgy technique, *Mater. Lett.* 53 (2002) 244
- [50] R. Asthana, Review reinforced cast metals. Part II. Evolution of the interface, *J. Mater. Sci.* 33 (1998) 1959

- [51] M.S. El-Eskandarany, A.A. Mahday, H.A. Ahmed, A.H. Amer, Synthesis and characterizations of ball-milled nanocrystalline WC and nanocomposite WC–Co powders and subsequent consolidations, *J. Alloys Compd.* 312 (2000) 315
- [52] X. Yu, Z. Xu, Z. Shen, Metal copper films deposited on cenosphere particles by magnetron sputtering method, *J. Phys. D: Appl. Phys.* 40 (2007) 2894
- [53] J.E. Cline, J. Wulf, Vapor deposition of metals on ceramic particles, *J. Electrochem. Soc.* 98 (1951) 385
- [54] Z. Jiang, C. Liu, Seed-mediated growth technique for the preparation of a silver nanoshell on a silica sphere, *J. Phys. Chem. B* 107 (2003) 12411
- [55] N. Kulyk, S. Cherevko, C.-H. Chung, Copper electroless plating in weakly alkaline electrolytes using DMAB as a reducing agent for metallization on polymer films, *Electrochim. Acta* 59 (2012) 179
- [56] S. Shukla, S. Seal, Z. Rahaman, K. Scammon, Electroless copper coating of cenospheres using silver nitrate activator, *Mater. Lett.* 57 (2002) 151
- [57] A. Kilicarslan, F. Toptan, I. Kerti, Electroless nickel–phosphorus coating on boron carbide particles, *Mater. Lett.* 76 (2012) 11
- [58] J. Lin, M. Yu, C. Lin, X. Liu, Multiform oxide optical materials via the versatile Pechini-type sol–gel process: synthesis and characteristics, *J. Phys. Chem. C* 111 (2007) 5835
- [59] B. Schumm, F.M. Wisser, G. Mondin, F. Hippauf, J. Fritsch, J. Grothe, S. Kaskel, Semi-transparent silver electrodes for flexible electronic devices prepared by nanoimprint lithography, *J. Mater. Chem. C* 1 (2013) 638
- [60] H. Lee, S.M. Dellatore, W.M. Miller, P.B. Messersmith, Mussel-inspired surface chemistry for multifunctional coatings, *Science* 318 (2007) 426
- [61] J.H. Waite, Surface chemistry - Mussel power, *Nature Mater.* 7 (2008) 8
- [62] F. Yu, S. Chen, Y. Chen, H. Li, L. Yang, Y. Chen, Y. Yin, Experimental and theoretical analysis of polymerization reaction process on the polydopamine membranes and its corrosion protection properties for 304 Stainless Steel, *J. Mol. Struct.* 982 (2010) 152
- [63] X.-B. Yin, Polydopamine-based permanent coating capillary electrochromatography for auxin determination, *J. Chromatogr. A* 1212 (2008) 130
- [64] J. Liebscher, R. Mrowczynski, H.A. Scheidt, C. Filip, N.D. Hadade, R. Turcu, A. Bende, S. Beck, Structure of Polydopamine: A Never-Ending Story?, *Langmuir* 29 (2013) 10539

- [65] D.R. Dreyer, D.J. Miller, B.D. Freeman, D.R. Paul, C.W. Bielawski, Elucidating the Structure of Poly(dopamine), *Langmuir* 28 (2012) 6428
- [66] M.-H. Ryou, Y.M. Lee, J.-K. Park, J.W. Choi, Mussel-inspired polydopamine-treated polyethylene separators for high-power Li-ion batteries, *Adv. Mater.* 23 (2011) 3066
- [67] M.-H. Ryou, D.J. Lee, J.-N. Lee, Y.M. Lee, J.-K. Park, J.W. Choi, Excellent cycle life of lithium-metal anodes in lithium-ion batteries with mussel-inspired polydopamine-coated separators, *Adv. Energy Mater.* 2 (2012) 645
- [68] J. Kong, W.A. Yee, L. Yang, Y. Wei, S.L. Phua, H.G. Ong, J.M. Ang, X. Li, X. Lu, Highly electrically conductive layered carbon derived from polydopamine and its functions in SnO₂-based lithium ion battery anodes, *Chem. Commun.* 48 (2012) 10316
- [69] H. Li, L. Shen, K. Yin, J. Ji, J. Wang, X. Wang, X. Zhang, Facile synthesis of N-doped carbon-coated Li₄Ti₅O₁₂ microspheres using polydopamine as a carbon source for high rate lithium ion batteries, *J. Mater. Chem. A* 1 (2013) 7270
- [70] J. Cui, Y. Wang, A. Postma, J. Hao, L. Hosta-Rigau, F. Caruso, Monodisperse polymer capsules: tailoring size, shell thickness, and hydrophobic cargo loading via emulsion templating, *Adv. Funct. Mater.* 20 (2010) 1625
- [71] B. Yu, D.A. Wang, Q. Ye, F. Zhou, W. Liu, Robust polydopamine nano/microcapsules and their loading and release behavior, *Chem. Commun.* 44 (2009) 6789
- [72] G. Yeroslavsky, M. Richman, L. Dawidowicz, S. Rahimipour, Sonochemically produced polydopamine nanocapsules with selective antimicrobial activity, *Chem. Commun.* 49 (2013) 5721
- [73] T.S. Sileika, H.-D. Kim, P. Maniak, P.B. Messersmith, Antibacterial performance of polydopamine-modified polymer surfaces containing passive and active components, *ACS Appl. Mater. Interfaces* 3 (2011) 4602
- [74] D.E. Fullenkamp, J.G. Rivera, Y.-K. Gong, K.H.A. Lau, L. He, R. Varshney, P.B. Messersmith, Mussel-inspired silver-releasing antibacterial hydrogels, *Biomaterials* 33 (2012) 3783
- [75] V. Ball, I. Nguyen, M. Haupt, C. Oehr, C. Arnoult, V. Toniazzi, D. Ruch, The reduction of Ag⁺ in metallic silver on pseudomelanin films allows for antibacterial activity but does not imply unpaired electrons, *J. Colloid Interface Sci.* 364 (2011) 359

- [76] L. Zhang, J. Wu, Y. Wang, Y. Long, N. Zhao, J. Xu, Combination of bioinspiration: a general route to superhydrophobic particles, *J. Am. Chem. Soc.* 134 (2012) 9879
- [77] S.M. Kang, I. You, W.K. Cho, H.K. Shon, T.G. Lee, I.S. Choi, J.M. Karp, H. Lee, One-step modification of superhydrophobic surfaces by a mussel-inspired polymer coating, *Angew. Chem. Int. Ed.* 49 (2010) 9401
- [78] W.-B. Tsai, W.-T. Chen, H.-W. Chien, W.-H. Kuo, M.-J. Wang, Poly(dopamine) coating of scaffolds for articular cartilage tissue engineering, *Acta Biomater.* 7 (2011) 4187
- [79] S.H. Ku, C.B. Park, Human endothelial cell growth on mussel-inspired nanofiber scaffold for vascular tissue engineering, *Biomaterials* 31 (2010) 9431
- [80] B. Fei, B. Qian, Z. Yang, R. Wang, W.C. Liu, C.L. Mak, J.H. Xin, Coating carbon nanotubes by spontaneous oxidative polymerization of dopamine, *Carbon* 46 (2008) 1795
- [81] Y. Jiang, Y. Lu, L. Zhang, L. Liu, Y. Dai, W. Wang, Preparation and characterization of silver nanoparticles immobilized on multi-walled carbon nanotubes by poly(dopamine) functionalization, *J. Nanopart. Res.* 14 (2012) 938
- [82] J. Si, H. Yang, Preparation and characterization of bio-compatible Fe₃O₄@Polydopamine spheres with core/shell nanostructure, *Mater. Chem. Phys.* 128 (2011) 519
- [83] W.-H. Zhou, C.-H. Lu, X.-C. Guo, F.-R. Chen, H.-H. Yang, X.-R. Wang, Mussel-inspired molecularly imprinted polymer coating superparamagnetic nanoparticles for protein recognition, *J. Mater. Chem.* 20 (2010) 880
- [84] Q. Li, M. Tian, L. Liu, H. Zou, L. Zhang, W.C. Wang, Facile preparation of alpha-Fe₂O₃@Ag core shell structured nanoparticles, *Electrochim. Acta* 91 (2013) 114
- [85] W. Wang, Y. Jiang, Y. Liao, M. Tian, H. Zou, L. Zhang, Fabrication of silver-coated silica microspheres through mussel-inspired surface functionalization, *J. Colloid Interface Sci.* 358 (2011) 567
- [86] J. Gao, F. Tang, J. Ren, Electroless nickel deposition on amino-functionalized silica spheres, *Surf. Coat. Tech.* 200 (2005) 2249
- [87] L. Zhang, Y.-G. Feng, L.-Y. Wang, J.-Y. Zhang, M. Chen, D.-J. Qian, Comparative studies between synthetic routes of SiO₂@Au composite nanoparticles, *Mater. Res. Bull.* 42 (2007) 1457–1467

- [88] H. Dai, H. Li, F. Wang, Electroless Ni–P coating preparation of conductive mica powder by a modified activation process, *Appl. Surf. Sci.* 253 (2006) 2474
- [89] I.A. Ibrahim, F.A. Mohamed, E.J. Lavernia, Particulate reinforced metal matrix composites - A review, *J. Mater. Sci.* 26 (1991) 1137
- [90] D.B. Miracle, Metal matrix composites - From science to technological significance, *Compos. Sci. Technol.* 65 (2005) 2526
- [91] M. Rosso, Ceramic and metal matrix composites: routes and properties, *J. Mater. Process. Technol.* 175 (2006) 364
- [92] M. Lekka, C. Zanella, A. Klorikowska, P.L. Bonora, Scaling-up of the electrodeposition process of nano-composite coating for corrosion and wear protection, *Electrochim. Acta* 55 (2010) 7876
- [93] R. Asthana, P.K. Rohatgi, On the melt infiltration of plain and nickel-coated reinforcements with aluminium alloys, *J. Mater. Sci. Lett.* 11 (1993) 442
- [94] C.A. Leon-Patiño, R.A.L. Drew, Role of metal interlayers in the infiltration of metal–ceramic composites, *Curr. Opin. Solid State Mater. Sci.* 9 (2005) 211
- [95] W.-S. Chung, S.-J Lin, Ni-coated SiC reinforced aluminum composites processed by vacuum infiltration, *Mater. Res. Bull.* 31 (1996) 1437
- [96] P. Yih, D.D.L. Chung, A comparative study of the coated filler method and the admixture method of powder metallurgy for making metal–matrix composites, *J. Mater. Sci.* 32 (1997) 2873
- [97] C.A. Leon, R.A.L. Drew, The influence of nickel coating on the wettability of aluminum on ceramics, *Composites Part A* 33 (2002) 1429
- [98] C.S. Ramesh, R. Keshavamurthy, B.H. Channabasappa, Abrar Ahmed, Microstructure and mechanical properties of Ni–P coated Si₃N₄ reinforced Al6061 composites, *Mater. Sci. Eng. A* 502 (2009) 99
- [99] C.S. Ramesh, R. Keshavamurthy, B.H. Channabasappa, Abrar Ahmed, Friction and wear behavior of Ni–P coated Si₃N₄ reinforced Al6061 composites, *Tribol. Int.* 43 (2010) 623
- [100] Y. Xia, G.M. Whitesides, Softlithography, *Annu. Rev. Mater. Sci.* 28 (1998) 153
- [101] D.B. Weibel, W.R. DiLuzio, G.M. Whitesides, Microfabrication meets microbiology, *Nature Reviews* 5 (2007) 209

-
- [102] A. Kumar, G.M. Whitesides, Features of gold having micrometer to centimeter dimensions can be formed through a combination of stamping with an elastomeric stamp and an alkanethiol ink followed by chemical etching, *Appl. Phys. Lett.* 63 (1993) 2002
- [103] A. Bietsch, B. Michel, Conformal contact and pattern stability of stamps used for soft lithography, *J. Appl. Phys.* 88 (2000) 4310
- [104] C. Donzel, M. Geissler, A. Bernard, H. Wolf, B. Michel, J. Hilborn, E. Delamarche, Hydrophilic poly(dimethylsiloxane) stamps for microcontact printing, *Adv. Mater.* 13 (2001) 1164
- [105] S.A. Ruiz, C.S. Chen, Microcontact printing: A tool to pattern, *Soft Matter* 3 (2007) 168
- [106] D.J. Campbell, K.J. Beckman, C.E. Calderon, P.W. Doolan, R.M. Ottosen, A.B. Ellis, G.C. Lisensky, *J. Chem. Educ.* 75 (1999) 537
- [107] A. Perl, D.N. Reinhoudt, J. Huskens, Microcontact Printing: Limitations and Achievements, *Adv. Mater.* 21 (2009) 2257
- [108] K.G. Sharp, G.S. Blackman, N.J. Glassmaker, A. Jagota, C.Y. Hui, Effect of stamp deformation on the quality of microcontact printing: Theory and experiment, *Langmuir* 20 (2004) 6430
- [109] H.W. Li, B.V.O. Muir, G. Fichet, W.T.S. Huck, Nanocontact printing: A route to sub-50-nm-scale chemical and biological patterning, *Langmuir* 19 (2003) 1963
- [110] T. Kaufmann, B.J. Ravoo, Stamps, inks and substrates: polymers in microcontact printing, *Polym. Chem.* 1 (2010) 371
- [111] N.B. Larsen, H.A. Biebuyk, E. Delamarche, B.J. Michel, Order in microcontact printed self-assembled monolayers, *J. Am. Chem. Soc.* 119 (1997) 3017
- [112] E. Delamarche, H. Schmid, A. Bietsch, N.B. Larsen, H. Rothuizen, B. Michel, H.A. Biebuyk, Transport mechanisms of alkanethiols during microcontact printing on gold, *J. Phys. Chem. B* 102 (1998) 3324
- [113] T.P. Moffat, H. Yang, Patterned metal electrodeposition using an alkanethiolate mask, *J. Electrochem. Soc.* 142 (1995) L220
- [114] J. Aizenberg, A.J. Black, G.M. Whitesides, Control of crystal nucleation by patterned self-assembled monolayers, *Nature* 398 (1999) 495
- [115] Y.-T. Tao, K. Pandian, W.-C. Lee, Microfabrication of interdigitated polyaniline/polymethylene patterns on a gold surface, *Langmuir* 14 (1998) 6158

-
- [116] M. Böltau, S. Walheim, J. Mlynek, G. Krausch, U. Steiner, Surface-induced structure formation of polymer blends on patterned substrates, *Nature* 391 (1998) 877
- [117] T.E. Balmer, H. Schmid, R. Stutz, E. Delamarche, B. Michel, N.D. Spencer, H. Wolf, Diffusion of alkanethiols in PDMS and its implications on microcontact printing (μ CP), *Langmuir* 21 (2005) 622
- [118] G.E. Poirier, M.J. Tarlov, H.E. Rushmeier, 2-Dimensional liquid-phase and the PX-Root-3-Phase of alkanethiol self-assembled monolayers on Au(111), *Langmuir* 10 (1994) 3383
- [119] K.Y. Suh, Y.S. Kim, H.H. Lee, Capillary force lithography, *Adv. Mater.* 13 (2001) 1386
- [120] A. Del Campo, E. Arzt, Fabrication approaches for generating complex micro- and nanopatterns on polymeric surfaces, *Chem. Rev.* 108 (2008) 911
- [121] Y.S. Kim, K.Y. Suh, H.H. Lee, Fabrication of three-dimensional microstructures by soft molding, *Appl. Phys. Lett.* 79 (2001) 2285
- [122] K.Y. Suh, H.H. Lee, Capillary force lithography: Large-area patterning, self-organization, and anisotropic dewetting, *Adv. Funct. Mater.* 12 (2002) 405
- [123] S.K. Lee, J.M. Jung, J.S. Lee, H.T. Jung, Fabrication of complex patterns with a wide range of feature sizes from a single line prepattern by successive application of capillary force lithography, *Langmuir* 26 (2010) 14359
- [124] K.Y. Suh, J. Seong, A. Khademhosseini, P.E. Laibinis, R. Langer, A simple soft lithographic route to fabrication of poly(ethylene glycol) microstructures for protein and cell patterning *Biomaterials* 25 (2004) 557
- [125] X.H. Yu, Z. Wang, R.B. Xing, S.F. Luan, Y.C. Han, Fabrication of structures with tunable morphologies and sizes by soft molding, *Appl. Surf. Sci.* 252 (2005) 1947
- [126] Y. Xia, J.A. Rogers, K.E. Paul, G.M. Whitesides, Unconventional methods for fabricating and patterning nanostructures, *Chem. Rev.* 99 (1999) 1823
- [127] B.D. Gates, Q. Xu, C. Love, D.B. Wolfe, G.M. Whitesides, Unconventional nanofabrication, *Annu. Rev. Mater. Res.* 34 (2004) 339
- [128] W.A. Murray, W.L. Barnes, Plasmonic materials, *Adv. Mater.* 19 (2007) 3771
- [129] J. Henzie, J. Lee, M.H. Lee, W. Hasan, T.W. Odom, Nanofabrication of Plasmonic Structures, *Annu. Rev. Phys. Chem.* 60 (2009) 147

-
- [130] C. Caliendo, P. Verardi, E. Verona, A. D'Amico, C. Di Natale, G. Saggio, M. Serafini, R. Paolesse, S.E. Huq, Advances in SAW-based gas sensors, *Smart Mater. Struct.* 6 (1997) 689
- [131] G. Luo, I. Maximov, D. Adolph, M. Graczyk, P. Carlberg, S. Ghatnekar-Nilsson, D. Hessman, T. Zhu, Z. Liu, H.Q. Xu, L. Montelius, Nanoimprint lithography for the fabrication of interdigitated cantilever arrays, *Nanotechnology* 17 (2006) 1906
- [132] S. De, P.J. King, P.E. Lyons, U. Khan, J.N. Coleman, Size Effects and the Problem with Percolation in Nanostructured Transparent Conductors, *ACS Nano* 4 (2010) 7064
- [133] D.S. Ghosh, L. Martinez, S. Giurgola, P. Vergani, V. Pruneri, Widely transparent electrodes based on ultrathin metals, *Opt. Lett.* 34 (2009) 325
- [134] C.-H. Hsu, M.-C. Yeh, K.-L. Lo, and L.-J. Chen, Application of microcontact printing to electroless plating for the fabrication of microscale silver patterns on glass, *Langmuir* 23 (2007) 12111
- [135] H. Kind, M. Geissler, H. Schmid, B. Michel, K. Kern, E. Delamarche, Patterned electroless deposition of copper by microcontact printing palladium(II) complexes on titanium-covered surfaces, *Langmuir* 16 (2000) 6367
- [136] N. Yoshida, T. Tasaki, T.F.M. Chang, A. Shibata, C. Ishiyama, M. Sone, Pd-Ni-P metallic glass pattern with controllable microstructure fabricated by electroless alloy plating, *Microelectron. Eng.* 88 (2011) 2401
- [137] F. Guan, M. Chen, W. Yang, J. Wang, S. Yong, Q. Xue, Fabrication of patterned gold microstructure by selective electroless plating, *Appl. Surf. Sci.* 240 (2005) 24
- [138] A.M. Bittner, X.C. Wu, K. Kern, Electroless metallization of dendrimer-coated micropatterns, *Adv. Funct. Mater.* 12 (2002) 432
- [139] C.E. Moran, C. Radloff, N.J. Halas, Benchtop fabrication of submicrometer metal line and island Arrays using passivative microcontact printing and electroless plating, *Adv. Mater.* 15 (2003) 804
- [140] S.S. Yoon, D.O. Kim, S.C. Park, Y.K. Lee, H.Y. Chae, S.B. Jung, J.-D. Nam, Direct metallization of gold patterns on polyimide substrate by microcontact printing and selective surface modification, *Microelectron. Eng.* 85 (2008) 136
- [141] J.C. Meyer, C.O. Girit, M.F. Crommie, A. Zettl, Imaging and dynamics of light atoms and molecules on graphene, *Nature* 454 (2008) 319

-
- [142] JEOL JEM 2100 instruction manual (2004)
- [143] F.J. Giessibl, Advances in atomic force microscopy, *Rev. Mod. Phys.* 75 (2003) 949
- [144] E. Meyer, Atomic force microscopy, *Prog. Surf. Sci.* 41 (1992) 3
- [145] G. Mondin, M.R. Lohe, F.M. Wisser, J. Grothe, N. Mohamed-Noriega, A. Leifert, S. Dörfler, A. Bachmatiuk, M.H. Rummeli, S. Kaskel, Electroless copper deposition on (3-mercaptopropyl)-triethoxysilane-coated silica and alumina nanoparticles, *Electrochim. Acta* 114 (2013) 521
- [146] G. Mondin, F.M. Wisser, A. Leifert, N. Mohamed-Noriega, J. Grothe, S. Dörfler, S. Kaskel, Metal deposition by electroless plating on polydopamine functionalized micro- and nanoparticles, *J. Colloid Interface Sci.* 411 (2013) 187
- [147] J.P. Rolland, R.M. Van Dam, D.A. Schorzman, S.R. Quake, J.M. DeSimone, Solvent-Resistant Photocurable “Liquid Teflon” for Microfluidic Device Fabrication, *J. Am. Chem. Soc.* 126 (2004) 2322
- [148] M. Hu, S. Noda, T. Okubo, Y. Yamaguchi, H. Komiyama, Structure and morphology of self-assembled 3-mercaptopropyltrimethoxysilane layers on silicon oxide, *Appl. Surf. Sci.* 181 (2001) 307
- [149] F. Basarir, T.-H. Yoon, Preparation of gamma-APS monolayer with complete coverage via contact printing, *J. Colloid. Interf. Sci.* 336 (2009) 393
- [150] A. Ulman, Formation and structure of self-assembled monolayers, *Chem. Rev.* 96 (1996) 1533
- [151] G. Mondin, B. Schumm, J. Fritsch, J. Grothe, S. Kaskel, Fabrication of micro- and submicrometer silver patterns by microcontact printing of mercaptosilanes and direct electroless metallization, *Microelectron. Eng.* 104 (2013) 100
- [152] H.V. Wartenberg, Über die Beschleunigung der Glasversilberung mit Zinnchlorür, *Z. Anorg. Allg. Chem.* 190 (1930) 185
- [153] C.M. Bruinink, M. Peter, P.A. Maury, M. De Boer, L. Kuipers, J. Huskens, D.N. Reinhoudt, Capillary force lithography: Fabrication of functional polymer templates as versatile tools for nanolithography, *Adv. Funct. Mater.* 16 (2006) 1555
- [154] S.D. Vaidya, N.V. Thakkar, Study of phase transformations during hydration of rho alumina by combined loss on ignition and X-ray diffraction technique, *J. Phys. Chem. Solids* 62 (2001) 977

- [155] F.M. Wisser, M. Abele, M. Gasthauer, K. Müller, N. Moszner, G. Kickelbick, Detection of surface silanol groups on pristine and functionalized silica mixed oxides and zirconia, *J. Colloid Interface Sci.* 374 (2012) 77
- [156] C.A. Ribeiro, W.R. de Souza, M. Spirandeli Crespi, J.A. Gomes Neto, F.L. Fertonani, Non-isothermal kinetic of oxidation of tungsten carbide, *J. Therm. Anal. Calorim.* 90 (2007) 801
- [157] F. Zucchi, A. Frignani, V. Grassi, G. Trabanelli, M. DalColle, The formation of a protective layer of 3-mercaptopropyl-trimethoxy-silane on copper, *Corros. Sci.* 49 (2007) 1570
- [158] R.M. Pasternack, S. Rivillon Amy, Y.J. Chabal, Attachment of 3-(aminopropyl)triethoxysilane on silicon oxide surfaces: dependence on solution temperature, *Langmuir* 24 (2008) 12963
- [159] E.T. Vandenberg, L. Bertilsson, B. Liedberg, K. Uvdal, R. Erlandsson, H. Elwing, I. Lundstrom, Structure of 3-aminopropyl triethoxy silane on silicon oxide, *J. Colloid Interface Sci.* 147 (1991) 103
- [160] H. Okabayashi, K. Izawa, T. Yamamoto, H. Masuda, E. Nishio, C.J. O'Connor, Surface structure of silica gel reacted with 3-mercaptopropyltriethoxysilane and 3-aminopropyltriethoxysilane: formation of the S–S bridge structure and its characterization by Raman scattering and diffuse reflectance Fourier transform spectroscopic studies, *Colloid. Polym. Sci.* 280 (2002) 135
- [161] K.M.K. Yu, D. Thompsett, S.C. Tsang, Ultra-thin porous silica coated silver–platinum alloy nano-particle as a new catalyst precursor, *Chem. Commun.* 13 (2003) 1522
- [162] C. Hernandez, A.C. Pierre, Evolution of the texture and structure of $\text{SiO}_2\text{--Al}_2\text{O}_3$ Xerogels and Aerogels as a function of the Si to Al molar ratio, *J. Sol-Gel Sci. Technol.* 20 (2001) 227
- [163] A. Baptiste, A. Gibaud, J.F. Bardeau, K. Wen, R. Maoz, J. Sagiv, B.M. Ocko, X-ray micro-Raman and infrared spectroscopy structural characterization of selfassembled multilayer silane films with variable numbers of stacked layers, *Langmuir* 18 (2002) 3916
- [164] P. Thissen, M. Valtiner, G. Grundmeier, Stability of phosphonic acid self-assembled monolayers on amorphous and single-crystalline aluminum oxide surfaces in aqueous solution, *Langmuir* 26 (2010) 156

-
- [165] B. Zhang, T. Kong, W. Xu, R. Su, Y. Gao, G. Cheng, surface functionalization of zinc oxide by carboxyalkylphosphonic acid self-assembled monolayers, *Langmuir* 26 (2010) 4514
- [166] I. Maege, E. Jaehne, A. Henke, H.-J.P. Adler, C. Bramb, C. Jung, M. Stratmann, Ultrathin organic layers for corrosion protection, *Macromol. Symp.* 126 (1997) 7
- [167] G. Guerrero, P.H. Mutin, A. Vioux, Anchoring of phosphonate and phosphinate coupling molecules on titania particles, *Chem. Mater.* 13 (2001) 4367
- [168] A.S. Kurlov, A.I. Gusev, Effect of particle size on the oxidation of WC powders during heating, *Inorg. Mater.* 47 (2011) 133
- [169] R. Ouyang, J. Lei, H. Ju, Artificial receptor-functionalized nanoshell: facile preparation, fast separation and specific protein recognition, *Nanotechnology* 21 (2010) 185502
- [170] J.-H. Jiang, L.-P. Zhu, X.-L. Li, Y.-Y. Xu, B.-K. Zhu, Surface modification of PE porous membranes based on the strong adhesion of polydopamine and covalent immobilization of heparin, *J. Membrane Sci.* 364 (2010) 194
- [171] G. Busca, The surface of transitional aluminas: A critical review, *Catal. Today* 226 (2014) 2
- [172] J. Fritsch, B. Schumm, R. Biedermann, J. Grothe, S. Kaskel, A new silver-based precursor as ink for soft printing techniques, *Eur. J. Inorg. Chem.* 5 (2012) 878
- [173] M. Schneider, M. Weiser, S. Doerfler, H. Althues, S. Kaskel, A. Michaelis, Electrodeposition of copper on aligned multi-walled carbon nanotubes, *Surf. Eng.* 28 (2012) 435
- [174] D.I. Rozkiewicz, D. Janczewski, W. Verboom, B.J. Ravoo, D.N. Reinhoudt, "Click" chemistry by microcontact printing, *Angew. Chem. Int. Ed.* 45 (2006) 5292
- [175] A.W. Adamson, A.P. Gast, *Physical Chemistry of Surfaces*, sixth ed., Wiley, New York, 1997
- [176] M. Bender, U. Plachetka, J. Ran, A. Fuchs, B. Vratzov, H. Kurz, T. Glinsner, F. Lindner, High resolution lithography with PDMS molds, *J. Vac. Sci. Technol. B* 22 (2004) 3229
- [177] O.D. Gordan, B.N.J. Persson, C.M. Cesa, D. Mayer, B. Hoffmann, S. Dieluweit, R. Merkel, On pattern transfer in replica molding, *Langmuir* 24 (2008) 6636
- [178] J.N. Lee, C. Park, G.M. Whitesides, Solvent compatibility of poly(dimethylsiloxane)-based microfluidic devices, *Anal. Chem.* 75 (2003) 6544

-
- [179] Q.U. He, Z.C. Liu, P.F. Xiao, N.Y. He, Z.H. Lu, Angular evaluation to quantify planar distortions of PDMS stamps in soft lithography, *Mater. Chem. Phys.* 83 (2004) 60
- [180] D. Myers, *Surfaces, Interfaces, and Colloids-principles and Applications*, second ed., Wiley, New York, 1999
- [181] K. Liu, F. Schuch, E. Kiran, High-pressure viscosity and density of poly(methyl methacrylate) plus acetone and poly(methyl methacrylate) plus acetone plus CO₂ systems, *J. Supercrit. Fluids* 39 (2006) 89
- [182] L. Martínez, D.S. Ghosh, S. Giurgola, P. Vergani, V. Pruneri, Stable transparent Ni electrodes, *Opt. Mater.* 31 (2009) 1115

List of publications of Giovanni Mondin

Peer-reviewed articles

- [1] **G. Mondin**, M.R. Lohe, F.M. Wissler, J. Grothe, N. Mohamed-Noriega, A. Leifert, S. Dörfler, A. Bachmatiuk, M.H. Rummeli, S. Kaskel, “Electroless copper deposition on (3-mercaptopropyl)-triethoxysilane-coated silica and alumina nanoparticles”, *Electrochimica Acta* 114 (2013) 521
- [2] **G. Mondin**, F.M. Wissler, A. Leifert, N. Mohamed-Noriega, J. Grothe, S. Dörfler, S. Kaskel, “Metal deposition by electroless plating on polydopamine functionalized micro- and nanoparticles”, *Journal of Colloid and Interface Science* 411 (2013) 187
- [3] **G. Mondin**, B. Schumm, J. Fritsch, R. Hensel, J. Grothe, S. Kaskel, “Fast patterning of poly(methyl methacrylate) by a novel soft molding approach and its application to the fabrication of silver structures”, *Materials Chemistry and Physics* 137 (2013) 884
- [4] **G. Mondin**, B. Schumm, J. Fritsch, J. Grothe, S. Kaskel, “Fabrication of micro- and submicrometer silver patterns by microcontact printing of mercaptosilanes and direct electroless plating”, *Microelectronic Engineering* 104 (2013) 100
- [5] B. Schumm, F.M. Wissler, **G. Mondin**, F. Hippauf, J. Grothe, S. Kaskel, “Semi-transparent Silver Electrodes for Flexible Electronic Devices Prepared by Nanoimprint Lithography”, *Journal of Materials Chemistry C* 1 (2013) 638
- [6] J. Fritsch, F.M. Wissler, K. Eckhardt, V. Bon, **G. Mondin**, B. Schumm, J. Grothe, S. Kaskel, “A new molecular silver precursor for the preparation of thin conductive silver films”, *Journal of Physics and Chemistry of Solids* 74 (2013) 1546
- [7] J.R. Martin, L. Borchardt, M. Oschatz, **G. Mondin**, S. Kaskel, “Titanium Carbide and Carbide-Derived Carbon Composite Nanofibers by Electrospinning of Ti-Resin Precursor”, *Chemie Ingenieur Technik* 85 (2013) 1742
- [8] T. Biemelt, C. Selzer, F. Schmidt, **G. Mondin**, A. Seifert, K. Pinkert, S. Spange, T. Gemming, S. Kaskel, “Hierarchical porous zeolite ZSM-58 derived by desilication and desilication re-assembly”, *Microporous and Mesoporous Materials* 187 (2014) 114

- [9] **G. Mondin**, M. Haft, F.M. Wissler, A. Leifert, N. Mohamed-Noriega, S. Dörfler, S. Hampel, J. Grothe, S. Kaskel, “Investigations of mussel-inspired polydopamine deposition on WC and Al₂O₃ particles: the influence of particle size and material”, Journal of Colloid and Interface Science (2014) submitted
- [10] A. Leifert, **G. Mondin**, S. Dörfler, S. Hampel, S. Kaskel, E. Hofmann, J. Zschetzsche, E. Pflug, G. Dietrich, M. Rühl, S. Braun, S. Schädlich, “Fabrication of nanoparticle-containing films and nano layers for alloying and joining”, Advanced Engineering Materials (2014) submitted
- [11] A. Leifert, B. Schumm, N. Mohamed-Noriega, A. Meier, C. Nowka, **G. Mondin**, S. Dörfler, J. Grothe, S. Hampel, E.M. López Cuéllar, S. Kaskel “Enhanced Hardness in Nanoparticle-Reinforced Copper Films Prepared from Polymeric Precursor”, J. Mater. Sci. (2014) submitted
- [12] K. Faber, F. Badaczewski, M. Oschatz, G. Mondin, W. Nickel, S. Kaskel, B. Smarsly, “In depth investigation of the carbon microstructure of silicon carbide-derived carbons by wide-angle X-Ray scattering”, Journal of Physical Chemistry C (2014) submitted
- [13] M. Oschatz, W. Nickel, M. Thommes, K.A. Cychosz, M. Leistner, M. Adam, **G. Mondin**, P. Strubel, L. Borchardt, S. Kaskel, “Evolution of Porosity in Carbide-Derived Carbon Aerogels for Efficient Carbon Dioxide Adsorption”, Small (2014) submitted

Patents

- [1] **G. Mondin**, F. Wissler, S. Doerfler, S. Kaskel, „Verfahren zur Metallbeschichtung von anorganischen Partikeln mittels stromloser Metallabscheidung“ 800298265 (2013) submitted

Versicherung

Hiermit versichere ich, dass ich die vorliegende Arbeit ohne unzulässige Hilfe Dritter und ohne Benutzung anderer als der angegebenen Hilfsmittel angefertigt habe; die aus fremden Quellen direkt oder indirekt übernommenen Gedanken sind als solche kenntlich gemacht. Die Arbeit wurde bisher weder im Inland noch im Ausland in gleicher oder ähnlicher Form einer anderen Prüfungsbehörde vorgelegt.

Dresden, den

Giovanni Mondin

Erklärung

Die vorliegende Arbeit wurde an der Professur für Anorganische Chemie I der Fachrichtung Chemie und Lebensmittelchemie der Technische Universität Dresden in dem Zeitraum vom August 2011 bis Mai 2014 unter wissenschaftlicher Betreuung von Herrn Prof. Dr. S. Kaskel angefertigt. Es haben bisher keine früheren erfolglosen Promotionsverfahren stattgefunden.

Hiermit erkenne ich die Promotionsordnung der Fakultät Mathematik und Naturwissenschaften der Technischen Universität Dresden vom 23. Februar 2011 an.

Dresden, den

Giovanni Mondin